RIGA TECHNICAL UNIVERSITY

Ilya Balmages

LASER SPECKLE IMAGE PROCESSING SYSTEM FOR THE ANALYSIS OF LARGE AREA SUBMICRON ACTIVITY

Doctoral Thesis

RTU Press
Riga 2025

RIGA TECHNICAL UNIVERSITY
Faculty of Computer Science, Information Technology and Energy
Institute of Applied Computer Systems

Ilya Balmages
Doctoral Student of the Study Program "Computer Systems"

LASER SPECKLE IMAGE PROCESSING SYSTEM FOR THE ANALYSIS OF LARGE AREA SUBMICRON ACTIVITY

The Doctoral Thesis

Scientific supervisor
Associate Professor Dr. sc. ing.
DMITRIJS BĻIZŅUKS

RTU Press
Riga 2025

Balmages, I. Laser Speckle Image Processing System for the Analysis of Large Area Submicron Activity. – Riga: RTU Press, 2025. – 121 p.

Published in accordance with the decision of the Promotion Council “P-07” of 9 May 2025, Minutes No. 04030-9.7/3.

DOCTORAL THESIS PROPOSED TO RIGA TECHNICAL UNIVERSITY FOR PROMOTION TO THE SCIENTIFIC DEGREE OF DOCTOR OF SCIENCE

To be granted the scientific degree of Doctor of Science (Ph.D.), the present Doctoral Thesis has been submitted for defence at the open meeting of RTU Promotion Council on September 22, 2025 at the Faculty of Computer Science, Information Technology and Energy of Riga Technical University, 10 Zundas krastmala, Room 104.

OFFICIAL REVIEWERS

Professor Dr. sc. ing. Agris Ņikitenko,
Riga Technical University

Ph.D. Viktor Dremin,
Aston University, UK

Ph.D. Mihails Birjukovs,
University of Latvia, Latvia

DECLARATION OF ACADEMIC INTEGRITY

I hereby declare that the Doctoral Thesis submitted for review to Riga Technical University for promotion to the scientific degree of Doctor of Science (Ph.D.) is my own. I confirm that this Doctoral Thesis has not been submitted to any other university for promotion to a scientific degree.

Ilya Balmages…… (signature)
Date: ……

The Doctoral Thesis has been written in English. It consists of an Introduction, six chapters, Conclusions, 65 figures, and three tables; the total number of pages is 121. The Bibliography contains 150 titles.

Acknowledgments

I would like to express my sincere gratitude to my supervisor, Assoc. Professor Dr. sc. ing. Dmitrijs Bļizņuks, for his invaluable support throughout my academic journey: from the initial stages of applying to the program to the completion of this research. I am deeply thankful for the opportunities he provided for growth and advancement, for the freedom to explore and develop my own ideas, and for his thoughtful guidance during the many challenges of study, work, and scientific inquiry. His understanding and encouragement were essential to this endeavor.

I thank Dr. Phys. Ilze Ļihačova and Dr. Phys. Alexey Lihachev (Institute of Atomic Physics and Spectroscopy, University of Latvia) for their contributions; Dr. biol. Jānis Liepiņš and his team (Institute of Microbiology and Biotechnology) for their help with experimental data and modeling; and M.D., Ph.D. Aigars Reinis and his colleagues (Pauls Stradins Clinical University Hospital) for providing experimental data.

I thank the reviewers: Prof. Dr. sc. ing. Agris Ņikitenko, Dr. Viktor Dremin, and Dr. Mihails Birjukovs, for their thorough and fair evaluation. I am also grateful to the Doctoral Committee and its chair, Dr. habil. sc. ing. Jānis Grundspeņkis, for reviewing my dissertation and granting approval for its defense.

My gratitude extends to the academic and research staff of Riga Technical University (RTU), Faculty of Computer Science, Information Technology, and Energy, for their support and contributions throughout my studies.

I would like to express my appreciation to Gymnasium No. 299 in Kyiv, Ukraine, especially to my physics teacher, A.V. Kabanovsky, who, despite my resistance and many challenges, managed to inspire me to study his subject.

I am thankful to the faculty of the Sami Shamoon College of Engineering (SCE), Faculty of Engineering Sciences, in Beer-Sheva, Israel, particularly Prof. Alexander Abramovitz, whose teaching sparked my interest in electronics.

My sincere appreciation also goes to the academic and teaching staff of Ben-Gurion University of the Negev, Faculty of Engineering Sciences, in Beer-Sheva, Israel, especially my M.Sc. supervisor, Prof. Boaz Rafaely, from whom I learned how to conduct research.

I am also grateful to the team of the now-defunct company EORD, especially my first manager, Dr. Yoram Tal, and also Mr. Alon Heimer, for their patience and guidance, which helped shape me as both an engineer and a researcher.

A special thank-you goes to my family for their unwavering support throughout this journey: to my parents, Yeva Mitelman and Grigory Balmages; to my wife, Anna Korb-Balmages (thanks to whom I moved to Latvia); and to my sister, Anna Shparberg, along with her family.

My deepest gratitude goes to my son, Semuel Korb-Balmages, who greatly contributed to my ability to adapt under the most unpredictable circumstances.

This work is dedicated to the memory of my grandmother, Haya Halfina, who so dearly wished that, despite my restlessness and disobedience, I would one day receive a higher education.

Abstract

The development of new technologies and data processing algorithms is drawing increasing attention to the field of processing very low-frequency signals. The most well-known applications are aimed at observing "global scale" processes, such as volcano eruptions, mountain-associated waves, earthquakes, and mineral exploration and require complex equipment. However, there are other industries where very low-frequency signals need to be processed. One of these is monitoring changes in the growth and inhibition of microorganisms. Optical contactless technology (laser speckle patterns analysis) has been proposed for this aim. The technological advantage lies in the small size of compact equipment and change-sensitive granular structure.

The sensitive correlation subpixel algorithm allows the conversion of a speckle image sequence into an array of temporal signals and is capable of highlighting hidden effects. An important advantage of this approach is that any subsequent signal processing algorithms can be applied to the array of obtained signals, such as filtering, operations in the time, frequency, or time-frequency domains, and also use the algorithms of spatial signal processing, analysing the behavior and changes in the time-spatial domain.

The application of artificial neural networks with additional post-processing based on understanding the properties of the signals has yielded high achievements in the classification of growing (active) and inactive zones.

The research results were applied in the ERDF and LZP projects.

Anotācija

Jaunu tehnoloģiju un datu apstrādes algoritmu attīstība piesaista arvien lielāku uzmanību ļoti zemas frekvences signālu apstrādes jomai. Vispazīstamākie lietojumi ir paredzēti "globāla mēroga" procesu novērošanai, piemēram, vulkānu izvirdumu, ar kalniem saistītu viļņu, zemestrīču un minerālu izpētes novērošanai, un tiem ir nepieciešams sarežģīts aprīkojums. Tomēr ir arī citas nozares, kurās jāapstrādā ļoti zemas frekvences signāli. Viena no tām ir mikroorganismu augšanas un inhibīcijas izmaiņu uzraudzība. Šim nolūkam tiek piedāvāta optiskā bezkontakta tehnoloģija (lāzera speklu paraugu analīze). Tehnoloģiskā priekšrocība ir kompaktā aprīkojuma nelielais izmērs un uz izmaiņām jutīgā granulveida struktūra.

Jutīgais korelācijas apakšpikseļu algoritms ļauj pārveidot speklu attēlu sekvenci par laika signālu masīvu un spēj izcelt slēptos efektus. Svarīga šīs pieejas priekšrocība ir tā, ka iegūto signālu masīvam var piemērot jebkādus turpmākos signālu apstrādes algoritmus, piemēram, filtrēšanu, darbības laika, frekvences vai laika–frekvences apgabalā, kā arī izmantot telpiskās signālu apstrādes algoritmus, analizējot uzvedību un izmaiņas laika–telpas apgabalā.

Mākslīgo neironu tīklu izmantošana ar papildu pēcapstrādi, kas balstīta uz signālu īpašību izpratni, ir devusi augstus sasniegumus augošu (aktīvu) un neaktīvu zonu klasifikācijā.

Pētījumu rezultāti tika izmantoti ERAF un LZP projektos.

Contents

GENERAL DESCRIPTION OF THE THESIS

Introduction

Very low-frequency signals. Several different technologies have analysed and processed very low-frequency signals (mHz (milliHertz)).

The most common technologies are:

1. Infrasound. Infrasonic waves are sub-audible acoustic waves, typically in the frequency range 0.01 <f < 10 Hz, and can result from many natural and man-made phenomena. A known example is an international infrasonic monitoring network that is capable of detecting and verifying nuclear explosions. Infrasonic waves can also result from mountain-associated waves, volcano, microbaroms, and gravity waves, among others. Infrasound has the ability to reach large distances, ranging from 100 to 500 km.

Low-frequency infrasound (one oscillation in a few seconds), cannot be physically recorded by microphones. In general, infrasound sensor stations consist of an array of sensors that measure pressure variations in the air and consist of many large components.

2. Gravity gradiometry is the field of study of variations or anomalies in the Earth's gravity field via measurements of the spatial gradient of gravitational acceleration. Understanding of subsurface anomalies can be used to more accurately target oil, gas, and mineral deposits. The greatest interest lies in the developments of the last decade of airborne gravity gradiometers for gravitational field measurements with improved signal-to-noise and resolution in the bandwidth from 0.001 to 1 Hz.

3. Seismic tomography or seismology. The frequency of seismic waves ranges from fractions of a Hz (mHz) to a few hundred Hz. Normal modes or free oscillations of the Earth are very long-period (very low frequency – mHz) standing surface waves.

4. Magnetotellurics – electromagnetic geophysical method for inferring the Earth's subsurface electrical conductivity. Electric and magnetic fields of Earth are measured over a frequency range 0.1 mHz – 10 kHz. The higher frequency ranges give information on the shallow Earth, whereas deeper information is provided by the low-frequency range.

Very low-frequency signals for analysing spatiotemporal micro-activity. All of the techniques described above require complex equipment and observing global-scale processes. However, there are other industries where very low-frequency signals need to be processed. For example, monitoring changes in growth and inhibition of microorganisms. The growth of microorganisms in space looks like a one-directional progression process. However, microorganisms create many different, multidirectional, random movements on the occupied surface. When considering these processes in the time domain, fluctuations characterising alternating processes occurring over time are observed. Accordingly, in the temporal frequency domain, frequencies corresponding to these fluctuations (located in the very low-frequency region) can be observed. Spectrogram analysis provides additional insight by allowing simultaneous observation of changes over time and frequency. Thus, temporary signals created by the activity of microorganisms are also very low-frequency signals. This thesis proposes an optical contactless technology (laser speckle patterns analysis), including signal processing algorithms for monitoring such phenomena.

The technological advantage lies in the small size of compact equipment, change-sensitive granular structure, and the set of image and signal processing techniques to extract useful

information. The application of laser speckle patterns analysis to measure acoustic and seismic signals (in the higher frequency region) has been demonstrated in the literature. Accordingly, potentially, this method can be used for acoustic, seismic, and other applications where processing of very low-frequency signals is required.

Laser speckle patterns technique. The operation of the first laser in 1960 demonstrated that objects viewed in laser light acquire a chaotic granular structure with an irregular pattern, which has no obvious relationship to the macroscopic properties of the illuminated object. The reason is that the surfaces of most materials are extremely rough on the scale of an optical wavelength. When monochromatic light is reflected from such a surface, the optical wave resulting at any distant point consists of many coherent components, each arising from a different microscopic element of the surface, the interference of which results in the granular pattern of intensity that is called “laser speckle”.

It is worth noting that speckle can appear not only from free-space propagation but also within the imaging system.

Initially, the laser speckle effect was only considered a main drawback in using coherent light sources. However, it was later noted that the speckle can also provide useful information. Currently, laser speckle techniques are used in a variety of optical metrology techniques, including displacement, distortion, and strain measurement, surface roughness assessment, velocity measurement, etc. Quite a few of these applications are used in the biomedical field, and in particular in microbiology, to observe microorganisms' development.

Submicron activity analysis. According to available literature, none of the laser speckle-based methods has been focused on 1) microbial growth (colony forming units (CFU) formation) monitoring in early stages; 2) detection and monitoring of differences in microbial activity in different parts of the colony; 3) classification of growing (active)/non-growing (non-active) bacterial colonies or zones; and 4) identifying dynamics and changes of microorganism's activity in the zone of inhibition (around the antibiotic disc).

To monitor these phenomena, in addition to the laser speckle technique, data processing algorithms are widely used. A comparison of the most well-known algorithms for processing speckle patterns was carried out, based on which the advantages of correlation analysis were noted. The application and development of correlation analysis algorithms were analysed, and based on data properties, an approach was proposed, taking into account time and frequency characteristics. The proposed sensitive correlation subpixels algorithm allows the conversion of a speckle image sequence into an array of temporal signals. An important advantage of this approach is that any subsequent signal processing algorithms can be applied to the array of obtained signals, such as filtering, operations in the time, frequency, or time-frequency domains, and also use the algorithms of spatial signal processing, analysing the behavior and changes in the time-spatial domain.

The application of artificial neural networks with additional post-processing based on understanding the properties of the signals has yielded high achievements in the classification of growing (active) and inactive zones.

The thesis uses both mathematical simulations and real experiments for algorithm development and data analysis.

The research **aim** is to develop a novel approach for non-contact detection and assessment of submicron activity or growth of submicron objects over a large area, and the ability to classify and evaluate specific submicron objects or events.

To achieve the aim, the following topics have been explored:

1. Development and adaptation of the use of correlation analysis of laser speckle images for submicron activity evaluation.
2. Comparison of the proposed correlation subpixel method with other methods based on the use of laser speckle techniques.
3. Development of tools for monitoring the growth dynamics of a microorganism colony, revealing the migration of activity zones within the colony and comparison with models.
4. Development and demonstration of capabilities of early detection of antibacterial susceptibility in disc diffusion tests using the proposed correlation subpixel method and comparison with models.
5. Classification of active (growing) and non-growing colonies or zones.

The proposed method demonstrated the ability to operate in noisy environments and reveal hidden effects (which were not detected by others described in the literature approaches). The application of artificial neural networks to signals obtained by the proposed algorithm from a sequence of images with additional post-processing has given high achievements in classifying growing (active) and inactive zones, which could not be achieved using raw speckle data.

Actuality

Observation of submicron activity by conventional devices such as microscopes cannot simultaneously cover a large observation area and examine it with high resolution. However, it may be important in many applications, such as the analysis of bacterial or fungal activity in a Petri dish. Therefore, it is necessary to scan the entire area, dividing it into smaller sections beforehand. In cases where the area is relatively large, and the activity changes occur quickly and only in certain places, i.e., the transition from one stage of the field to another takes longer than the scanning period, these changes can be missed. In this case, cameras with an adequate field of view may represent an alternative. It can be used for large field coverage, but it has limited optical resolution, which would not provide submicron resolution for areas above a square centimeter.

Accordingly, there is a need to use other approaches. Recently, the need to perform analysis, data processing, finding, and classification of searched objects or events in a non-contact manner, quickly, with high resolution, and with high quality is becoming more and more frequent. This is especially relevant if direct access to objects is difficult, as objects are small, imperceptible (like a submicron activity), and located in unknown places.

The proposed non-contact optical method is based on laser speckle processing algorithms with high sensitivity, which allows 1) to view the required observation area at the same time without scanning; and 2) the technology is sensitive to submicron movements and changes occurring in the observation field. The method is based on the ability of laser speckle (a specific granular structure) to change the intensity of each speckle (grain) when physical movements occur up to half of the laser wavelength (for example, 0.4 micrometers). On the other hand, the size of the speckle can be a few tens of microns, which allows it to be captured by a typical camera.

Developed and adapted signal processing algorithms will make an additional contribution to the analysis of object activity in the case when movements are minimal (for example, the division of bacteria) or only movements of a specific nature that need to be evaluated.

Thus, even using a low-resolution camera, it is possible to detect submicron activity and perform additional analysis of its parameters and properties significantly earlier than existing methods allow.

Objectives and Hypotheses

The **objectives** of the Thesis:

1. Perform a review of existing methods for processing speckle patterns. Demonstrate the outperformance of the proposed method in the Thesis.
2. Study of correlation analysis techniques of speckle patterns. Comparison of different algorithms, testing execution time, and accuracy. Proposal and adaptation for application to low-frequency signals characterising the activity of microorganisms.
3. Study of the possibility of the proposed method to perform quick and non-contact detection and assessment of submicron activity or growth of submicron objects.
4. Measurement of the spread speed of submicron objects or events in space. Comparison with mathematical models.
5. Study of the possibility of the proposed method to perform the determination of specific hidden phenomena and effects of certain types of submicron objects. Comparison with mathematical models.
6. Demonstrate the ability to classify and evaluate specific submicron objects or events.
7. Publish findings in scientific publications and include them in this Thesis.

During research and development of algorithms of laser speckle image processing for submicron activity evaluation, the following **hypotheses** were defined:

1. The correlation subpixel algorithm is sensitive to small changes caused by activity (in particular submicron activity of microorganisms) and is able to observe/detect them earlier than other widely used methods.
2. The correlation subpixel algorithm for a given type of signal (submicron activity of microorganisms) is more sensitive and provides more information than other widely used algorithms used in the laser speckle technique, such as contrast analysis, speckle size analysis, and decorrelation time analysis.
3. The correlation subpixel algorithm is able to observe/detect activity even when there is no direct vision of it. For example, the formation of colonies in a noisy environment (when the colonies are covered in noise).
4. The correlation subpixel algorithm allows for “emphasizing”/distinguishing the character of activity in the data, thereby providing the opportunity to implement classification based on it.

Research methods

Objectives of the Thesis are accomplished by analytical and experimental research that has been published in the scientific research papers listed in the continuation of this chapter. The

Thesis uses experimental, mathematical, and statistical data analysis, as well as machine learning research methods. Qualitative and quantitative research methods have been used to review the scientific literature and existing and novel methods. Within this research, the primary research subject has been the development of a non-contact optical approach based on laser speckle processing algorithms with high sensitivity for submicron activity observation. Methods for its implementation have also been studied in order to improve the performance and functionality results.

Scientific Novelty of the Thesis

The **scientific novelty** of the Thesis is based on the development and proposal of the system, methods, and algorithms that are aimed at solving practical tasks related to the fast and efficient detection of submicron activity and are able to provide the following:

1. quick and non-contact assessment of submicron activity or growth of submicron objects;
2. the ability to classify and evaluate specific submicron objects or events;
3. measurement of the spread speed of submicron objects or events in space;
4. determination of specific phenomena and effects of certain types of submicron objects.

Practical Significance of the Thesis

The **practical significance** lies in software implementation, experimental validation, and assessment of the discussed methods. The full list of practical achievements is as follows.

1. A review and comparison of methods described in the literature were performed, and the advantages of the proposed method were demonstrated.

2. Results were obtained that could not be observed using a conventional microscope or other non-invasive technology, such as movement of activity in microbial colonies from the center to the edges; classification: active or inactive colony, early detection of the formation of an inhibition zone, detection of fully covered by noise microbial colonies, etc.

3. In practice, the proposed method allows for earlier detection of submicron objects or events (significantly faster than conventional methods).

4. Potential application of the proposed method in practice can be aimed at the following benefits:

4.1. High potential for the development of cost-effective solutions for fast evaluation of bacterial activity in solid media.

4.2. The potential for real-time tracking could revolutionise the way bacteriophage-bacterial interactions are studied, providing empirical data that could complement current experimental data and enhance mathematical models.

4.3. Faster antimicrobial susceptibility results and, therefore, if necessary, faster replacement of empiric antimicrobial therapy with pathogen-targeted therapy, which has greater potential to reduce treatment duration and costs and to reduce mortality.

5. The approach, taking into account parameter adjustment, can be used in different tasks with similar features, for example: 1) monitoring the paint drying process; 2) observation of micro-vibrations; 3) detection of microcracks in the vehicle or aircraft body and identification

of various mechanical damages; 4) non-invasive diagnosis of skin diseases; 5) assessment of blood flow dynamics; 6) detection of objects covered with a thin layer of some material that interferes with direct view; and many other applications, some of which do not yet use the speckle technique, some of which are used, but with different (less sensitive) algorithms.

6. Software implementation has been created in MATLAB.

Approbation

The results of the research were presented at the following international conferences.

1. SPIE Conference 13196, Artificial Intelligence and Image and Signal Processing for Remote Sensing XXX, Edinburgh, Great Britain, 16–19 September 2024.
2. SPIE Conference 13006, Biomedical Spectroscopy, Microscopy, and Imaging III, Strasbourg, France, 7–11 April 2024.
3. SPIE Conference 12628, Diffuse Optical Spectroscopy and Imaging IX, Munich, Germany, 25–29 June 2023.
4. 19th Nordic-Baltic Conference (NBC) on Biomedical Engineering and Medical Physics, Liepaja, Latvia, 12-13 June 2023.
5. SPIE Conference 12572, Optical Sensors, Prague, Czech Republic, 24–26 April 2023.
6. 3rd Baltic Biophysics Conference, Vilnius, Lithuania, 6–7 October 2022.
7. SPIE Conference 12144, Biomedical Spectroscopy, Microscopy, and Imaging II, Strasbourg, France, 7–11 April 2022.
8. SPIE Conference 11920, Diffuse Optical Spectroscopy and Imaging VIII, Munich, Germany, 20–25 June 2021.
9. SPIE Conference 11359, Biomedical Spectroscopy, Microscopy, and Imaging, Strasbourg, France, 6–10 April 2020.

Research results that served as the basis for the Thesis published in the scientific papers

Q1 Journal Articles

1. I. Balmages, J. Liepins, S. Zolins, D. Bliznuks, R. Broks, I. Lihacova, A. Lihachev, "Tools for classification of growing/non-growing bacterial colonies using laser speckle imaging". Frontiers in Microbiology, 14, 1279667, (2023), DOI:10.3389/fmicb.2023.1279667 (**contribution 80 %).**
2. I. Balmages, A. Reinis, S. Kistkins, D. Bliznuks, E. V. Plorina, A. Lihachev, and I. Lihacova, "Laser speckle imaging for visualization of hidden effects for early detection of antibacterial susceptibility in disc diffusion tests", Frontiers in Microbiology, 14, 1221134, (2023), DOI: 10.3389/fmicb.2023.1221134 (**contribution 80 %**).
3. I. Balmages, J. Liepins, E. T. Auzins, D. Bliznuks, E. Baranovics, I. Lihacova, and A. Lihachev, "Use of the speckle imaging subpixel correlation analysis in revealing a mechanism of microbial colony growth," Sci. Rep. 13(1), 2613, (2023), DOI: 10.1038/s41598-023-29809-0 (**contribution 80 %**).

4. I. Balmages, J. Liepins, S. Zolins, D. Bliznuks, I. Lihacova, and A. Lihachev, "Laser speckle imaging for early detection of microbial colony forming units," Biomed. Opt. Express, 12(3), pp. 1609–1620 (2021), DOI: 10.1364/BOE.416456 (**contribution 80 %**).

Conference proceedings

1. I. Balmages, A. Reinis, S. Kistkins, D. Bliznuks, A. Lihachev, I. Lihacova, "Comparison of algorithms for monitoring the behavior of microorganisms based on remote laser speckle method", Proc. SPIE 13196, Artificial Intelligence and Image and Signal Processing for Remote Sensing XXX, 1319611 (2024), https://doi.org/10.1117/12.3032500 (**contribution 50 %**).
2. I. Balmages, A. Reinis, S. Kistkins, J. Liepins, M. Pogorielov, V. Korniienko, K. Diedkova, D. Bliznuks, A. Lihachev, I. Lihacova, "Determination of operating parameters of fungal growth signals analyzed by laser speckle contrast imaging", Proc. SPIE 13006, Biomedical Spectroscopy, Microscopy, and Imaging III, (2024), DOI: 10.1117/12.3016906 (**contribution 50 %**).
3. I. Balmages, D. Bliznuks, A. Reinis, S. Kistkins, E. V. Plorina, A. Lihachev, and I. Lihacova, "Laser speckle imaging-assisted disk diffusion test for early estimation of sterile zone radius", Proc. SPIE 12628, Diffuse Optical Spectroscopy and Imaging IX, 126281Y, (2023), DOI: 10.1117/12.2670618 (**contribution 50 %**).
4. I. Lihacova, I. Balmages, A. Reinis, S. Kistkins, D. Bliznuks, E. V. Plorina, A. Lihachev, "Dynamic laser speckle imaging for fast evaluation of the antibacterial susceptibility by the disc diffusion method", 19th Nordic-Baltic Conference (NBC) on Biomedical Engineering and Medical Physics (2023), DOI: 10.1007/978-3-031-37132-5_39 (**contribution 20 %**).
5. A. Lihachev, I. Balmages, J. Liepins, I. Lihacova, D. Bliznuks, "Dynamic laser speckle imaging for estimation of microbial colony growth in a noisy environment", Proc. SPIE 12572, Optical Sensors 2023; 1257220 (2023), DOI: 10.1117/12.2675953 (**contribution 20 %**).
6. I. Balmages, J. Liepins, E. T. Auzins, A. Zile, D. Bliznuks, I. Lihacova, A. Lihachev, "Evaluation of microbial colony growth parameters by laser speckle imaging", Proc. SPIE 12144, Biomedical Spectroscopy, Microscopy, and Imaging II, 121440B (2022), DOI: 10.1117/12.2621152 (**contribution 50 %**).
7. I. Balmages, J. Liepins, D. Bliznuks, S. Zolins, I. Lihacova, A. Lihachev, "Laser speckle imaging reveals bacterial activity within colony", Proc. SPIE 11920, Diffuse Optical Spectroscopy and Imaging VIII; 1192024 (2021), DOI: 10.1117/12.2615444 (**contribution 50 %**).
8. I. Balmages, D. Bliznuks, J. Liepins, S. Zolins, and A. Lihachev, "Laser speckle time-series correlation analysis for bacteria activity detection", Proc. SPIE 11359, Biomedical Spectroscopy, Microscopy, and Imaging, 113591D (2020), DOI: 10.1117/12.2541663 (**contribution 50 %**).

The results of the Doctoral Thesis research have been used in the following projects

1. Latvian Council of Science project "Fast and non-contact optical estimation of microorganisms activity" (agreement No. lzp-2018/2-0051), 12.2018–12.2020 (employed since August 2019).
2. European Regional Development Fund project "Fast and cost-effective machine learning based system for microorganism growth analysis" (agreement No. 1.1.1.1/19/A/147) (07.2020–06.2023).
3. European Regional Development Fund project "Rapid assessment system of antibacterial resistance for patients with secondary bacterial infections" (No. 1.1.1.1/21/A/034), (2021.01–2023.11).
4. Latvian Council of Science funded project "Dynamic laser speckle imaging for evaluation of fungal growth activity" (agreement No. lzp-2022/1-0247), (2023.01–2025.12).

Structure and Content of the Thesis

The Doctoral Thesis contains an introduction, six main chapters, results analysis, and conclusions. The full Thesis is written in the form of a collection of publications with extended explanations.

The structure of the Doctoral Thesis

The **introduction** validates the topicality of the conducted investigations and formulates the object, the aim, and the research tasks. It describes the scientific novelty and practical significance.

Chapter 1 provides the literature review of non-contact optical measurement methods based on laser speckle method.

Chapter 2 provides an analysis of the development of the laser speckle correlation method and the rationale for its use in estimating submicron activity.

Chapter 3 describes the algorithm's ability to analyse bacterial colonies, with a focus on 1) early detection of bacterial colonies and monitoring growth dynamics, and 2) visualisation of differences in microbial activity over time in different parts of the colony.

Chapter 4 describes the algorithm's ability to early detect antibacterial susceptibility in disc diffusion tests.

Chapter 5 describes the ability to classify between active and inactive colonies (or zones).

Chapter 6 compares the results between the proposed method and other laser speckle methods

The Results and Conclusions chapter summarises the main contributions of this study and draws conclusions, covers the scientific and practical novelty of the Thesis, and discusses future research directions.

Relationship between aims, topics, and publications

1. Objective 1: Perform a review of existing methods for processing speckle patterns. Demonstrate the outperformance of the proposed method in the Thesis; Conference paper 1; Chapters 1 and 6.
2. Objective 2: Study of correlation analysis techniques of speckle patterns. Comparison of different algorithms, testing execution time and accuracy. Proposal and adaptation for application to low-frequency signals characterising the activity of microorganisms; Journal Article "Correlation analysis techniques of laser speckle images and rationale for its use to assess the growth and behaviour of fungi and bacteria" (in preparation process); Chapter 2.
3. Objective 3: Study of the possibility of the proposed method to perform quick and non-contact detection and assessment of submicron activity or growth of submicron objects; Journal article 4; Conference papers 2, 5, 6, and 8; Chapter 3.
4. Objective 4: Measurement of the spread speed of submicron objects or events in space. Comparison with mathematical models; Journal articles 2 and 4; Conference papers 3 and 4; Chapters 3 and 4.
5. Objective 5: Study the possibility of the proposed method to determine specific hidden phenomena and effects of certain types of submicron objects. Comparison with mathematical models; Journal Article 3; Conference paper 7; Chapter 3.
6. Objective 6: Demonstrate the ability to classify and evaluate specific submicron objects or events; Journal Articles: 1, and "Laser speckle technique for classifying between inhibition and active bacteria growth zones around the antibiotic's discs using a neural network" (in preparation process); Chapter 5.

1. LITERATURE REVIEW OF NON-CONTACT OPTICAL MEASUREMENT METHODS BASED ON LASER SPECKLE TECHNIQUE

This chapter of the Doctoral Thesis provides an overview of non-contact optical measurement methods based on the laser speckle technique. The chapter covers techniques that are most popular specifically for measuring biological phenomena.

1.1 A brief overview of the discovery and study of the speckle phenomenon

The speckle phenomenon has been investigated by many scientists since Newton, who interpreted the fact that twinkling may be observed for stars but not for planets [1]. In 1877, Exner [2,3] sketched the radially granular speckle pattern that he observed within the bright central Fraunhofer ring. In 1914, von Laue [4] published a photograph of Fraunhofer rings obtained from a plate covered with lycopodium powder, which clearly shows the radially granular structure noted by Exner. Exner explained the radial shape of the pattern because the light source used was not very monochromatic, and de Haas later confirmed this statement [5]. Von Laue [6,7] described the statistical properties of the speckle pattern found within the central Fraunhofer ring, including a derivation of the second-order probability density function and the autocorrelation function of the intensity.

The operation of the first laser in 1960 demonstrated an interesting phenomenon: objects viewed in laser light acquire a granular structure. This granularity bears no obvious relationship to the macroscopic properties of the illuminated object. It looks chaotic with an irregular pattern that is described by the methods of statistics and probability theory.

The physical origin of the observed granularity was investigated (Rigden and Gordon [8], Oliver [9]). As it turned out, the surfaces of most materials are extremely rough on the scale of an optical wavelength (about $\lambda = 500(nm)$). When monochromatic light is reflected from such a surface, the optical wave resulting at any distant point consists of many coherent components, each arising from a different microscopic element of the surface. If the surface is really rough, the distances travelled by these various components may differ by many wavelengths.

Interference of the de-phased but coherent components results in the granular pattern of intensity, which is called "laser speckle".

It was observed that for an “ideal” (aberration-free) imaging system (with a lens), the intensity at a given image point can result from the coherent addition of contributions from many independent surface areas. Thus, speckles can appear not only from free-space propagation but also in imaging systems.

Similar phenomena (speckle noise or granular noise texture) are observed in the operation of other technologies, such as synthetic aperture radar [10] and medical ultrasound [11], in photographs of stars taken at high magnification from telescopes located on Earth [12]. In these coherent imaging systems, degrading of the quality also occurs for the same reason: as a consequence of interference among wavefronts. That is, the laser speckle effect was considered as a main drawback in the use of coherent light sources. The optical speckle limits the spatial resolution and decreases the signal-to-noise ratio (SNR) of many optical techniques. Accordingly, this side effect was undesirable. However, it was later noted that the speckle can

also provide useful information. For example, for measuring surface characteristics [13,14]. It also allows the detection of dynamic changes (or motion) on the observed surface [15]. That is, the changes in the spatial speckle pattern over time can be used as a measurement of the surface's activity, such as which is useful for measuring displacement fields via digital image correlation.

Thus, laser speckle techniques are used in various optical metrology techniques, including displacement, distortion and strain measurement, surface roughness assessment, velocity measurement etc. Quite a few of these applications are used in the biomedical field.

It is worth mentioning the laser Doppler technique. This is a traditional approach to blood flow monitoring. Much laser-speckle medical research has been carried out in this field. The Laser Doppler technique can only measure from a single point with a very narrow (less than 0.1 mm3) acquisition field. Obtaining an instantaneous two-dimensional map of velocities or spatiotemporal flow dynamics in real-time is an advantage of the speckle method compared to the Doppler method [16]. This advantage gave impetus to the development and use of laser speckle techniques for medical purposes. Not only blood flow measurements.

Various techniques have been used to characterize bacterial activity in liquid and solid media, such as infrared thermography, [17] microcalorimetry, [18] flow cytometry [19] and optical coherence tomography [20]. All those techniques require expensive equipment and also a well-trained personal to carry out the experimental work. The dynamic speckle technique is simple and practical, and the analysis based on its principles requires minimal resources. Therefore, this technique has many advantages over others.

In the following subsections consider the speckle patterns mathematics and simulations and methods and parameters most popular for laser speckle techniques measurements.

1.2 Speckle patterns mathematics and simulations

1.2.1 A basic speckle pattern model

For a deep understanding of laser speckle patterns behaviour, simulation can be a promising direction and allows separate considering different processes of observed phenomena: the physics, the optical system, and data processing, to study their properties and easily make changes depending on changing environmental conditions. Dynamic events can be added to the model according to their characteristics and properties. Also, speckle patterns can be simulated in a noiseless environment (which is impossible to do in a real experiment), and then different types of noise can be evaluated for their effect on the measurement result. A preliminary understanding of what will be obtained as a result of a real experiment would allow a more precise design and a better interpretation of its results. Simulation of measurements by the laser speckle method provides such opportunities.

In the current subsection, the most well-known methods for speckle pattern simulations are considered and compared. The aim is to select a model that describes the behavior and changes in submicron activity observed using the laser speckle technique.

The speckle phenomenon results from the superposition of randomly phased elementary components and can be simulated by implementing a numerical model that sums these components on the observation plane [21]. This is the basic model from which many studies of

the speckle phenomena begin, and accordingly, it is an important step both in understanding the speckle image and in modelling it. This model can be described using equation (1.1).

$$U(x,y) = \frac{1}{\sqrt{N}} \sum_{k=1}^{N} |a_k| \cdot e^{j\phi_k} \tag{1.1}$$

where $\frac{a_k}{\sqrt{N}}$ and ϕ_k the amplitude and the phase of the kth statistically independent phasor, respectively, and U represents the phasor amplitude of the field, which is a complex-valued function of space. However, the directly observable quantity is the irradiance or intensity of a pixel belonging to a speckle pattern which is acquired with a camera:

$$I(x,y) = \lim_{T\to\infty} \frac{1}{T} \int_{-T/2}^{T/2} |U(x,y;t)|^2 dt \propto U(x,y)U^*(x,y) \tag{1.2}$$

In the next subsections, the most well-known methods for simulating static and dynamic speckle patterns will be discussed in detail.

1.2.2 Static speckle patterns simulation

The model described by equation (1.1) allows the creation of a static speckle pattern without reference to geometry. Another study allows binding to the geometry, where the coordinates of the region of interest are set [22]. The speckle pattern simulation is a summarizing of Gaussian modes on the grid with a fixed width of the Gaussian mode σ. To each of the mode is associate a random term of phase ϕ_k, (with uniform distributed: $[0-2\pi]$) with and random positions: $R_k = (x_k, y_k)$.

$$I(x,y) = \left(\sum_{k=1}^{N} e^{\frac{(x-x_k)^2+(y-y_k)^2}{2\sigma^2}} \cdot e^{j\phi_k} \right)^2 \tag{1.3}$$

where the point $R_k = (x_k, y_k)$ determines the position of the kth mode on the grid.

Another way to create objective (nonimaged) speckle patterns states that: Every point in the detector plane receives contributions from all the scattering centers in the input plane. Then, the distribution intensity at the image plane can be calculated from the Fourier transform of multiplying the light field from the object by the optical pupil function (low pass filter) [23]. The light field can be expressed as the phase in which the roughness measured of the reflected surface is included measured in wavelengths, which is proportional to the optical path also expressed in wavelengths [24]. The optical pupil function is the function which projects the light to the detectors.

$$I(x,y) = \left| FT\left(H \cdot e^{j\varphi(x,y)}\right) \right|^2 \tag{1.4}$$

where H is a circular spatial low-pass filter with radius r. A circular region produces a statistically isotropic speckle pattern. However, other patterns also may be used. FT is a Fourier transform. Fourier transforms in objective laser speckle patterns is performs the observed effect of the many-to-one mapping. (x,y) are the pixel coordinates of the detector and $\phi(x, y)$ is a phase distribution of the scattered light from the rough surface.

The pupil diameter determines the minimum size of the speckles. For example, if the ratio of the length of the screen to the diameter is 2, the Nyquist criterion is met, and the smallest speckle is two pixels wide [25].

In the case of subjective (imaged) speckle patterns, which corresponds to systems with lenses (cameras), Eq. 1.4 will look different:

$$I(x,y) = \left| FT^{-1}\left(H \cdot FT\left(e^{j\varphi(x,y)}\right)\right)\right|^2 \tag{1.5}$$

where H represents the circular aperture of the camera lens FT and $FT^{-1}$are the direct and inverse Fourier transforms, respectively.

Now compare the simulation results performed using these methods: 1) by Eq. 1.3 - the sum of the waves; 2) by Eq. 1.5 - Fourier transform. The simulation also used different speckle sizes, which were also calculated and compared with the actual values. The time of simulation for each method was also tested. Both methods provide similar patterns (Fig. 1.1). It becomes obvious that by the sum of the waves method, the implementation time is significantly longer. Although this method works with waves and their parameters, which is intuitive, for a quick implementation, one needs to choose the second method - using the Fourier transform.

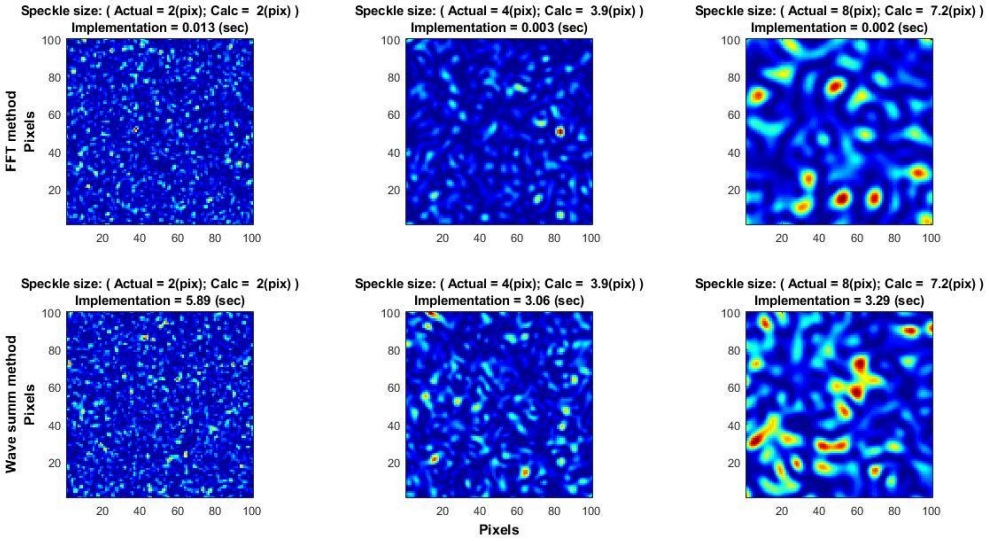

Figure 1.1. Static simulation of speckle images. Top row using the Fourier transform. The bottom row uses the sum of the waves. The speckle sizes increase from left to right: 2,4,8.

The examples discussed in this subsection refer to a static situation that does not change in time. If the observation is for time-varying events, then it is necessary to understand how "dynamic speckle" can be simulated.

1.2.3 Dynamic speckle patterns simulation

Dynamic speckle is a phenomenon that occurs when laser light is scattered by objects that exhibit some kind of activity. Activity is a situation in which the observed surface changes its properties. This may be due to the random movement of scattering centers, or a change in configuration, or a change in the optical path due to refractive index variations, or a combination of these situations. To describe the behavior of dynamic speckles in simplified situations, the following model was proposed [26]. Here, the geometry of both the reflectors' position and the screen (detectors) is fully taken into account. The dynamic process is simulated by changing

the distance between the scattering particles and the detectors. Changing the distance leads to a change in the amplitude and phase obtained in the detectors.

$$I(x,y) = \left| \sum_n \sum_m \frac{A_{n,m}}{R_{nx,my}} \cdot e^{\left(jkR_{nx,my} + \phi_{n,m} \right)} \right|^2 \tag{1.6}$$

where $A_{n,m}$ amplitude (comparing equations 1.1 and 1.6, can conclude that is should not be negative), $R_{nx,my}$ is the distance between the scattering center (n,m) and pixel (x,y), $k = \frac{2\pi}{\lambda}$ is the wavenumber, and λ is the wavelength.

That is, the authors simulated only the movement of the scatterers. The movement is added to the model as follows: In calculating the distance between the center of scattering where the activity was and the pixel of the detector, add v_{nm} - the speed of this center of scattering (equation 1.7). Thus, in the areas of activity, changes in amplitude and, most importantly, phase will be noticed.

$$R_{nx,my}(t) = R_{nx,my} + v_{nm} \tag{1.7}$$

The obtained results are in agreement with what is expected from the theory and qualitatively with the experimental results outlined in their previous works. Only a one-dimensional model was used in the [26]. It consists of a one-dimensional diffuser at some distance from a linear array detector. However, this model can be "expanded" to two-dimensional. But, as in the case of simulating formula (1.3), this simulation also will take much time.

Another approach to dynamic speckle modeling uses two-dimensional modeling [27]. If an activity occurs on a rough surface that changes the microstructure but its reflectivity is maintained constant, then some change in the optical phase due to the variation of the microtopography is added to the phase. It is assumed that changes in microstructure occur due to an alteration in the height of the scattering centers normal to the surface [28].

$$\Delta\phi_j = (2\pi/\lambda)(1+\cos(\theta))\Delta h_j \tag{1.8}$$

where $\Delta\phi_j$ the phase changes, Δh_j the alteration in the height of the scattering centers, and θ is the angle between the parallel illuminating beam and the observation direction normal to the surface.

Based on equation (1.8), to calculate the changing phase, equation (1.9) is obtained:

$$\phi(x,y,n) = \phi(x,y,n-1) + G(x,y,n)\sigma\left[\Delta\phi(x,y,n-1,n)\right] \tag{1.9}$$

where n is the frame number, σ is the standard deviation of the phase change between consecutive frames, G(x,y,n) is an N by N random matrix with Gaussian distribution, and recalculated at every frame.

Further, the formula with Fourier transform (1.4) or (1.5) (objective or subjective speckle) is used, with the difference that the changes in the phase described above occur, which create dynamics.

One more approach to dynamic speckle modelling will be covered in this subsection. The study [25] describes the process of creating continuous phase trajectories between two given limits. Since phase continuity occurs, then the evolution of the speckle pattern is also continuous.

To implement this process, two sets of statistically independent random numbers X_1, X_2 with a uniform distribution are created. With the Box–Mueller transformation from these two sets, two new sets of random variables are created, also statistically independent, but with a Gaussian distribution:

$$\begin{aligned} Y_1 &= \mu + \sigma \cdot \sqrt{-2\ln(X_1)} \cdot \cos(2\pi \cdot X_2); \\ Y_2 &= \mu + \sigma \cdot \sqrt{-2\ln(X_1)} \cdot \sin(2\pi \cdot X_2) \end{aligned} \tag{1.10}$$

The μ, σ values can be determined: $\mu = 0$, $\sigma = 1$, and the following procedure realisation:

$$\begin{vmatrix} Z_1 \\ Z_2 \end{vmatrix} = \frac{1}{\sqrt{2}} \cdot \begin{vmatrix} 1 & -1 \\ 1 & 1 \end{vmatrix} \begin{vmatrix} \sqrt{1+r} & 0 \\ 0 & \sqrt{1-r} \end{vmatrix} \begin{vmatrix} Y_1 \\ Y_2 \end{vmatrix} \tag{1.11}$$

Two sets of random numbers are obtained, which are bivariate normal with correlation coefficient r. The next step uses the percentile transformation:

$$T_1 = F_z(Z_1),\ T_2 = F_z(Z_2) \tag{1.12}$$

where normal cumulative distribution function is written as F_z.

Obtained two sets of random numbers with a uniform distribution on the unit interval. The new sets are no longer statistically independent, since they have correlation coefficient r, that gradually changes from 1 to -1. Sets T_1 and T_2 are brought into the phase:

$$\phi_n(x, y) = 2\pi T_n \tag{1.13}$$

Then 2 speckle - patterns are created using formula (1.4) or (1.5) (objective or subjective speckle).

According to [29], such a generated speckle patterns has an exponential probability density function associated with polarisation. To get speckle patterns with an arbitrary degree of polarisation, the two resulting speckle - patterns are averaged:

$$I(x, y) = \frac{I_1(x, y) \cdot (1 + p) + I_2(x, y) \cdot (1 - p)}{2} \tag{1.14}$$

where 0<p<1, is the degree of polarisation. When p=0, this is a simple average of two speckle patterns. The new probability density function becomes Rayleigh.

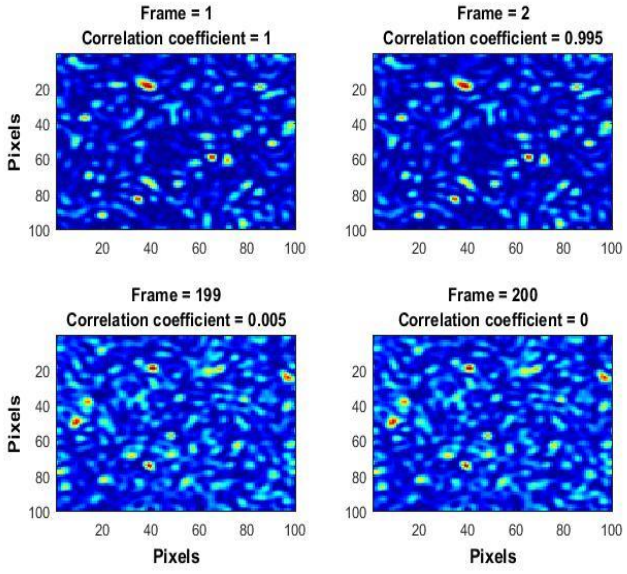

Figure 1.2. The first two frames (top) and the last two frames (bottom) in a sequence of speckle images, with a correlation coefficient smoothly changing from 1 to 0.

This behavior corresponds to a real physical process [30]. This is the main difference from the study [27], where each step in the sequence adds an increment of a statistically independent phase. Accordingly, if the phase increment is discontinuous, then the evolution of the speckle pattern sequence is also discontinuous. The speckle images generated by this method [25] change smoothly from frame to frame. The difference between each pair of consecutive frames is almost no noticeable. However, this becomes apparent when comparing frames that are temporally distant from one another in the sequence (Fig. 1.2).

Based on the models described in [25] and [27], or even a combination of them, as shown in the study [31], a series of dynamic speckle simulations studies has been performed.

Adding a contribution of the biological models of submicron activity behavior will provide a full simulation of the phenomena being studied.

1.3 The speckle size

1.3.1 Speckle size determination from system parameters

The speckle parameters like size, contrast, intensity and polarisation carry information on the scattering media. For example, the speckle size can be used to measure the roughness of a surface [32].

Therefore, it is important to know how to get these parameters. The average speckle size (diameter) in an objective speckle (nonimaged) pattern formed on a screen at a distance L by scattering of coherent light from a circular region of diameter D and wavelength λ of the laser light [33] is given by:

$$S \approx 1.2\lambda \frac{L}{D} \tag{1.15}$$

The objective speckle is created when there is no imaging lens in the system. This situation is almost non practical use in measurement. However, it helps to understand the formation of the more useful second type of speckle - subjective speckle. The subjective speckle is observed when a lens is used to create an image of an object that is illuminated by coherent light [33]. This pattern is called subjective because it is dependent on the parameters of the imaging optics used. The average speckle size, in this case, is given by:

$$S \approx 1.2\lambda(1+M)\frac{f}{\alpha} \tag{1.16}$$

where M is the magnification and $\frac{f}{\alpha}$ the F-number of the lens (focal length over aperture).

It is emphasised in [34] that although the value of S is frequently reported as the mean speckle size, this is actually an expression for the minimum speckle size. Because the speckle effect is the result of a pairwise scattering process, while the most widely spaced scatterers give rise to the smallest speckle in the pattern.

1.3.2 Speckle size calculation from experimental or simulated image

The average speckle size is estimated as the normalised autocovariance function of the intensity speckle pattern acquired in the observation plane [35].

$$c_I(x,y) = \frac{R_I(x,y) - \langle I(x,y)\rangle^2}{\langle I(x,y)^2\rangle - \langle I(x,y)\rangle^2} \tag{1.17}$$

where I(x,y) is the intensities in the observation plane (x, y), $R_I(x,y)$ the intensity autocorrelation function and $\langle\ \rangle$ corresponds to a spatial average.

The autocovariance function can be calculated using the Wiener–Khinchin theorem [36] and shown in:

$$R_I(x,y) = \langle I(x_1,y_1)I(x_2,y_2)\rangle = FT^{-1}\left[PSD_I(\nu_x,\nu_y)\right] = \\ = FT^{-1}\left[\left|FT[I((x,y)]\right|^2\right] \tag{1.18}$$

where $I(x_1,y_1), I(x_2,y_2)$ are the intensities of two points in the observation plane (x, y), FT, FT^{-1} the direct and inverse Fourier transform, and PSD - the Power Spectral Density of the intensity.

Thus, the formula for finding the normalised autocovariance function of the intensity speckle pattern can be written as follows:

$$c_I(x,y) = \frac{FT^{-1}\left[\left|FT[I((x,y)]\right|^2\right] - \langle I(x,y)\rangle^2}{\langle I(x,y)^2\rangle - \langle I(x,y)\rangle^2} \tag{1.19}$$

The average (or by [34] minimum) speckle size may be estimated by the full width at half maximum (FWHM) of the autocovariance function. Moreover, for the x-axis and the y-axis, this can be done separately.

Thus, having speckle images from experiments or simulations with a given speckle size can be tested on how much the given speckle size corresponds to the calculated. If the given speckle size is unknown, it can be calculated from the speckle image. Also, it can be useful if the speckle size can be used to measure the roughness of a surface, etc.

1.3.3 Criteria for speckle size determining

The size defined by 2 pixels/speckle is ambiguous since it is expected that each speckle has a circular shape. Study [37] assumes that it is necessary to have 4 pixels to sample a speckle with 2 pixels of diameter. That is, the speckle size should be maintained above the Nyquist criteria for both dimensions (x and y). To ensure a correct sampling of a 2-dimensional structure, at least two points should be sampled in each dimension.

On the other hand, the increase in the speckle size leads to a strong decrease in spatial resolution. First, fewer speckles are present in the same region, and second, larger processing windows must be used to ensure enough statistical relevance in the computation of the contrast.

1.4 The speckle contrast parameter

1.4.1 Relationship between motion of particles and contrast of speckle images

Another important parameter in speckle measurements is contrast. Laser speckle contrast techniques are based on the spatial and temporal statistics of the speckle pattern. The motion of particles in the illuminated medium causes fluctuations in the speckle pattern on the detector. These intensity fluctuations blur the image and reduce the contrast to an extent that is related to the speed of the illuminated (observed) objects [38].

The contrast (K) of speckle images is usually defined as the ratio between the standard deviation and the mean intensity [39].

$$K = \frac{\sigma}{\langle I \rangle} = \frac{\sqrt{\langle I^2 \rangle - \langle I \rangle^2}}{\langle I \rangle} \quad (1.20)$$

where <I> is the spatial mean intensity and σ is the spatial standard deviation of intensity. In ideal conditions (using a completely coherent and polarised light source), the resulting speckle pattern is fully developed, which means that speckles are perfectly defined. For a fully developed speckle pattern, there is equality between its spatial standard deviation (σ) and its spatial average intensity <I> [40]. That is, the contrast of an ideal speckle pattern is equal to 1 (for example, a static speckle pattern under ideal conditions). However, in a real situation, the contrast is lower than 1 and follows the condition $0 \leq K \leq 1$ [41]. The lower values of K correspond to more intense dynamic changes in the observed medium. This is explained by the fact that as the object moves, the speckle pattern will be blurred, and the standard deviation of the intensity will be small compared to the unchanged mean intensity, resulting in reduced speckle contrast.

This property of the speckle interference effect is useful for its application in the biomedical field [42].

1.4.2 Relationship between contrast, exposure time and decorrelation time

The temporal fluctuations of the intensity of the speckle contain information concerning the dynamic properties of the medium. These intensity fluctuations are produced by electric field changes caused by the light scattered by moving particles. The normalised temporal autocorrelation function of the electric field is used to analyse these fluctuations [43]:

$$g_1(\tau) = \frac{\langle E(t)E^*(t+\tau) \rangle}{\langle E(t)E^*(t) \rangle} \quad (1.21)$$

where E(t) is the electric field over time t, E^* denotes the complex conjugate of the electric field, τ the autocorrelation delay time and < > the time average. This is the first-order autocorrelation function. However, imaging systems obtain not an electric field but intensity. Therefore, for analysis used signal information as the normalised temporal autocorrelation function of the intensity (the second-order correlation function) [44]:

$$g_2(\tau) = \frac{\langle I(t)I(t+\tau) \rangle}{\langle I(t)^2 \rangle} \quad (1.22)$$

The relation (Siegert relation) between these two functions is known [45]:

$$g_2(\tau) = 1 + \beta |g_1(\tau)|^2 \quad (1.23)$$

where $\beta \leq 1$ is a number that takes into account the absence of light stability and is determined by the ratio of detector size to speckle spot size (if do not follow the correct ratio, (Nyquist condition) can get the speckle averaging due to spatial aliasing in the image detector) [46].

That is, for the analysis is to measure $g_2(\tau)$ and to extract $g_1(\tau)$ using Eq. (1.23). Subsequent connection is then to be made between $g_1(\tau)$ and scattering site dynamics, depending on details of the illumination and detection geometry and on the optical properties of the sample.

From the definition of the correlation functions, it can be assumed stationarity:

$$g_2(\tau) = 1 + \frac{C_t^{(2)}}{\langle I \rangle_t{}^2} \quad (1.24)$$

where $C_t^{(2)}$ is the autocovariance of the temporal fluctuations in the intensity of a single speckle:

$$C_t^{(2)} = \langle (I(t) - \langle I \rangle_t)(I(t+\tau) - \langle I \rangle_t) \rangle_t \quad (1.25)$$

From equations (1.23) and (1.24) it can be obtained:

$$C_t^{(2)} = \langle I \rangle_t{}^2 * \beta |g_1(\tau)|^2 \quad (1.26)$$

For random motion of the scatterers, the speckle pattern will decorrelate in time but will not drift. Accordingly, using Goodman's result [40], the spatial variance in a time-averaged speckle pattern is given by:

$$\sigma_s^2 = \frac{1}{T}\int_0^T C_t^{(2)}(\tau)d\tau \quad (1.27)$$

where T is the exposure time (integration time). Substituting equation (1.26) into (1.27) can be obtained:

$$K(T) = \frac{\sigma_s}{\langle I\rangle_s} = \left(\frac{\beta}{T}\int_0^T |g_1(\tau)|^2 d\tau\right)^{1/2} \quad (1.28)$$

where K(T) is the speckle contrast as function of the exposure time (T) of the used imaging system. The original study [47] assumed that $\beta = 1$.

This equation show the relationship between speckle contrast and the normalized temporal autocorrelation function of the electric field (or normalized temporal autocorrelation function of the intensity). This approach [48] allows to measure the differences between a pair of successive speckle images as a simpler alternative to the measurement of the complete autocorrelation function of fluctuating speckle. That is allows to use it in many studies and systems developments.

A number of authors argue that for a correct expression and to obtain accurate results in Eq (1.28), it is necessary to multiply by term 2*(1−τ /T) [16,49,50]:

$$K(T) = \left(\frac{2\beta}{T}\int_0^T |g_1(\tau)|^2 \left(1-\frac{\tau}{T}\right) d\tau\right)^{1/2} \quad (1.29)$$

This term falls from the transformation of the variance into the correlation, where a triangular weighting must be multiplied by the autocorrelation function [51].

1.4.3 Speckle contrast measurement techniques

The laser speckle contrast methods can be classified into three categories: spatial contrast, temporal contrast, and, a combination of both, spatio-temporal [52].

1) The spatial contrast consists in computing the contrast in a small spatial window (NxN pixels) of the laser speckle raw image. where N = not a large number of pixels (3,5,7,...). The spatial contrast calculation moved along the x and y directions. The window displacement is often used without overlapping. In the study [52], this particular method is called Laser speckle contrast analysis (LASCA).

The larger the window, (the processing area), the better the contrast estimation. However, the increase of the window size causes a decrease in the spatial resolution of the contrast images and, therefore, of the contrast map.

To select a correct window size, it is necessary to take into account the speckle size present in the raw images. The window size should be proportional to the speckle size to estimate the contrast in a statistically relevant number of speckles. Consequently, when the value of pixels/speckle is high, the larger window should be used.

2) In order to improve the spatial resolution study [53] propose the temporal contrast technique. The temporal contrast is calculated by using a set of statistically independent frames. These frames can only be consecutive when the interframe times (Δt) is large enough that is not occur in high-speed systems [54]. In the study [52], this method is called Laser Speckle Imaging (LSI) or also Laser Speckle Temporal Contrast Analysis (LSTCA). Cases: a) no dynamic speckle pattern and b) complete blurred dynamic speckle pattern give a contrast equal to 0. This makes LSI unsuitable for samples with regions where dynamic speckle patterns are not present.

3) A combination of both spatial and temporal algorithms can be applied to compute the speckle contrast [55]. The used window is usually a cuboid. This window is displaced in the spatial and temporal dimensions.

1.4.4 Decorrelation of time-varying speckle

When an object moves, the speckle pattern it produces changes. For small movements of a solid object, the speckles move with the object, i.e. they remain correlated; for larger motions, they decorrelate and the speckle pattern changes completely. Decorrelation also occurs when the light is scattered from a large number of individual moving scatterers, such as particles in a ~~fluid~~ media. An individual speckle appears to 'twinkle' like a star. Time-varying speckles are frequently observed when biological samples are observed under laser-light illumination.

For each pixel n of a speckle image with N pixels, in a sequence consisting of K images with exposure time t_e and time interval between images δt, the temporal normalized autocorrelation intensity function can be calculated as [56]:

$$C(n,k) = \frac{1}{K-k}\sum_{i=1}^{K-k}\frac{I_n(t_i)I_n(t_i+k)}{\bar{I}_n^2} \tag{1.30}$$

where k is the lag time, $I_n(t_i)$ the intensity of pixel n at time t_i and $\bar{I}_n$ the temporally averaged intensity of pixel n. The minimum lag time is given by $k_{min} = \delta t + t_e$.

The temporal autocorrelation intensity function $C(n,k)$ (Eq. 1.30) obtained from substituting (Eq. 1.25) into (Eq. 1.24), for $g_2(\tau) - 1$. For more accurate observation of decorrelation caused by dynamic events, studies [56] operate not on every each pixel individually, but on the averaging speckle of the image (or sections of it) over pixels:

$$C(\tau) = \frac{1}{N}\sum_{n=1}^{N} C(n,k) \tag{1.31}$$

A similar, but with several differences approach (decorrelation analysis) is also used in many studies. Study [30] claim that the statistical properties of a limited sample of a random process differ from their theoretical prediction. Consequently, the intensity correlation formula (Eq.1.22) of $g_2(\tau)$ must be modified in order to take into account the finite number of samples to be used, and after mathematical derivation and normalization, the following formula was obtained:

$$C_t(k*\delta t,x,y) = \frac{\langle I(t,x,y)I(t+k*\delta t)\rangle - \langle I(t,x,y)\rangle\langle I(t+k*\delta t)\rangle}{\sqrt{[\langle I^2(t,x,y)\rangle - \langle I(t,x,y)\rangle^2][\langle I^2(t+k*\delta t,x,y)\rangle - \langle I(t+k*\delta t,x,y)\rangle^2]}} \tag{1.32}$$

where x and y are the pixel positions in the image, k is the frame number, δt is the time interval between two adjacent frames (time step). A series of the acquired speckle images are analyzed using the first speckle frame as a template with subsequent images. This expression is used in many studies for decorrelation time or rate analysis [57,58].

Thus, there is a relationship between spatial contrast and temporal autocorrelation intensity function. As mentioned above, when observing dynamic events, the contrast decreases. In this case, the temporal autocorrelation function of the intensity also decreases.

One of the important parameters of the correlation function is the decorrelation time. Decorrelation time is the time during which the correlation between the original image and the subsequently acquired images is reduced to 50 % (up to 0.5). For biological specimens, study [30] proposes to use (1/e = 0.368).

1.4.5 Velocity of scattering particles

This subsection mentions attempts to calculate the speed of scattering particles using decorrelation time. Potentially, this approach could become a useful tool for working with microorganisms.

In study [59], using the fact that coherence time is the time duration over which signals have a strong potential for amplitude correlation, uses the coherence time formula to find correlation time (Eq. 1.33):

$$\tau_c = \frac{\overline{\lambda}^2}{(c*\delta\lambda)} \tag{1.33}$$

where $\delta\lambda$ is wavelength spread > 0.1 (nm) and a mean wavelength $\delta\lambda$ ~ 600-800 (nm), c - speed of light. This yields a coherence time of $10^{-12} - 10^{-11}$sec. For T~1 ms, T/τ_c is > 10^9. Based on the fact that this is a large number, the study [59] demonstrates that for both cases described by formulas 1.28 and 1.29 can obtain the relation (Eq. 1.34):

$$\frac{1}{K^2} = n * \frac{T}{\tau_c} \tag{1.34}$$

where τ_c is the correlation time, T is the camera exposure time, T/τ_c is the flow index and is proportional to the mean velocity V [60], and n is the constant that determines the difference between formulas 1.28 and 1.29. Accordingly, the $\frac{1}{K^2}$ parameter can be used for an approximate estimation of T/τ_c.

A number of studies believe that (under some statistical assumption) there is a relation between the decorrelation time of speckles and the speed of observed scattering particles [46]:

$$V = \frac{\lambda}{2\pi\tau_c} \tag{1.35}$$

That is, the relationship between decorrelation time and velocity is inverse. Accordingly, a small value of the contrast (that corresponds with a small τc) means that speckles move quickly (high velocity). In the case when contrast is close to unity (that corresponds to a large τc value), the speed is low. That is, this is an almost stationary speckle pattern. In this way, the $\frac{1}{K^2}$ parameter can be considered a parameter showing the absolute velocity of moving particles. Accordingly, the exact determination of the speckle decorrelation time is required, which is not so simple.

It is also worth mentioning that the study [61] demonstrates that the concentration of scattering particles influences the relationship between the contrast value K and the speed of moving particles in the low concentration range.

Although several studies believe that the $\frac{1}{\tau_c}$ ratio is a useful indicator of velocity (V), in other studies, the linearity between the scatterer speed and $\frac{1}{\tau_c}$ has been questioned. Accordingly, velocity values are not often used in laser speckle studies because it have not yet been proven to be a quantitative tool for complex systems [39]. For this reason, the current study will not cover this topic, but it is worth emphasising that such studies are being conducted.

1.4.6 Dynamic and static scatterers.

One of the factors that complicates the use of Laser speckle contrast imaging (LSCI) as a quantitative technique is the effect of static scatterers. In some situations, the dynamic events that need to be measured are covered by some static, massive object (for example: imaging of local changes in cerebral blood flow through a mouse skull). It is necessary to determine how

the effects of static and dynamic scatterer concentrations separately affect the correlation and contrast of laser speckles. The influence is a static object covering the measured object on the laser speckle signal has been quantitatively addressed [50]. The quantitative interpretation of the acquired data is not straightforward for the common case of a speckle field formed by both by moving and localised scatterers. Study [62], without modifications of the typical laser speckle contrast analysis (LASCA) experimental settings and image acquisition procedure, proposes a processing algorithm which takes into account the effect of static contribution on the optical signal and thus allows for a correct computation of dynamic events.

Another example of the influence of static scatterers can be observed when performing a microcirculation assessment, where the tissues are low vascularised, for example, the forearm [63]. There containing high concentrations of static scatterers, which influence the blood flow evaluation.

Consequently, there was a need to take into account the effect of "static scatterers" and understand where and how to use this technique.

The static speckles influence is proposed to be calculated using cross-correlating between two consecutive speckle images. To do this, the following condition must be met: the time interval between successive frames is larger than the exposure time, and the exposure time is larger than the intensity correlation time. In this case, there are no correlations of the dynamic speckles between successive frames. This means that two speckle patterns detected in two sequential frames are correlated only due to the presence of static speckles. After calculating the influence of static parameters, it is possible to obtain the contribution only of dynamic. The suppressing contributions of non-uniformly distributed specular reflections obtained is also an advantage of the proposed method.

In investigating the changes in concentrations of static and dynamic scatterers, the study [64] demonstrated that the laser speckle correlation could be used to estimate the relative concentration of static/dynamic scatterers within a sample. The authors also claim that speckle correlation is independent of the dynamic scatterer velocity, which is a fundamental characteristic to be used in contrast correction.

The Siegert relation is only valid if the light electric field is a random Gaussian variable [65]. This relation has been applied to both ordered flow [44, 50] and Brownian motion [42, 66]. The study [67] describes the two statistical models used for ordered flow (Gaussian) and Brownian motion (Lorentzian).

The original LSCI theory [47] has been improved, and the correction factor (ρ) has been included in the field autocorrelation function as a way to estimate the fraction of static scatterers present in the sample. In the study [62] value of the correction factor was determined as:

$$\rho = \frac{\langle I_s \rangle}{\langle I_s \rangle + \langle I_d \rangle} \tag{1.36}$$

where $\langle I_s \rangle$ represents the average light intensity scattered by the static scatterers, and $\langle I_d \rangle$ the average light intensity scattered by dynamic scatterers.

Accordingly, the field autocorrelation function will be separated into two parts: for the dynamic scatterers $g_{1d}(\tau)$ and for the static scatterers $g_{1s}(\tau)$ [16]. Static scatterers will generate a constant speckle signal over time. The static autocorrelation function independent of τ, and between consecutive patterns is equal to 1 [68]. Thus $g_{1s}(\tau) = 1$. The correlation function of the mixed field and of the mixed intensity can be written as in Eq. (1.37) and (1.38) respectively:

$$g_1(\tau) = (1 - \rho)|g_{1d}(\tau)| + \rho \tag{1.37}$$

$$g_2(\tau) = 1 + \beta|(1-\rho)|g_{1d}(\tau)| + \rho|^2 \quad (1.38)$$

The contrast of both static and dynamic speckles is a substituting Eq. (1.37) into Eq. (1.29):

$$K(T) = \left(\frac{2\beta}{T}\int_0^T |(1-\rho)|g_{1d}(\tau)| + \rho|^2 \left(1-\frac{\tau}{T}\right) d\tau\right)^{\frac{1}{2}} = ((1-\rho)^2 K_{2d}^2 + 2\rho(1-\rho)K_{1d}^2 + \beta\rho^2)^{\frac{1}{2}} = (K_{12d}^2 + \beta\rho^2)^{\frac{1}{2}} \quad (1.39)$$

where the K_{1d} and K_{2d} represent the contrast of the dynamic field and the dynamic intensity respectively, and K_{12d} is a mixed (total) dynamic part of the contrast.

This function cannot be solved quantitatively. When the time interval between successive frames is much larger than the scatterers' decorrelation time, the dynamic autocorrelation function becomes close to zero $g_{1d}(\tau) \approx 0$. Then from Eq. (1.38) is obtained only static contribution:

$$g_2(\delta t) = 1 + \beta\rho^2 \quad (1.40)$$

where δt the time interval between successive frames.

Next, Eq. 1.40 allows to estimate of the static contribution from two sequential images $I_1(x_i)$ and $I_2(x_i)$ with i =1...N over a chosen area containing N pixel.

$$\rho = \frac{1}{\beta^{\frac{1}{2}}}(g_2(\delta t) - 1)^{\frac{1}{2}} = \frac{1}{\beta^{\frac{1}{2}}}\left(\frac{\langle I_1 I_2\rangle}{\langle I_1\rangle\langle I_2\rangle} - 1\right) = \frac{1}{\beta^{\frac{1}{2}}}\left(\frac{\frac{1}{N}\sum_{i=1}^{N}(I_1(x_i) * I_2(x_i))}{\langle I_1\rangle\langle I_2\rangle} - 1\right) \quad (1.41)$$

It should be noted that this method is only valid when the time interval between two successive speckle images is much longer than the expected decorrelation time.

The contrast is obtained using Eq.1.20 for the same selected area containing N pixels. Knowing ρ and contrast, the mixed (total) dynamic contrast K_{12d} from Eq. 1.39 can be obtained as:

$$K_{12d} = (K^2 - \beta\rho^2)^{\frac{1}{2}} \quad (1.42)$$

Then the correlation time witch corresponding to mixed (total) dynamic contrast is found.

The increase of static scattered light produces an increase in the decorrelation time (contrast increase) of the speckle pattern [50, 69]. An increase of the dynamic scattered light leads to a decrease of the decorrelation time, (contrast decrease). In fact, it is the relation between the light scattered from dynamic and static scatterers that defines the ρ value. Therefore, correlation is used to estimate the amount of light reflected by static and dynamic diffusers.

As already mentioned, this approach is used to measure cerebral blood flow through the skull of an animal (blood flow is a dynamic object, the skull is static). For laser speckle contrast analysis to measure the behavior of microorganisms on a Petri dish, this approach could also provide additional benefit by treating the dish as a static object and the microorganisms as dynamic.

1.4.7 The exposure time

As has been noticed throughout the current chapter, an important parameter is the exposure time of the camera. The changing speckle pattern is recorded with a camera that has an exposure time in the order of the speckle decorrelation time. Due to the long exposure time compared to the typical decorrelation time of the speckle pattern, the speckle pattern will be blurred in the recorded image. The level of blurring is quantified by the speckle contrast.

Different exposure times are sensitive to different scatterers' velocities. For example, shorter exposure times are more suitable to analyse fast-moving scatterers [70]. At short exposure times, only rapid movements will cause blurring.

The detector used has a finite integration time. If this integration time is long compared with the correlation time of the speckle fluctuations, the intensity fluctuations are averaged out, and a constant intensity is recorded. At shorter integration times, the modulation depth depends on the integration time and on the velocity of the scatterers. Hence, the depth of modulation of time-integrated speckle as a function of integration time contains information about the velocity of the scatterers [71], and the integration time can be used as an additional degree of freedom.

1.5 Frequency analysis of time-varying speckle

Studies [72-73] showed that the velocity is proportional to the mean frequency of the fluctuations and that this, in turn, is proportional to the root mean square of the time-differentiated intensity.

A study [74] demonstrated that the gradient of the power spectral distribution, conveniently expressed as the ratio of the high-frequency component to the low-frequency component, is an indicator of the mean velocity. They used band-pass filters to facilitate the calculation of this ratio and applied the technique to measure blood flow in the skin. However study [75] showed that this approach was not always applicable, and the mean frequency of the oscillations was used as the velocity indicator instead. The mean frequency was also used in later work on blood flow in the retina and choroid of rabbits.

However, the advantages of using the simpler parameters, the standard deviation of the intensity fluctuations and intensity (which allows speckle contrast analysis), are obvious.

In newer studies [76], using proven techniques, part of the calculations are performed in the frequency domain, which provides certain benefits.

Another notable recent study proposes a rapid, phenotype-based antibacterial susceptibility testing method for predicting the minimum inhibitory concentration (MIC) of antibiotics for *Escherichia coli* bacteria [77]. Measurements in this study were conducted periodically during the experiment, with each measurement lasting 10 seconds and a sampling frequency of 50 Hz. Each 10-second dataset was processed as follows: the raw speckle images were decreased by a factor of 10 along both spatial axes using the nearest neighbor method. A Fourier Transform was applied along the time axis of the resulting data array. Taking into account that spectral intensity distributions with significant high-frequency content generally correspond to more active motion, only the spectral intensity (excluding phase information) was utilised for analysis. To prepare the data, the DC term in each individual pixel spectrum was normalised to 1 and subsequently removed. The processed dataset was then used as input for a machine learning classifier.

Although this dataset was not directly employed for analysis in the study [77] (only as input for a machine learning classifier), it has the potential to provide valuable additional information. Therefore, the current study will take advantage of working not only in the time domain but also in the frequency domain and time-frequency domain. In aims to achieve more higher performance this technique will be implemented differently and will be discussed in the following chapters.

1.6 Chapter conclusions

In this chapter, speckle patterns mathematics and simulations and also speckle patterns parameters for the dynamic events analysis (suitable also for the medical/biological field) were considered. There is a relationship between all of them with correlation analysis. Thus, it becomes clear that correlation analysis is an important, powerful and promising tool for analysing speckle patterns (also in the medical/biological field). The next chapter will consider the development of correlation analysis of laser speckle images and the rationale for its use for submicron activity evaluation.

2. A REVIEW OF THE DEVELOPMENT OF CORRELATION ANALYSIS OF LASER SPECKLE IMAGES AND THE RATIONALE FOR ITS USE FOR SUBMICRON ACTIVITY EVALUATION

Based on the posed aim and tasks, the second chapter of the Doctoral Thesis performs an overview of the development of correlation analysis (signal processing algorithms with high sensitivity) of laser speckle images and the rationale for its use for microbiological data and submicron activity evaluation as a research object.

2.1 Introduction to the chapter

One of the frequently used approaches in speckle measurements is contrast analysis. Studies [40,47] show the relationship between speckle contrast and the normalised temporal autocorrelation function of the electric field (or normalised temporal autocorrelation function of the intensity). Contrast analysis allows the measurement of the differences between a pair of successive speckle images as a simpler alternative to the measurement of the complete autocorrelation function of fluctuating speckles [48]. However, there are differences between contrast analysis and correlation analysis. Correlation analysis can provide more accurate information about displacements, allowing more sensitive monitoring of moving dynamic events or objects.

Correlation algorithms have found wide application in mechanics, acoustics, and to a much lesser extent in microbiology. In the current chapter, the evolution of correlation analysis techniques of laser speckle images will be reviewed. Approaches will also be proposed and provide a rationale for their use in assessing of fungal and bacterial growth and behavior.

2.2 Speckle-displacement measurement

The first computer based digital image speckle correlation system was presented in the early 1980s for the analysis of mechanical deformations [78,79]. In applications of experimental mechanics, in cases where the wanted deformation field tends to be hidden by the larger, rigid body motion and is difficult to distinguish, the speckle correlation method makes it possible to determine small deformations even with overlaying large, rigid body motions. Images before and after deformation are on different frames.

The image before deformation is - the reference image, and the image after deformation - is the displaced image. The images are divided into small sub-images. In order for a small sub-image to indicate its position (displacement), a pattern has to be completely random, be of a high contrast and high frequent. A laser speckle pattern is a good example of such a characteristic pattern. If the changes between reference and deformed sub-images are very large, the similarity between them is not great, resulting in a low signal-to-noise ratio.

The size of these sub-images determines the spatial resolution of the final result. Too large sub-image - low spatial resolution. Too small sub-image can lead to difficulty matching images (low correlation between them).

The cross-correlation algorithm compares the sub-images (from the reference and shifted images) and finds a displacement for each of the sub-images (Eq. 2.1).

$$CC(u,v) = \sum_x \sum_y ((a(x,y)) * (b(x-u, y-v))) \quad (2.1)$$

where *a(x,y)* and *b(x,y)* are two frames (before and after deformation), u and v are spatial displacements between two frames in the directions of x and y, respectively.

The displacement between sub-images occurs and is measured in two directions, x and y, respectively. The height of the correlation peak determines the accuracy of the measurement. The accuracy of correlation decreases with increased speckle size and increased speckle decorrelation. To obtain a more accurate result, interpolation around the peak is performed. Interpolation methods can be different: parabolic, gaussian, etc. [80]. Or, as discussed in [81], subpixel accuracy is obtained by a Fourier series expansion around the cross-correlation peak. This method gives a sharper correlation peak and, therefore, may provide a better estimate of true sub-pixel displacement than parabolic interpolation.

Fig. 2.1 shows the displacement field resulting from the simulated mechanical shift. In order to compare how a simple shift differs from the behavior of fungi, a similar analysis was performed with real experiments with the *Candida albicans* fungi (Fig. 2.2). Fungal behave chaotically.

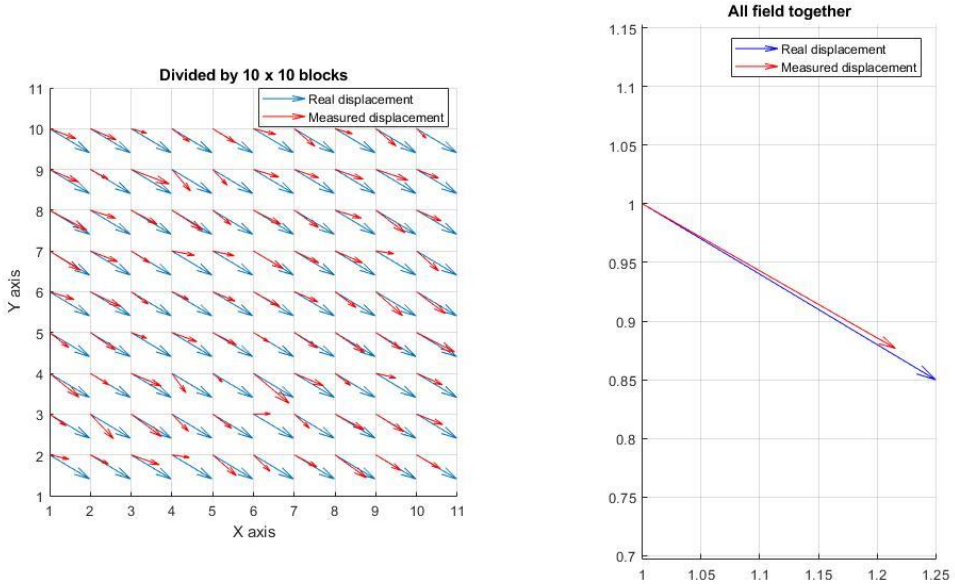

Figure 2.1. Simulation of mechanical shift or deformation. On the left side, the displacement field of the 100 by 100 pixels speckle image is divided into blocks of 10 by 10 pixels (100 blocks); on the right side, the analysis was performed on the entire image at once.

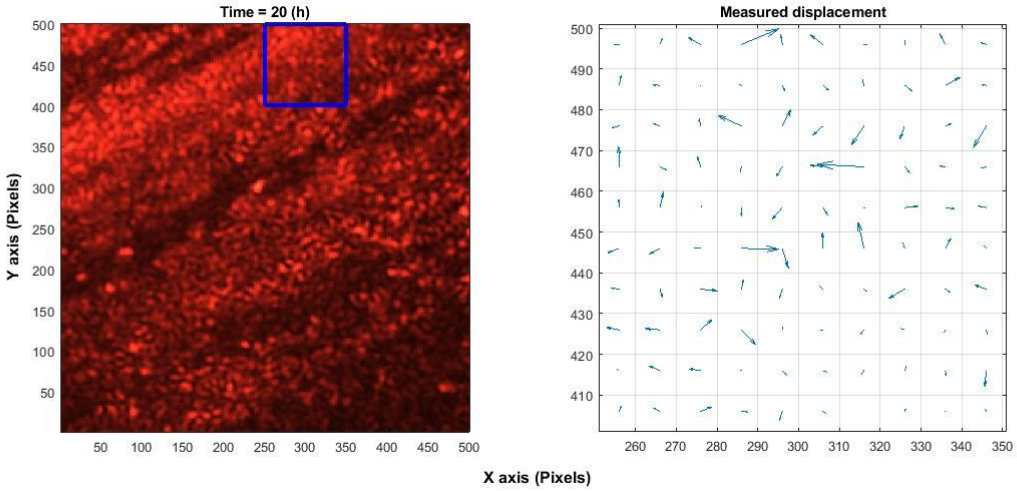

Figure 2.2. Experiment with fungi *Candida albicans*. On the right is a speckle image for a time of 20 hours from the experiment beginning. A square of 100 by 100 pixels is highlighted in blue. Left - displacement field between two frames (1 second). A speckle image of 100 by 100 pixels is divided into blocks of 10 by 10 pixels (100 blocks).

A similar method to measure displacements of speckle patterns but in the frequency domain was also proposed [81,82]. In [82], it is proposed to normalise the cross-correlation. In subsequent works, the Zero mean Normalized Cross-Correlation is used. The reasons will be discussed in the subsections 2.6.

Thus, by comparing the speckle image before and after the deformation, the cross-correlation method is used to construct (and analyse) the spatial displacement field caused by this deformation.

It is also worth noting that the width of the correlation peak is twice the width of the speckle size in the image [34]. This can lead to errors in estimating displacement using cross-correlation analysis.

2.3 Signal reconstruction by zero mean normalised cross-correlation between images

Influenced by the method for detecting mechanical deformations described in the previous subsection, another method has been developed for detecting vibrations caused by acoustic signals and reconstructing audio signals, which will be described in the current chapter.

Verification and comparison of six different algorithms for speech reconstruction based on laser speckle Images [83] showed that the cross-correlation method is one of the best options for this purpose.

Changes that, as a result of the influence of the appearance of a signal, can be decomposed into three components: transverse, axial and tilt movements. With a strong defocusing of speckle images, only the tilt movement significantly affects the shift between successive speckle images. The influence of the other two movements on the shape and displacement can

be ignored [84]. It has also been demonstrated [84] that in laser speckle processed audio signals under appropriate conditions, there is only speckle movement between speckle images (frames) but no shape change. That is, the difference between two successive images will be expressed as displacements in the plane (xy). These displacements can be detected. In the first (reference) image, a template (NxN pixels) is selected, or several different templates. By zero mean normalised cross-correlation (Eq. 2.2), a larger area is scanned in the next-in-time ("deformed") image to locate the template position and determine the displacement.

$$ZNCC(u,v) = \frac{\sum_x \sum_y ((a(x,y)-\overline{a})*(b(x-u,y-v)-\overline{b}))}{\sqrt{\sum_x \sum_y (a(x,y)-\overline{a})^2 * \sum_x \sum_y (b(x-u,y-v)-\overline{b})^2}} \quad (2.2)$$

where *a(x,y)* is a part of the first (template) frame and *b(x,y)* part of the next frames in a sequence, $\overline{a}$ and $\overline{b}$ are the average values of these frame parts.

Interpolation is performed around the correlation peak to detect a more accurate (sub-pixels) displacement. This procedure is carried out with every speckle image until the end of the experiment [85,86]. Thus, the displacement value is calculated between the template image and each subsequent image. Depending on the external influence, these displacements can be of different values and positively and negatively directed. By sequentially inserting all these displacements into the array, from the first to the last, a signal is obtained whose values change (displacements are positive and negative). This signal can also be considered in the frequency domain. Accordingly, the audio signal will be reconstructed from a sequence of laser speckle images. To illustrate the algorithm's performance, different signals, such as speech, noise, etc., can be selected. However, since speech or noise are random processes, for a more pronounced demonstration, it is worth using a deterministic signal, for example, sine, pulses, or linear sweep. Then the difference is visible both in the time and frequency domains.

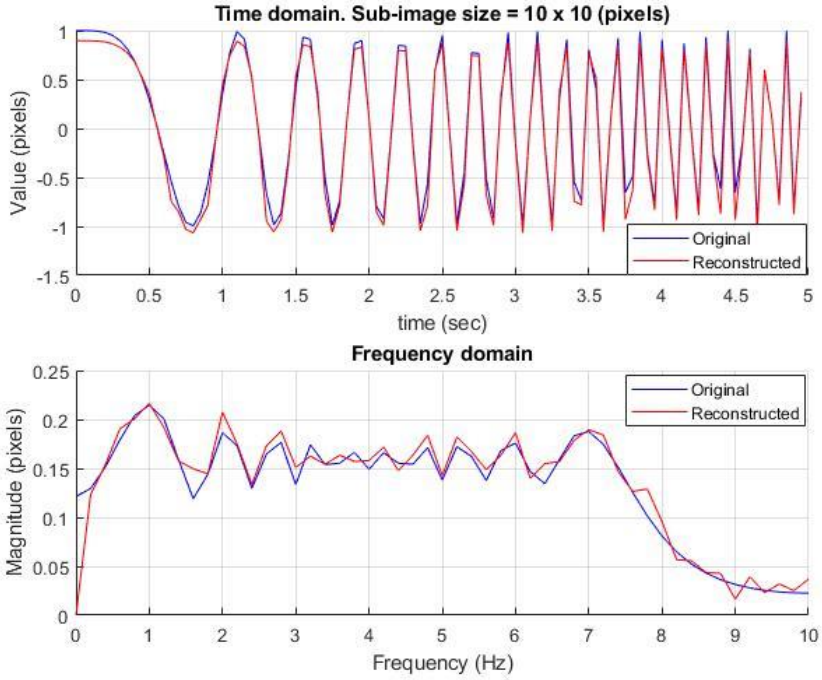

Figure 2.3 Reconstruction of the simulated acoustic signal from speckle images. Signal parameters: linear sweep, frequency increase: 0-8 Hz during 4.95 sec, Fs = 20 Hz, time between consecutive frames 50 msec. Top subplot – time domain, bottom – frequency domain

Fig. 2.3 shows the result of the reconstruction of the simulated acoustic signal (linear sweep, frequency increase: 0-8 Hz during 4.95 sec, Fs = 20 Hz, time between consecutive frames 50 msec). The template is taken from the first frame. All calculations are made in relation to it.

2.4 Temporal decorrelation effect

In the previous two subsections, have been described detection methods that, based on spatial cross-correlation, allow the detection of displacement. This subsection will use the temporal and spatiotemporal correlation to detect changes in the specimen's behavior over time.

Another common method of laser speckle correlation technique is measuring the time or rate of decorrelation. This technique is often used in applying the laser speckle method in medicine and microbiology for monitoring processes related to the movement of the particles. The method is considered to be non-destructive. When a laser light illuminates the biological material, usually light can penetrate into tissue and backscattered or from the surface or by internal inhomogeneity. In addition, living material is not stable in space and in time, so the speckle pattern has a dynamic component. A study [52] suggested that this dynamic behavior is caused by Doppler shifts of the light that interacts with the moving particles. The speckle's activity can provide information about various living processes occurring inside a cell.

Two approaches to obtaining decorrelation times are described in the literature. It was described in Chapter 1, equations 1.30-1.31 and equations 1.32, respectively.

Decorrelation curves for different biological species differed from each other. The shape of the decorrelation curve characterises the biological activity of the different samples. Thus, the correlation coefficients can be used as an analysis tool for the temporal behavior of biological samples.

The study [57] describes correlation analysis for assessing fruit quality (by temporal degradation of a correlation peak). Decorrelation curves of botanical specimens were found to change with different speeds subject to conditions of their freshness, moisture and preservation.

In a study [87], a similar analysis was used for measuring an index of atherosclerotic plaque viscoelasticity. The method can provide important information about plaque rupture.

This method is used to measure the behavior of other biological organisms and assess changes in bacterial activity [88]. Measuring the dynamic speckle patterns from specimen enables the detection of living microorganisms present. By decorrelation curves of laser speckle patterns from tissues, the living activities of microorganisms can be detected.

Specimen with living microorganisms (due to their spontaneous movements) have a shorter correlation time than those without microorganisms.

The presence and activity of microorganisms can be quantitatively analysed by measuring the decorrelation time of scattered light from samples.

For an agar dish with microorganism colonies, the correlation value significantly decreased over time. Considering a dish without colonies, the correlation value theoretically should remain constant, but in reality, it also decreased, albeit slowly. This occurs due to mechanical instability of the optical system, water evaporation and other factors. Thus, laser speckle decorrelation is proportional to microorganisms' activity and concentration.

A study [88] also demonstrated that ultraviolet (UV) light radiation, due to its antibacterial effects [89,90] can be used for sterilization of specimen with high concentration of bacteria.

After a longer UV radiation period, correlation values become high, which is interpreted as suppression of the bacterial activity.

It is worth noting that this method is sensitive to external vibrations. When some vibration in the system occurs, a large decorrelation is detected.

Fig. 2.4 shows the change in the value of the zero mean normalised cross-correlation over time between the 1st frame and subsequent frames in 2 cases: 1) without bacteria and 2) with S. aureus bacteria.

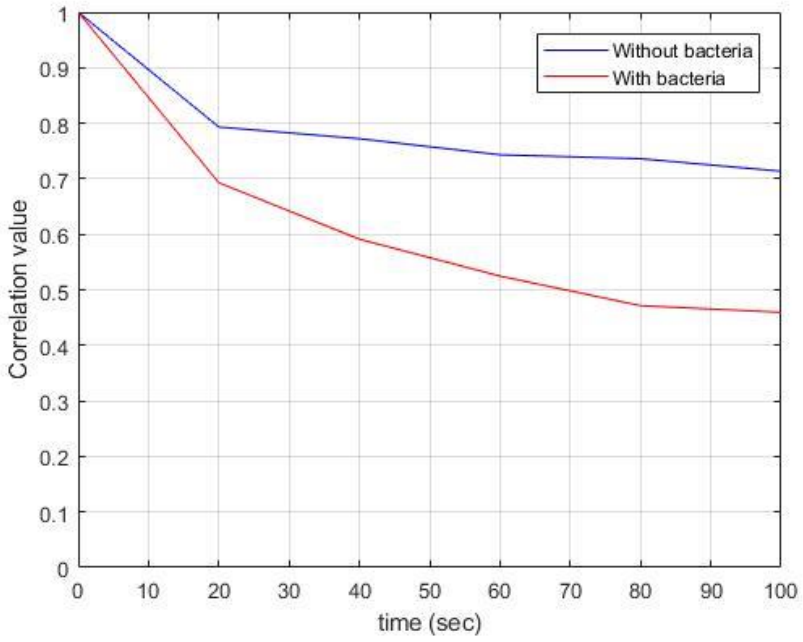

Figure 2.4 change in the value of the zero mean normalized cross-correlation over time between the 1st frame and subsequent frames in 2 cases: 1) without bacteria (blue) and 2) with S. aureus bacteria (red)

2.5 Sequence of laser speckle images of microorganisms activity converted into time signals

Having considered and analysed the methods described in the previous subsections, to study the activity of microorganisms, is was decided to use a technique similar to the reconstruction of an acoustic signal (subsection 2.3). That is to convert speckle - images into signals. Thus, the received reconstructed signals will correspond to the measurement as if made by a sensitive to micro-vibrations sensor.

The difference between the method that will be used in this subsection and the method described in subsection 2.3:

Working with the reconstruction of the acoustic signal (subsection 2.3), it is assumed that under the action of vibrations the speckle - pattern does not change, but only displaced in space. In the case of fungi or bacteria, this is the wrong statement. Firstly, due to random processes in the behavior and activity of microorganisms, micro-vibrations will be local and directed in

different directions. That is, the pattern itself will change over time from frame to frame (Fig.2.2). This is confirmed by subsection 2.4, where it is shown that the decorrelation between the first (reference) image and subsequent images in which bacterial activity occurs is very quickly, in a tens seconds (Fig. 4). For this reason, we cannot take the first image as a template and perform a correlation with respect to it, but we will do this with each pair of consecutive images: 1 with 2, 2 with 3, 3 with 4, etc. (In Eq. 2.2, *a(x,y)* and *b(x,y)* in this case not first (template) frame and next frames in a sequence, but are two adjacent frames in a sequence).

Since, in this case, the correlation has been performed not between the template image and all subsequent images but between each pair of adjacent images, to take this effect into account when reconstructing the signal, the previous displacements are accumulated (separately for x and y axis) (Eq. 2.3).

$$sig[n] = \sum_{i=1}^{n} \hat{\delta}[i] \tag{2.3}$$

where $\hat{\delta}$ is all previous displacements.

Secondly, there will be no strong vibrations caused by an external signal, and the bacteria themselves create micro-vibrations, so there should not be strong displacements capable of shifting the template image by several pixels in a short time interval. Accordingly, we will not scan the area around the template image but will concentrate on the same position.

To obtain signals over the entire field, it is necessary to divide it into NxN pixels and in each of these sections zero mean normalised cross-correlation (and interpolation) between successive frames will be performed.

Fig. 2.5 compares the reconstructed signal inside the bacterial and fungal colony and outside it.

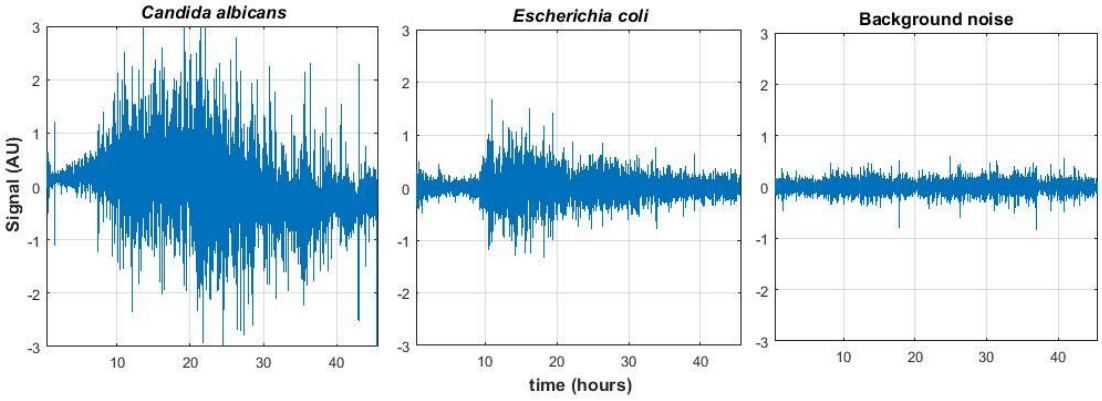

Figure 2.5 The signal obtained using the algorithm. Left - a signal from a *Candida albicans* (fungi) colony; center - a signal from an *E. coli* (bacteria) colony; right - a signal out of the colony.

2.6 Measurement accuracy and algorithm implementation time

This subsection discusses several ways to implement the cross-correlation algorithm so that it provides high accuracy on the one hand but is also fast on the other. The development of

microorganisms is a slow process, processing a large area (the entire Petri dish), and many hours of experiments with many frames, large amounts of data are obtained, and the processing time is long. For this reason, performance speed is important. Processing time assessments were conducted for a typical work section in the studies: 10 by 10 pixels, corresponding to a 100-150 by 100-150 micrometer area.

In cases where the brightness of the images can vary due to lighting and exposure conditions, the images should be normalised before processing. Accordingly, normalised cross-correlation is particularly useful since it is insensitive to both signal strength and level. The main advantage of the normalized cross-correlation over the non-normalized cross-correlation is that it is less sensitive to linear changes in the amplitudes of the two compared signals [91]. On the other hand, non-normalized cross-correlation is faster.

In a number of studies, for example [92], when they describe normalized cross-correlation, they present 2 options: Zero mean Normalized Cross-Correlation (ZNCC), that is, the function that we consider in this work, and Normalized Cross-Correlation (NCC) - a function which we are considering, but without subtracting the means of the images. Due to the subtraction of the local mean, the ZNCC provides better robustness than the NCC since it tolerates uniform brightness variations as well.

Now consider several implementation options and compare them: first and most importantly - in terms of accuracy (Fig. 2.6-2.7), and then in terms of processing time (Tables 1-3).

1) To implement NCC, we can calculate a non-normalized cross-correlation (from Eq. 2.1) and perform a division (normalisation) at the end. That is, this function will preserve the non-accuracy of the non-normalized cross-correlation, with that difference the values will be in the range from -1 to 1 (Eq.2.4).

$$NCC(u,v) = \frac{\sum_x \sum_y ((a(x,y)) * (b(x-u,y-v)))}{\sqrt{\sum_x \sum_y (a(x,y))^2 * \sum_x \sum_y (b(x-u,y-v))^2}} \quad (2.4)$$

2) The implementation of ZNCC follows Eq. 2.2.

3) To reduce the computation time, it is worth implementing the algorithm in the frequency domain. The formula for non-normalized cross-correlation in the frequency domain is known. However, how to implement normalised cross-correlation in the frequency domain? One approach is to implement phase correlation, which is also normalised [93] (Eq.2.5). This method will work much faster. Still, the result will differ from the implementation of zero mean normalised cross–correlation (Eq. 2.2).

$$PC(u,v) = FT^{-1}\left(\frac{[FT[a((x,y)] * FT[b((x,y)]^*]}{|FT[a((x,y)] * FT[b((x,y)]|}\right) \quad (2.5)$$

where FT^{-1} and FT – inverse and direct Fourier transform, and $()^*$ - complex conjugate.

4) In the study of J. P. Lewis [94], an algorithm is presented that, after a known finding of a fast non-normalized cross-correlation in the frequency domain, allows to convert it into a normalized. The accuracy is the same as the ZNCC. This method was apparently designed to work with relatively large matrices, where the implementation is quite fast; however, for small matrices, for example, 10 by 10 pixels, the normalization process is slow, and this method will be quite a bit faster than the ZNCC, but much slower than phase correlation.

5) Another implementation option proposed in the current study: the average is subtracted from the speckle images, and then the images are normalized. Then, frequency domain correlation is performed with two normalized images, (according to the formula for non-normalized frequency domain cross-correlation) (Eq.2.6). The accuracy is the same as in the

ZNCC or in the previous method by (J. P. Lewis), and the processing time is comparable (slightly slower) with phase correlation.

$$An(x,y) = \frac{a(x,y)-\overline{a}}{\sqrt{\sum_x \sum_y (a(x,y)-\overline{a})^2}} \; ; \; Bn(x,y) = \frac{b(x,y)-\overline{b}}{\sqrt{\sum_x \sum_y (b(x,y)-\overline{b})^2}} \; ; \qquad (2.6)$$

$$ZNCC(u,v) = FT^{-1}([FT[An((x,y)] * FT[Bn((x,y)]^*])$$

6) If the speckle images are large in size, not 10 by 10, but for example, 100 by 100 or more, then to calculate the ZNCC, the formula in the time domain (Eq. 2.2) can be used. However, not use all the shifts, but only a couple in the central part (to obtain a correlation peak only) for which the interpolation is made. If the images are large in size, then the method will be a faster implementation than in the frequency domain. For small sizes in the frequency domain, it is slightly faster.

Fig. 2.6 and Fig. 2.7 show different correlation functions' results. Whereas Fig. 2.6 shows the results of correlating a frame with itself. It can be seen that the phase correlation, in this case, gives the best result of accuracy. Fig. 2.7 shows the correlation results between two frames shifted by a non-integer number of pixels (0.5 pixels) along each axis. In this case, the result will either not be shifted or shifted by 1 pixel, and only sub-pixel interpolation can find a more accurate value.

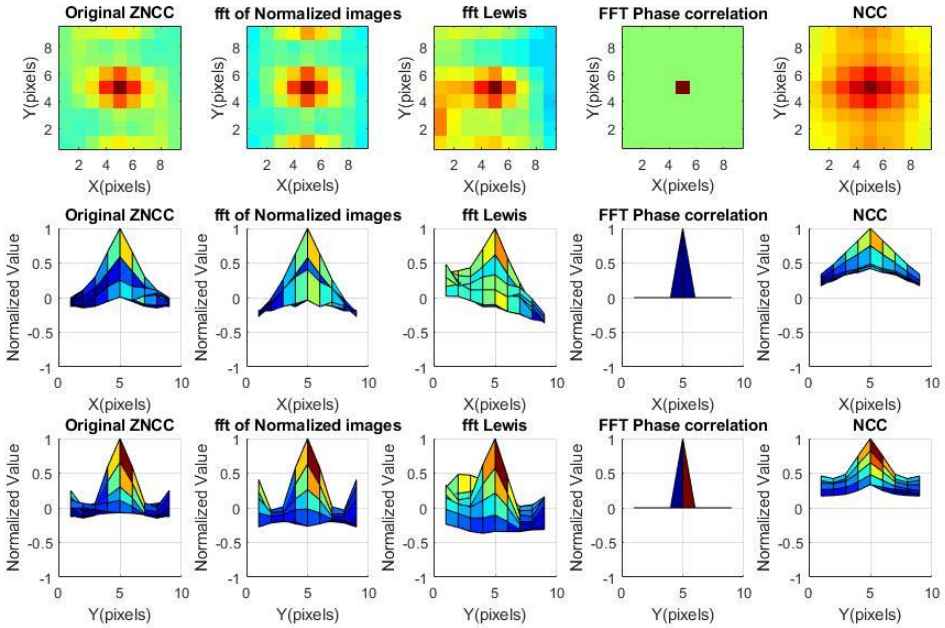

Figure 2.6 Comparison of different correlation functions. The results of correlating a frame with itself. Observing the advantage of phase correlation method

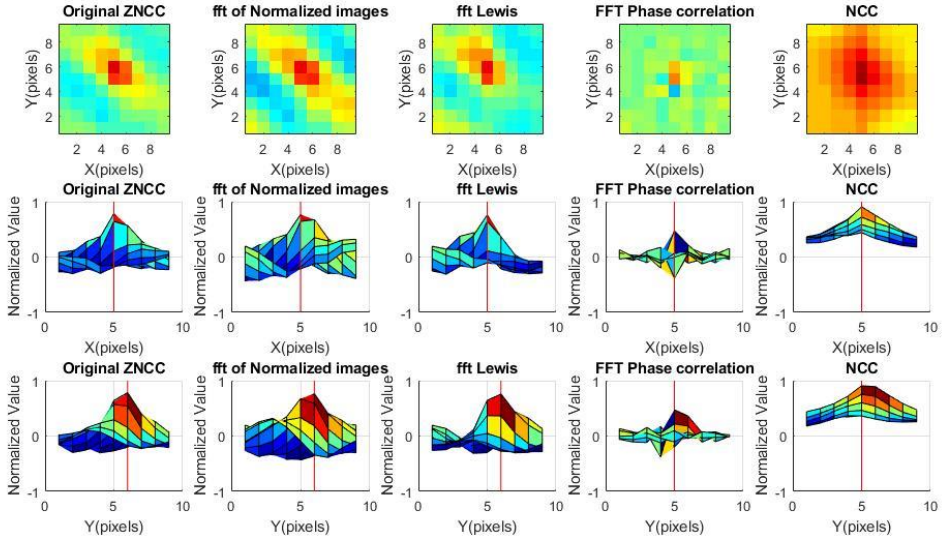

Figure 2.7 Comparison of different correlation functions. The results of correlating a frame with a frame shifted by 0.5 pixels. Deviations from the reference method are visible. The performance of phase correlation worsened.

The results of all algorithms were compared with the original implementation (ZNCC). It can be seen that already in this case, with a small displacement, the phase correlation and NCC show differences from the original, while the implementations in the frequency domain according to the Lewis method and proposed by current study method show closeness to the original.

It can be concluded that phase correlation works best when searching for an identical template within an image. However, its accuracy and peak value decrease with shifts or deformations, while ZNCC maintains high performance in both time and frequency domains under such conditions.

Below are tables describing processing time for different correlation algorithms and for different speckle image section sizes.

Table 1

The differences in processing time for these different algorithms. The section size of the speckle image is 6 by 6 pixels.

Speckle image section size = 6x6 pixels	**NCC (Eq.2.4).**	**Original ZNCC (Eq.2.2).**	**ZNCC use only 3 shift around the peak**	**Lewis method**	**Phase correlation (Eq.2.5)**	**Frequency domain correlation of normalised images (Eq.2.6)**
Average (μs)	148.8	168.9	78.8	478.0	34.5	63.6
Standard deviation (μs)	23.0	25.1	13.1	49.1	6.6	11.0

Table 2

The differences in processing time for these different algorithms. The section size of the speckle image is 10 by 10 pixels.

Speckle image section size = 10x10 pixels	**NCC (Eq.2.4)**	**Original ZNCC (Eq.2.2)**	**ZNCC use only 3 shift around the peak**	**Lewis method**	**Phase correlation (Eq.2.5)**	**Frequency domain correlation of normalised images (Eq.2.6)**
Average (μs)	515.9	550.0	93.9	545.5	48.0	81.8
Standard deviation (μs)	117.3	150.4	82.7	78.5	34.7	64.9

Table 3

The differences in processing time for these different algorithms. The section size of the speckle image is 100 by 100 pixels.

Speckle image section size = 100x100 pixels	**NCC (Eq.2.4)**	**Original ZNCC (Eq.2.2)**	**ZNCC use only 3 shift around the peak**	**Lewis method**	**Phase correlation (Eq.2.5)**	**Frequency domain correlation of normalised images (Eq.2.6)**
Average (ms)	473.8	476.8	0.9	13.0	1.3	1.1
Standard deviation (ms)	30.5	27.4	0.1	1.4	1.5	0.2

The results are obtained statistically based on the calculation of 5000 speckle image sections for each algorithm and for each section size. The calculation was carried out on a home PC. For other computers the processing times will be different (depending on its parameters). However, the ratio between them should remain similar.

2.7 Chapter conclusions

In the chapter, several of the famous methods for using correlation algorithms for processing laser speckle images were considered. The methods for detecting mechanical vibrations and reconstructing audio signals were the motivation for employing the technique described in this chapter (in Subsection 2.5). However, unlike mechanical and acoustic deformations, the movement of fungi and bacteria is chaotic, which causes not only image displacements but also changes in the images themselves. The correlation coefficient between images drops rapidly

(Subsection 2.4). For this reason, in the case of microorganisms, the "signal reconstruction" algorithm cannot take the first frame as a reference, template image and compare all subsequent frames to it. Accordingly, comparisons occur between each pair of consecutive frames. The resulting shifts are accumulated to ensure the continuity of the signal.

For a more accurate result, it is necessary to perform interpolation around the correlation peak in any of the implementations. The current study focused on the analysis of different techniques for correlation functions implementation and only mentioned interpolation techniques (Subsection 2.2). This could be analysed in a future study.

Various methods for implementing Normalized Cross-Correlation were also considered. The fastest is the phase correlation algorithm, but with displacement, its accuracy drops (in relation to the ZNCC method). Also, the other two algorithms implemented in the frequency domain are fast but, in contrast to the phase correlation method, provide high accuracy even in displacement cases. When comparing relatively large image fragments (100 x 100), the fastest algorithm will be in the time domain, where there are only a few values closest to the correlation peak are calculated, and not the entire matrix.

3. CORRELATION SUBPIXEL ANALYSIS OF LASER SPECKLE IMAGES FOR MONITORING THE DYNAMICS OF THE COLONY OF MICROORGANISM'S GROWTH AND REVEALING THE MIGRATION OF ACTIVITY ZONES WITHIN THE COLONY

Based on the posed aims and tasks, the third chapter of the Doctoral Thesis describes in more detail the proposed analysis method and its application for microbiological data and submicron activity evaluation as a research object. The chapter covers experimental confirmation of the capabilities of earlier detection of submicron activity and the efficiency of growth models of submicron events.

3.1 Laser speckle imaging system

The system was assembled for capturing macro scale images under white light and laser illumination. The optical measurement system consists of a laser source, white light source LED, 35 mm CS lens @F18, optical attenuator, a testing agar plate (with inoculated bacteria) and IDS CMOS 10 MPix camera (or later IMX477 CMOS 12.3 Mpix camera) (Fig. 3.1). To avoid antimicrobial effects caused by blue and green irradiation, the red laser was selected for generation of laser speckles. At the first stages of the study, in experiments the laser speckles were generated by a linearly polarised 635 nm diode pumped solid state multimode laser (output power 50 mW). Later, it was replaced by a single mode 658nm diode-pumped solid-state laser (output power 60 mW).

To achieve optimal exposure for image capturing and to avoid the heating effects of the illuminated plate, the optical attenuator was used, enabling 3-5 mW/cm2 power density of the scattered laser light on the whole agar plate surface. The diameter of the laser beam on the surface was greater than 9 cm providing even illumination of the entire Petri dish. According to the available literature, the illumination conditions applied in the current research are optimal and do not affect microbial growth [95]. The system's main components are presented in Fig. 3.1. The speckle images were captured by a CMOS camera with 1-30-second intervals (depending on the microorganism types) for experiments with different durations (10-110 hours). The interval was chosen according to the location of the useful time signal region in the spectrogram (will be explained in the continuation of this chapter). Exposure time was set to 1 second and was chosen according to laser illumination and lens diaphragm. Parameters of optical setup, including camera resolution, lens diaphragm, camera distance to Petri plate and resulting region of interest, were chosen to achieve adequate spatial resolution for detecting laser speckles. According to previous research [34], the camera's resolution should be at least 2 pixels per speckle. Lens magnification was set to 0.2. The diaphragm value of F18 was chosen as the optimal balance between image sharpness, speckle size, and the required exposure. That results of spatial resolution of 9$\boldsymbol{\mu}$m and a speckle size of 33 $\boldsymbol{\mu}$m.

White light experiments were performed separately from the laser speckle imaging by using the same set-up (Fig. 3.1). For these experiments, images were taken every 15 minutes under white LED illumination.

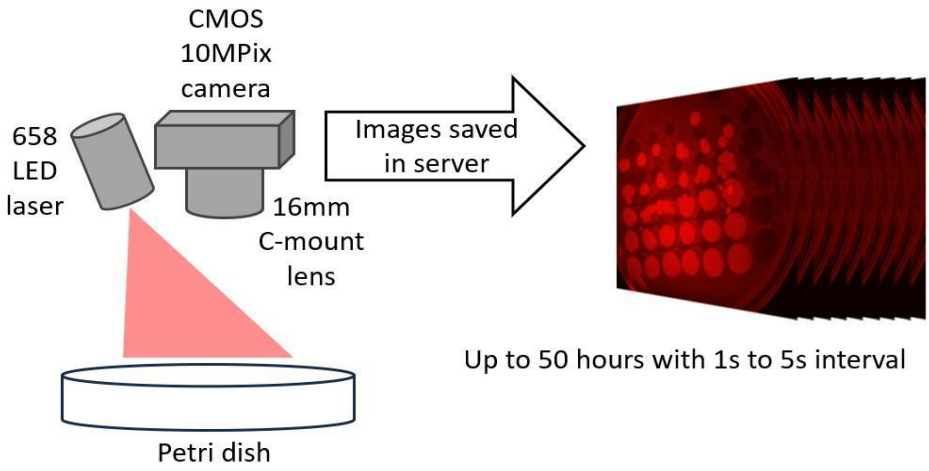

Figure 3.1. Setup scheme for burst image capturing of bacteria growing process under 658 nm laser illumination.

3.2 Challenge of early detection of bacterial colonies and monitoring growth dynamics

Determination of the viable microbial cells in a sample is one of the central tasks of epidemiology. Each viable cell initiates the development of one colony on an agar plate medium called colony forming units (CFU). Colonies are counted after they are clearly visible to the naked eye. A limitation of this method is the need to wait until colonies reach a certain size to be registered (detected). There is a risk that the two colonies can merge together, or fast-growing big colonies can overwhelm other smaller colonies, thus making correct CFU counting impossible [96]. Currently, counting microorganisms in the early stages of colony formation is possible only by microscope, which is limited to a small sample area. Automated counting of colony size increase dynamics is possible only by using regular cameras that are limited in optical resolution and, therefore, can detect signs of microbial colony only after a certain size threshold is reached. It would take 8 – 22 hours for the colony to reach the size of 0.2 mm, which is the detection limit for a photo camera. In standard methods, the waiting time is 18 – 40 hours for CFU's to "develop" before counting them [97].

One of the options for the fast and early evaluation of microorganisms' activity is a non-contact optical technique called – laser speckle patterns analysis. A laser speckle is an interference pattern produced by coherent light reflected or scattered from different parts of the illuminated surface. The growth of bacterial colonies on this surface leads to changes in scattering properties. As a result of this effect, the speckle pattern changes, and consequently, the behavior of the acquired image also varies [21]. This behavior as a function of time can be measured, detected and quantified. Thus, this technique allows monitoring moving particles in optically inhomogeneous media by analysing time-varying laser speckle patterns.

In general, the laser speckle approach is quite simple, providing early responses from microbiological activity compared to turbidity estimation methods or manual colony counting methods. However, according to available literature [55,77,88,98-102], none of the laser speckle-based methods have been focused on microbial growth (CFU formation) monitoring in

the early stages. The current Chapter will prove that dynamic laser speckle image analysis methods can be used to detect the CFU of different microbes in solid media.

3.3 Challenge of visualisation of differences in microbial activity over time in the different parts of the colony.

In many models, microbial colony growth is described to be uneven—colony growth depends on the active zones of the microbes, which, in turn, depend on nutrient supply from the media. For example, microbial growth on the colony's edge is more active than in its center due to the constant supply of nutrients from the surrounding media or the constant push of the cells on the lateral ones. The microscopic structure of the colony supports many of these presumptions. The cells in the center of the yeast colony stop proliferating and lose viability, while the cells on the edge of the same colony are alive and continue growing (proliferating) [103].

The differences in microbial activity in different parts of the colony cannot be accurately visualised with the existing live imaging methods. Currently, different microbial activity within colonies can be explored only with invasive procedures—colony cross-sectioning and viability staining [103].

The proposed speckle analysis system is capable not only of recording the growth of a microbial colony but also of visualising microbial growth activity in the different parts of the colony. The speckle patterns analysis reveals that colony growth is driven by cell proliferation on its edges rather than its center. This method was tested on three different microorganisms: *Vibrio natriegens*, *Escherichia coli*, and *Staphylococcus aureus*, and confirms the accuracy of the previous models of colony growth and provides a methodology for microbial activity analysis within the colony.

3.4 Converting subsequent frames of speckle images into a time signal

The previous chapter described the development of methods for correlation analysis of laser speckle images in the context of submicron activity detection. The proposed algorithm will now be described in more detail.

In cases where a rough surface is deformed, shaken, or displaced, the corresponding offset (displacement) can be observed in the speckle image [104]. This offset can be described by the position of the peak of the cross-correlation function between frames. The offset of the autocorrelation peak (the frame with itself) is always zero. A cross-correlation peak offset (between frames) indicates that there is a bias between them. The correlation coefficient can be used to analyse activity as a time-varying speckle pattern [27]. Each frame of the sequence is compared with the previous frame. Thus, a change in the correlation coefficient over time is obtained. Low temporal variation of the correlation coefficient in the observed area implies its relative inactivity in the frame of sensitivity of the detection method. The correlation coefficient graph, as a function of the frame number (or time), represents the activity of the observed process. Accordingly, the correlation method can be used to convert the change between subsequent frames into a temporal signal. By analysing the received time signal, it is possible

to detect events caused by the vibration of the measured surface or activity on it. For example, the dynamic spreading of a bacterial colony on the solid media surface.

A method for speckle image conversion into a time signal is described below.

1) First, two-dimensional normalised correlation between images following each other in time is performed. This allows detecting changes in the speckle image (between subsequent frames) because of dynamic activity. (Canonical Equation 2.2 or faster Equation 2.6 from Chapter 2 (where the correlation is performed between two adjacent frames in a sequence)).

2) Changes that occur between successive frames are characterised by an offset in the location of the maximum correlation value (Eq. 3.1).

$$\left(\hat{u},\hat{v}\right) = \arg\max_{u,v}\left(Corr(u,v)\right) \tag{3.1}$$

where u and v are spatial displacements between two adjacent frames in a sequence in the directions of x and y, respectively.

3) The growth of a bacterial colony is a random process. Therefore, the offset between each pair of successive frames cannot be exactly equal to an integer number of pixels. Hence, the offset between successive frames does not represent the integer number of pixels. For this reason, interpolation was performed within the maximum of the correlation function [105]. This was performed separately for x-axis and y-axis. Eq.3.2 shows the parabolic interpolation for the x-axis.

$$\hat{\delta}_x = -\frac{b_u}{2a_u} = \frac{Corr(\hat{u}-1,\hat{v}) - Corr(\hat{u}+1,\hat{v})}{2\left(Corr(\hat{u}-1,\hat{v}) - 2Corr(\hat{u},\hat{v}) + Corr(\hat{u}+1,\hat{v})\right)} \tag{3.2}$$

where a_u and b_u are the coefficients of the parabola.

4) Offsets obtained between each pair of adjacent samples were accumulated (separately for x and y axis) to consider previous offsets (Equation 2.3 from Chapter 2).

Running the described algorithm for consecutive N × N pixels images for the entire sequence creates a "time signal". This algorithm was implemented for all N × N pixel sections in the entire field of the experiment. Thus, a two-dimensional array from the "time signals", where time is the third dimension, was obtained in place of the considered fled of the experiment.

To find the local extrema and to avoid the influence of local transient spikes, it is expedient to smooth the signal [106] (obtain signal envelope function). A moving root-mean-square technique or another similar algorithm can be used for this purpose:

$$Env[n] = \sqrt{\frac{1}{N}\sum_{k=n-N+1}^{n} sig[k]^2} \tag{3.3}$$

where N is the length of the window, n is the current sample, and k is the index running inside the window. Accordingly, N—the length of the window—is responsible for the degree of signal smoothing. The extreme values can be truncated to avoid outliers when performing the RMS technique, as it is done by adopting the truncated mean technique [107].

An increase of signal values will be observed when bacterial growth occurs. Establishing a threshold or an adaptive threshold or constant false alarm rate (CFAR) - based threshold for this signal allows detecting the region and time where the growth of bacteria was observed.

In Fig. 3.2, it is also possible to compare the signal (inside the colony) and the noise (outside of the colony). The signal is much higher than the noise level.

The bottom row represents the spectrograms. A spectrogram represents a signal on a time-frequency domain using a short-time Fourier transform (STFT). The spectrogram shows how the spectral density was distributed over the frequencies by observing a signal indicating colony growth (Eq. 3.4-3.5):

$$STFT[k, f] = \sum_{n=-\infty}^{\infty} sig[n] \cdot w[n-k] \cdot e^{-j2\pi fn} \tag{3.4}$$

where w is the Hamming window function [108], and sig[n] is the signal to be transformed. Using the window w, the signal is divided into segments and performs windowing.

$$spectrogram[k, f] = |STFT[k, f]|^2 \tag{3.5}$$

STFT[k,f] is essentially the Fourier transform of $sig[n] \cdot w[n-k]$, a complex function representing the phase and magnitude of the signal over time and frequency.

The signal characterising the activity of bacteria is located in the low-frequency area: (0 - 15 mHz)). However, higher frequencies were observed in other experiments or with other bacteria, up to 20-25 mHz. From a practical point of view, this means that according to the Nyquist–Shannon sampling theorem [109, 110], the sampling frequency between frames must be at least 50 mHz, that is, the frame at least once every 20 seconds. However, it is worth taking a reserve and working with frames that are sampled every 10 seconds (which corresponds to operational frequencies up to 50 mHz) (Eq. 3.6):

$$t_s = \frac{1}{f_s} \geq \frac{1}{(2 * f_{max})} \tag{3.6}$$

where t_s is the time between frames (in seconds), accordingly f_s - sampling frequency, and f_{max} is the maximum frequency of the useful signal (in Hz).

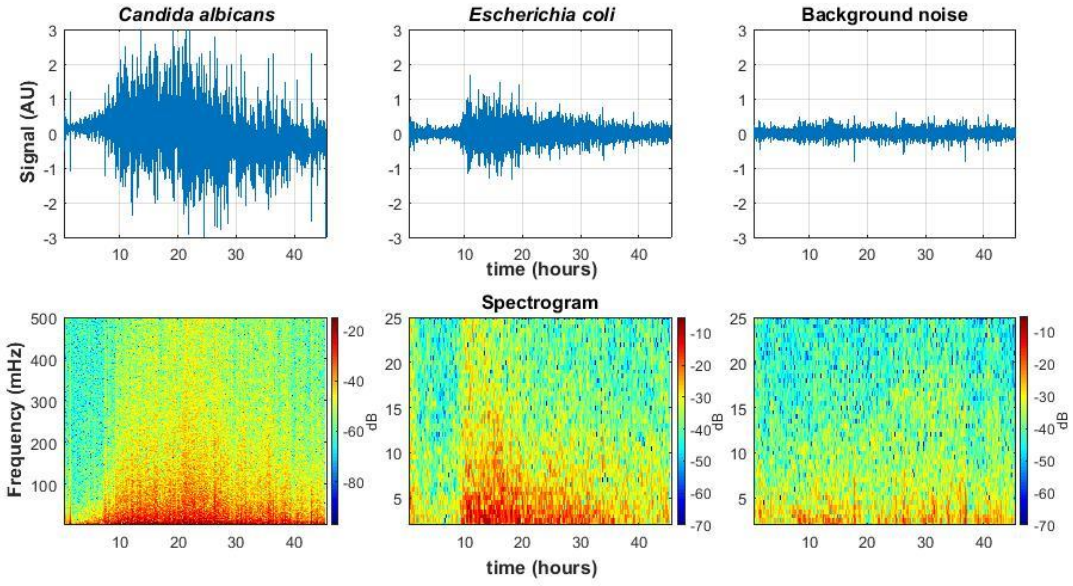

Figure 3.2. Top: The signal obtained using the algorithm (Signal from the colony center). The left column shows a signal from *Candida albicans* fungi, a similar speckle signal pattern was

observed also for *Aspergillus niger* fungi. The center column shows a signal from an E. coli bacterial colony; a similar speckle signal pattern was also observed for *S. aureus* and *V. natriegens* bacteria. Bottom row: A spectrogram is a representation of a signal on a time-frequency domain using a short-time Fourier transform (STFT), allowing simultaneously to observe the behavior of the signal and noise in time and frequency. Right side: the noise (out of the colony) obtained using the algorithm (top) and noise spectrogram (bottom).

Experiments conducted with the fungi *Aspergillus niger* and *Candida albicans* showed that the signal is in the frequency range from 0 to 150 mHz. Accordingly, the sampling frequency between frames must be at least 2 * 150 mHz, that is, a frame at least once every 3.33 seconds. However, it is worth taking a reserve and working with frames that are sampled every 2-3 seconds (which corresponds to operational frequencies up to 250-167 mHz, accordingly) (Fig. 3.2)

3.5 Operations in a noisy environment

The real systems must operate in different environments with an unknown noise level. Therefore, it is important that the system can work in noisy environments.

To analyse the algorithm's performance in a noisy environment, a bacterial colony detection experiment was performed using the laser speckle technique with noise added. A high noise level was set in the experimental field (3-4 times higher than normal background noise). Thus, the useful signal level, which should be observed in "characteristic for environment" background noise, was deeply covered by noise. Figure 3.3 shows the levels of 1) "characteristic for environment" background noise, 2) the noise level in which the experiment was carried out, and 3) the useful signal (as a function of time). A useful signal (characterising the appearance of a bacterial colony at this point in space) becomes noticeable after 7 hours. Taking a sample from the central area of the colony, it is possible to follow the change in time of the intensity of raw speckle and the result of the algorithm.

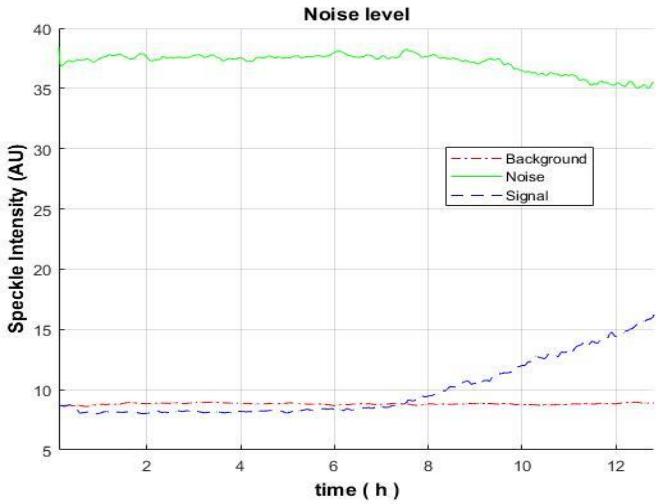

Figure 3.3. Average levels of useful signal and noise obtained by averaging M amount of 10x10 pixel section from the colony center (signal) and outside the colony (noise).

The intensity variability of raw speckle (Fig. 3.4 top) is similar to the noise level (Fig. 3.3), and the useful signal does not appear. In contrast, the application of correlation subpixel analysis enables the extraction of a useful signal (Fig. 3.4 bottom) - a signal becomes noticeable after 7 hours. Signals represented in Fig.3.4 were obtained from a 10x10 pixels section from the center of the colony. In cases where images can be observed in at least one of the domains in which they are processed (temporal, frequency, spatial or other), adaptive or optimal filters can help to extract the useful signal hidden in the noise. Using the correlation subpixel algorithm, it is possible to detect changes in activity that are not visible in raw images. Even when additional noise is added to the experiment, rendering the activity changes completely "invisible" to direct observation, the activity continues to occur, and the algorithm successfully detects these changes.

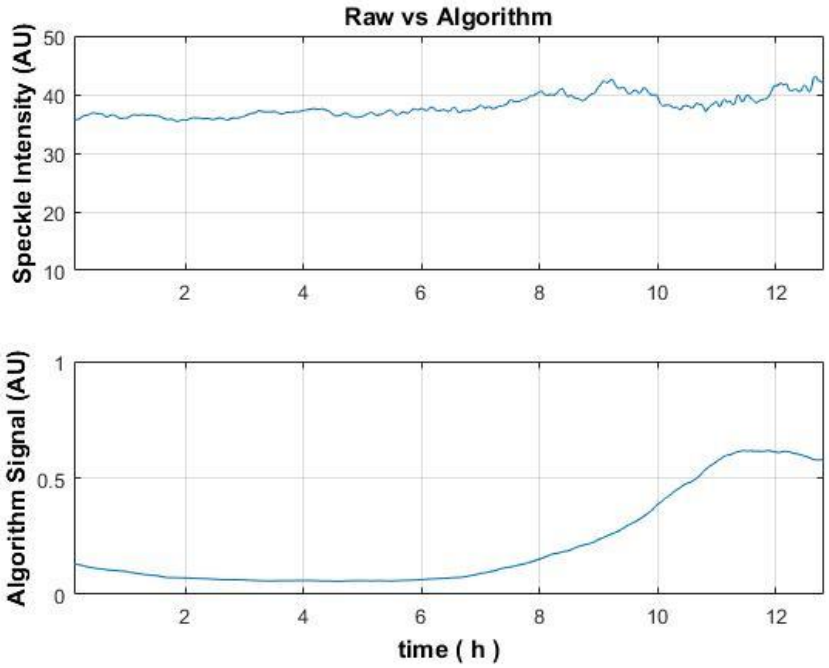

Figure 3.4. The raw speckle intensity (top) and signal calculated by the algorithm (bottom) obtained from a 10x10 pixel section from the colony center.

In high noise level conditions, speckle patterns do not clearly show the useful image, or the useful image may disappear completely (Fig.3.5, top row). Figure 3.5 shows an example where three bacterial colonies develop in a noisy environment. The colonies are not visible on raw speckle images (top row). Using the sub-pixel correlation algorithm (displacement finding using correlation and refining using subpixel interpolation), all three colonies will be detected (bottom row), and their evolution over time can be observed.

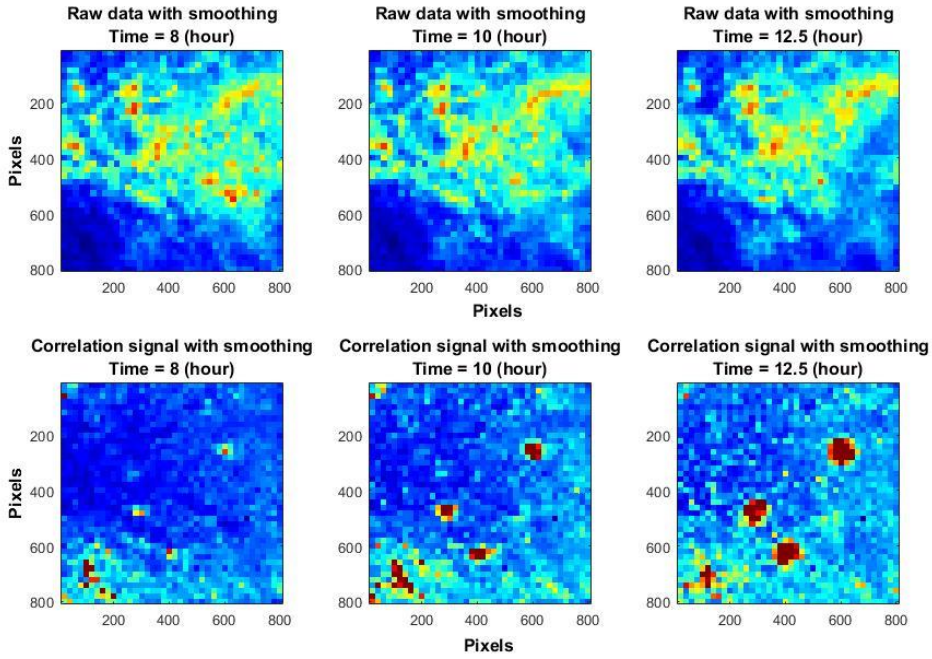

Figure 3.5. Raw laser speckle images with smoothing of *V. natriegens* sample at 8h, 10.5h and 12.5h (top row) and correlation signal with smoothing obtained using sub-pixel analysis at 8h, 10h, 12.5h (bottom row).

In the current subsection, it was demonstrated that the proposed method can give promising results in distinguishing the desired signal in a noisy environment.

3.6 Signal as a function of different initial cell numbers in the colony

One of the issues that is not neglected is the influence of the initial cell number in the colony on the signal.

It was analysed how the number of cells in a colony affects the signal obtained from the growing colony. The time of the maximum signal value of the laser speckle images was compared with the initial cell number within the macrocolony (Fig. 3.6). The time of the maximum signal value is defined as the time when the signal activity reaches its maximum. Overnight E. coli culture was serially diluted and inoculated on the LB agar media as macrocolonies (the volume of each inoculum was 5 μL). Macrocolony growth was recorded using a laser speckle imaging system. The time of the maximum signal value for each macrocolony was determined and plotted against the initial cell number per macrocolony. Signal peak time mean values and standard deviation of the three independent inoculation series were calculated (Fig. 3.6).

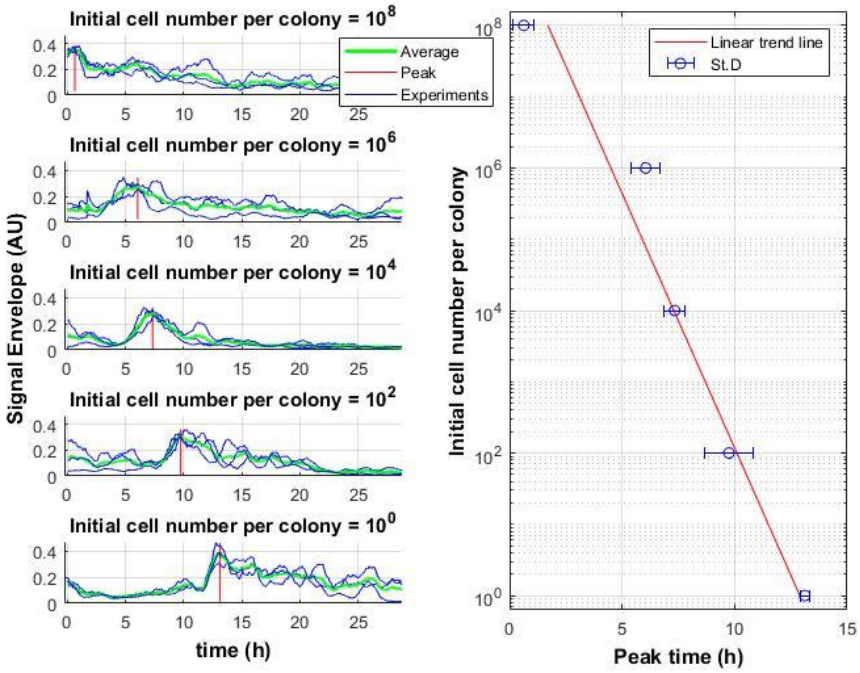

Figure 3.6. Dependance of the time of the maximum signal value (red lines on the graph on the left and blue circles on the graph on the right) obtained by the laser imaging system on the initial number of *E. coli* cells in the colony.

Obviously, the time of the maximum signal value depends on the initial cell number within the colony. If the initial number of cells in the colony is large, less time is required to reach the maximum signal. On the other hand, if the initial number of cells is small, it will take longer to reach the maximum signal value. Even though colony growth continues for more than 20 h (Fig. 3.6 for E. coli), the maximum of the signal is reached once and it never "repeats".

3.7 Early detection of microbial colony forming units

3.7.1 Analyses of colony growth under white light illumination

Microbial growth on the agar surface and colony formation is a self-limiting process that starts with the maximum rate, which is gradually inhibited by the exhaustion of necessary nutrients and accumulation of end products of microbial metabolism. Many mathematical models describe microbial colony growth; among them, the Gompertz model is one of the most common [111,112]. The mathematical expression of the Gompertz model is presented in Eq.3.7.

$$\mu(t) = \mu_0 \cdot e^{-\mu_i(t-t_0)} \tag{3.7}$$

where μ is the specific growth rate (h^{-1}), μ_0 – is the specific growth rate at the beginning of colony formation (h^{-1}), μ_i – specific growth rate at infliction (or specific inhibitory rate), t_0 represents the time at beginning of the colony growth and t is the actual time (h).

Eq.3.8 describes the growth of the colony radius as a function of time.

$$r(t) = r_{max} \cdot e^{-\left(ln\left(\frac{r_{max}}{r_0}\right)\cdot e^{-\left(\mu_i\cdot(t-t_0)\right)}\right)} \quad (3.8)$$

Eq.3.8 shows the growth of the colony radius, where r_{max} is the maximal radius that the colony can reach in the given environmental conditions, r_0 is the initial radius at t_0, μ_i is the specific growth rate at the inflexion point of the area curve. Over time gradual inhibition of colony growth occurs, which can be described by μ_i. To use these equations to simulate the growth of real CFU, μ_0 and μ_i should be found.

Using the Gompertz model, a specific set of parameters should be found to describe microbial colony growth. It was done experimentally for each microbial species and cultivation conditions (temperature and media). Data under white light illumination (bacteria *Vibrio natriegens*) were taken as a reference. Colony diameters were determined from the image series over time (see example of image series in Fig 3.7B). Using Eq. 3.8 the μ_i for *V. natriegens* were calculated at given temperature and media conditions. (See example of obtained results and mathematical approximation in Fig. 3.7A).

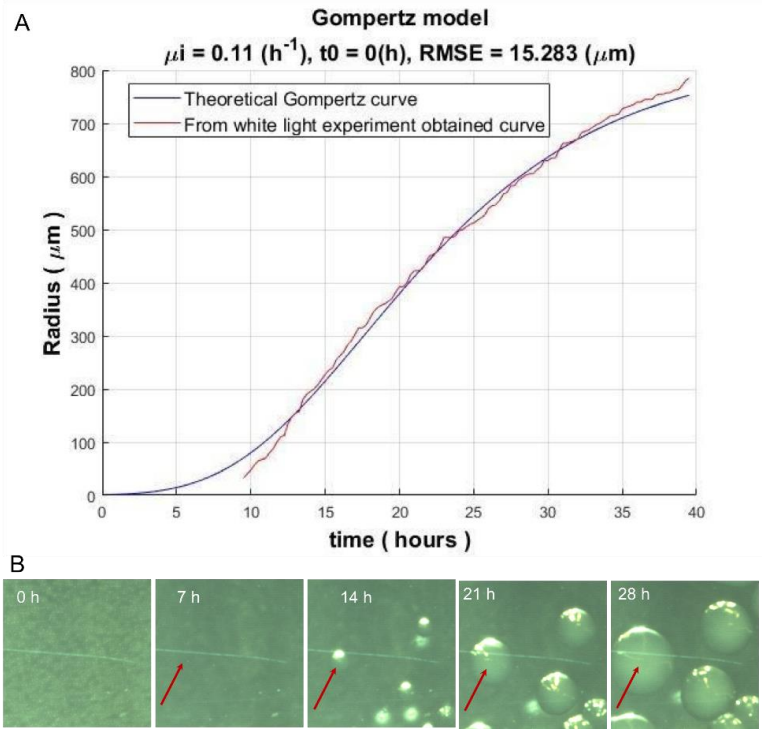

Figure 3.7. The growth dynamics of *V. natriegens* colony. (A) Theoretical Gompertz - curve (blue) and experimental curve (red) of *V. natriegens* colony radius dynamics over time. (B) Example of *V. natriegens* white light image time series. The red arrow indicates one colony. Colonies are not visible under white light until 8-12 h of growth. The size of each image is 500x500 pixels (2500 x 2500 micrometers). The colony radius was determined from the white light images.

Based on the experimentally obtained colony measurements, was set maximum colony radius to be 170 pixels and initial colony radius (r_0) 0.1 pixels (1 pixel equals 5 micrometers). When simulating μ_i for *V. natriegens* in the room temperature for the given colony growth, the μ_i was 0.11 h^{-1}. However, μ_i is not a fixed number. This coefficient characterises decreasing of the colony growth rate over time. The colony growth rate depends on many factors such as: temperature, number of surrounding colonies, and local concentration gradient of nutrients (compare Fig. 3.7 with Fig. 3.8 and Fig. 3.11). Usually, the μ_i can vary by 20-50 % among the same organism [111].

To extract parameters from the given experimental data set, a parameter scan was used. As a criterion Root Mean Square Error (RMSE) to minimum Eq. 3.9 to find μ_i and t_0 was used.

$$RMSE = \sqrt{\frac{1}{n}\sum_{i=1}^{n}\left(R_{Gompertz}[i] - R_{measured}[i]\right)^2} \tag{3.9}$$

where $R_{Gompertz}$ is the radius estimated from the Gompertz model, $R_{measured}$ is the radius determined experimentally, n is the number of measurement points.

RMSE values can vary in each experiment as they represent a match between theoretical and experimental curves.

3.7.2 Analyses of colony growth by processing of laser speckle images

For the speckle image analysis, the growth of the *V. natriegens* colony under laser light illumination was recorded. The analysis was performed after the correlation subpixel algorithm. By marking the growth start times of each 20x20 pixel square, knowing the location of each square in space and its distance from the colony center (marked manually), the colony radius was calculated as a function of time (Fig. 3.8).

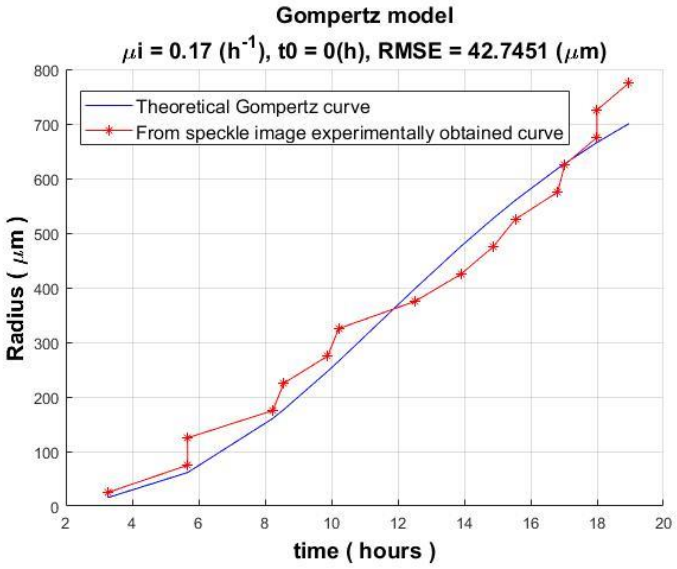

Figure 3.8. *Vibrio natriegens* colony radius obtained by speckle image experiment (red) and theoretical Gompertz curve (blue). Interestingly, first signals above the threshold level from speckle imaging can be extracted as fast as less than three hours from the beginning of the cultivation.

Fig. 3.8 represents the increase in colony radius in speckle images as a function of time obtained according to the Gompertz model (Eq.3.8). Using the scanning method for several parameters (growth rate, growth start time, maximum radius of colony) it is possible to get the most optimal suitable Gompertz curve in which the Root Mean Square Error (RMSE) value will be minimal. RMSE value (see Fig.3.8) shows how much the curve differs from the model. To summarise, the above-mentioned approach captures time events that characterise dynamic changes in speckle signals for all spatial sections (NxN pixels each) throughout the experimental data set.

3.7.3 Comparison of colony growth measurements in white light and speckle imaging experiments

Numerous experiments were performed using the speckle imaging techniques and images under white light illumination (Fig.3.8) to understand the typical signal dynamics of *V. natriegens* colony growth.

Comparing these two techniques, it was obtained that with the speckle imaging technique, it is possible to detect microbial activity earlier than using white light imaging. The colony formation on the agar media was observed 3 hours after bacterial inoculation, while the CFU growth of the colony in white light could be detected after 8-13 hours. However, there are speckle image experiments where growth was observed later than 3 hours from the beginning of the experiment (Fig.3.9). All signals depicting CFU growth (obtained from speckle and white light images) demonstrate similar dynamics (the graphs of radius increase over time are parallel to each other). However, the growth signal graphs are scattered across x-axes, which can be attributed to fluctuated room temperature across the experiments, thus affecting growth speed and colony detection.

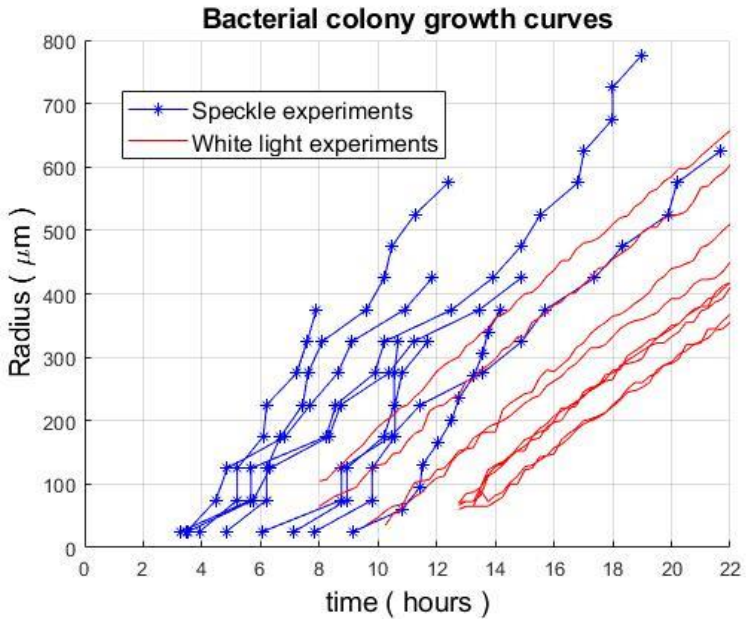

Figure 3.9. Comparison of growth curves of a colony of bacteria *Vibrio natriegens* measured by analysis of laser speckle images and visual examination under white light illumination.

Detection of the colony growth (increase of the colony radius) using speckle images demonstrates that it is possible to distinguish colony development from the background earlier than using white light images.

A comparison was also made not only for *Vibrio natriegens* but also for Escherichia coli and *Staphylococcus aureus* bacteria to study bacterial colony growth parameters.

Comparing colony growth under white light illumination and under laser with the following speckle imaging analysis method, highly similar growth curves were obtained (Fig. 3.10). Therefore, it may be concluded that the established laser speckle system does not affect the growth of microbial colonies. However, there is a tendency for the speckle imaging technique to reveal colony growth earlier than imaging under white light (Fig.3.10).

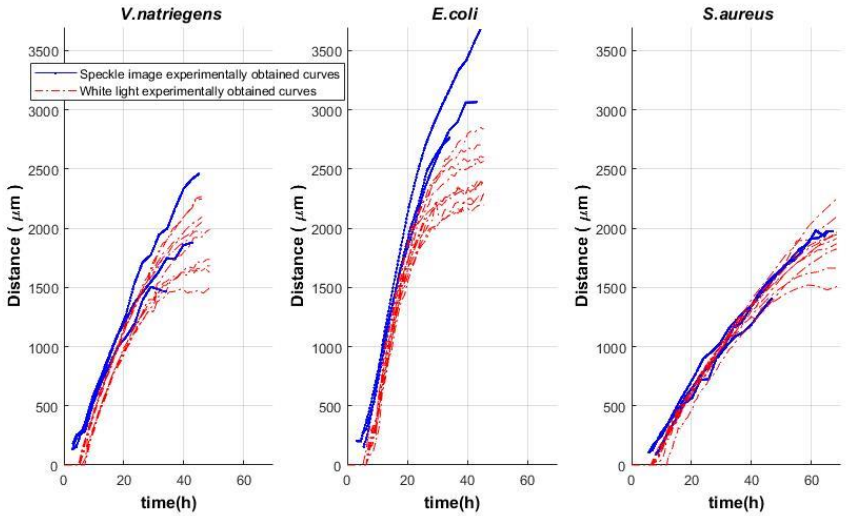

Figure 3.10. Dynamics of colony radius growth over time. The colony radius of the *Vibrio natriegens*, *Escherichia coli* and *Staphylococcus aureus* were measured by laser speckle image analyses (blue) or measured directly from photos taken by document scanner (Cannon 4400, 600 DPI) (red).

3.7.4 Influence of temperature on growth speed of microbial CFU on the agarised media

The growth speed of microbial CFU on the agarised media depends on many factors: temperature, distance from the neighboring colonies, and local concentrations of nutrients. To test the sensitivity of the laser speckle imaging method at different room temperatures, colony growth was recorded at “low” (~22°C) and “high” (~26°C) temperatures. It was observed that the *Vibrio natriegens* colony grew more slowly at low temperatures, and the laser speckle method began to observe it after 9 h (Fig. 3.11. blue curve). But at higher temperatures, bacterial colonies started to grow faster and were detected after 4 h (Fig. 3.11, green curve). The Gompertz model was applied for the samples at “low” and “high” temperatures to find the best parameter set for approximation of the experimental data. Specific growth rate μ_i, time when growth starts- t_0, and the error between the experimental and theoretical curves (RMSE) were found. The results are depicted in Fig. 3.11.

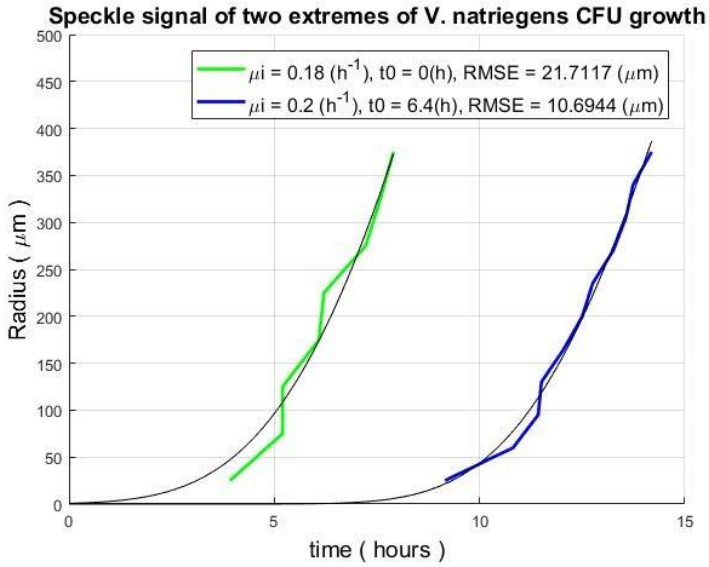

Figure 3.11. Comparison of *Vibrio natriegens* colony growth curves measured by laser speckle image analysis at low (22°C, blue curve) and high (26°C, green curve) room temperatures.

From the comparison shown in Fig. 3.11, the Gompertz parameters for these two "extremes" are quite alike. While the start time of the growth is different, the μ_i is similar. It was observed that at 26°C room temperature the growth of *V. natriegens* started immediately (Gompertz model start time t_0=0), but at 22°C room temperature, bacterial growth began after a 6.4 h delay. In both cases calculated colony growth radius can be fit by the theoretical model of colony growth.

3.8 Correlation subpixel analysis for determining spatiotemporal activity patterns during colony growth

3.8.1. Detection of high microbial activity zones using the laser speckle imaging system

The signal obtained by correlation subpixel analysis of laser speckle images, which characterises bacterial activity, increased inside the colony, reached its maximum, and then decreased. The signal strength had a remarkable spatiotemporal distribution. Different parts of the colony had different maximum signal peak times. The peak activity was initially observed at the center of the colony. Over time, the activity "wave" migrated from the center to the edges of the colony (Fig. 3.12 and Fig 3.13). This spatiotemporal behavior of the speckle signal was observed within all tested microbial colonies: *S. aureus*, *E. coli* and *V. natriegens*.

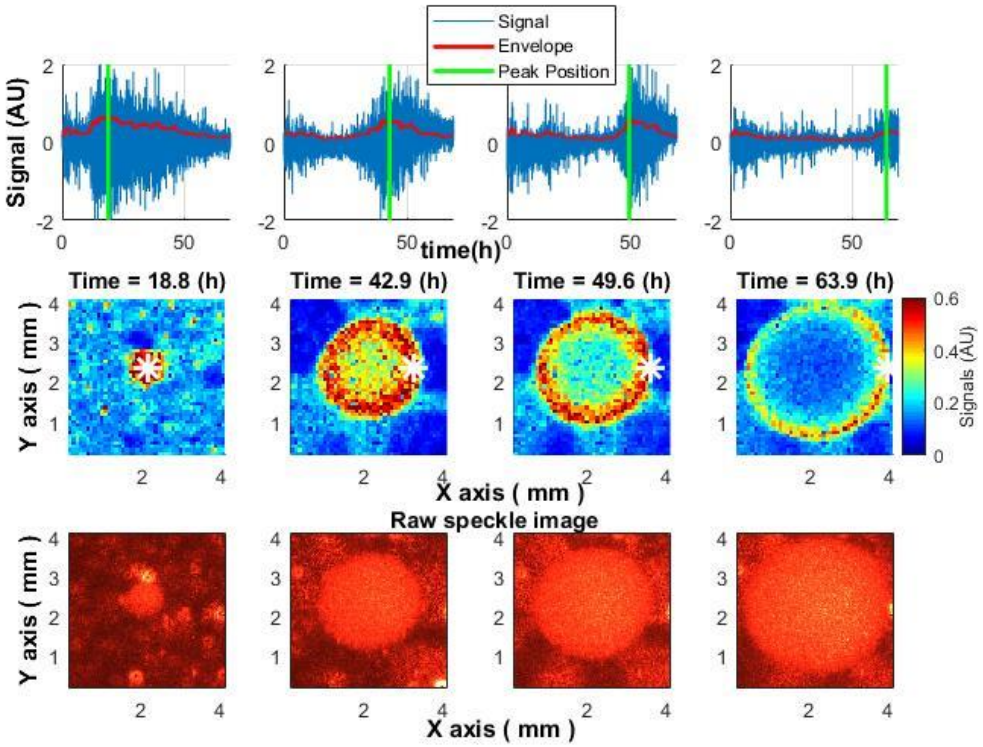

Figure 3.12. Spatiotemporal distribution of the speckle signal across *S. aureus* colony. Upper row: signal dynamics over time at different points within the colony (white star in the middle graphs). The green line marks the maximum activity, after which the signal decreases. Middle row: changes in the activity during colony growth. Bottom row: Raw speckle images

It is possible to obtain an image that illustrates the beginning of the decrease in activity throughout the colony (Fig. 3.13, top image) by choosing the times of the start of the decrease over the entire area of the colony and placing them on a two-dimensional spatial map with the corresponding coordinates.

The high-activity "ring" is formed around the center and then it migrates away together with the front of the growing colony. The color shows the time (in hours) when the activity started to decrease: the blue color (in the center) represents the earliest, red color represents the latest (edge of the colony).

The location of the first decrease on the map can be assumed as the starting point for the growth of a microbial colony. Knowing the coordinates of this starting point or center, obtaining a curve of the colony growth as a function of time is possible. However, since the growth of the colony depends on various factors (the availability of oxygen and nutrients, Brownian movement, push and/or pull from the neighboring cells within the colony, asynchrony of the cell growth and proliferation within the colony, etc.), the resulting curve will have a certain scatter of values (Fig 3.13, bottom graph). Therefore, a moving median filter was applied to smooth curve data [106]:

$$Dsmooth(n) = median[D(n-N+1), D(n-N+2), \ldots, D(n-1), D(n)] \quad (3.10)$$

where N is the length of the window, and n is the current sample. The median is the number that is situated in the middle of a set of numbers when sorted in ascending order. That is, half of the elements in the set of numbers are not less than the median, and the other half is not greater than the median:

$$median(x) = \begin{cases} x\left(\frac{N+1}{2}\right) & if N\ is\ Odd \\ \frac{x\left(\frac{N}{2}\right)+x\left(\frac{N}{2}+1\right)}{2} & otherwise \end{cases} \quad (3.11)$$

This method was applied for the following reasons: 1) It does not try to fit the curve into a specific shape: a straight line, or a parabola, etc. 2) Unlike a moving average, it does not take outliers into account.

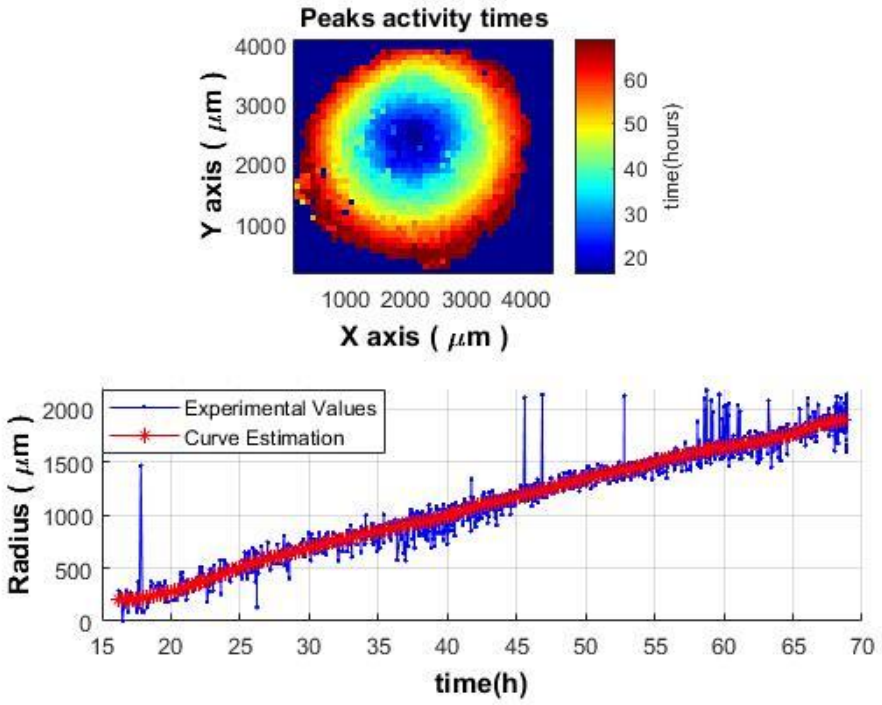

Figure 3.13. The time of colony peak activity (the start of the decrease in activity) during the growth of *S. aureus* colony. Top image – a two-dimensional spatiotemporal image; bottom image – the peak activity as a function of time. Similar spatiotemporal behavior of the signal was also observed within colonies of *E. coli* and *V. natriegens.*

3.8.2. Analysis of activity zones for different bacterial colonies in the time-space domain

The "ring" effect was obtained for all three types of the tested bacteria. The growth rate was the main difference that was observed (Fig. 3.14).

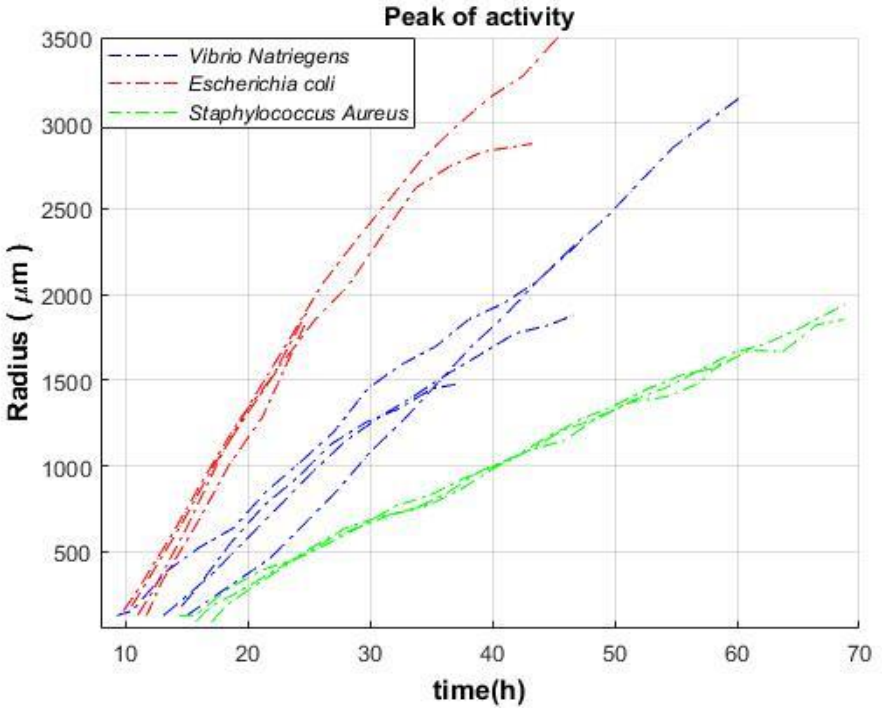

Figure 3.14. Colony peak activity curves as a function of time for 3-4 *V. natriegens* (blue), *E. coli* (red), and *S. aureus* (green) colonies.

Taking the points corresponding to the distance from the center of the colony according to the curve described in Fig. 3.13-3.14, the coordinates in space (x, y) for each "ring" is obtained. A smoothed envelope function of the signal is placed at each such point in space (Fig. 3.12). Thus, many signals will correspond to each specific radius (the distance from the center of the colony to the maximum activity point). In an ideal situation, all signals within the same "ring" (at the same distance from the colony center) would be the same. However, the growth of a bacterial colony is affected by various conditions mentioned above, so these signals are slightly different. Therefore, it is necessary to do some averaging of all signals for a given radius, so that each radius receives one signal that characterises it. Such averaging was performed by adopting the truncated average method [107], where the truncation was performed not in amplitude but in the time of the activity peak:

$$\overline{Env(D)} = \frac{1}{n-k_b-k_f}\left[Env(k_b+1)+,\ldots,+Env\left(L-k_f\right)\right] \qquad (3.12)$$

where L is the number of envelope signals at a given distance, $k_b$and k_f – the number of envelope signals that were truncated from each side. Those signals whose peak of activity in the given radius differed greatly from the general trend (premature or delayed) were not considered. The obtained averaged signals were mapped as a function of distance from the center and time (Fig. 3.15, top image).

By selecting several points in time on the map, it is possible to observe how the peak of activity will look as a function of the distance from the center of the colony. The width of the

peak is proportional to the width of the activity “ring”, and its change in time is shown in the bottom graph of Fig. 3.15.

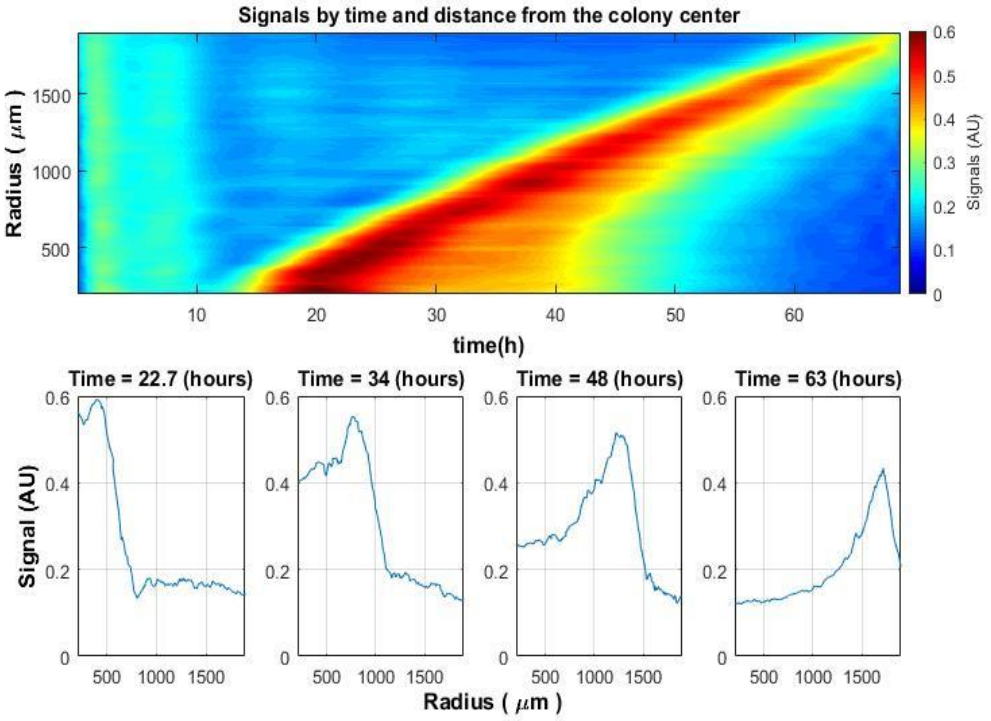

Figure 3.15. Envelopes of the averaged signals as a function of distance from the colony’s center and time (top) and the peak of activity as a function of the distance from the colony's center for different times (bottom) of *S. aureus*. Similar spatiotemporal behavior of the signal was observed also within colonies of *E. coli* and *V. natriegens.*

3.8.3. Spatial width of the activity zones

The spatial width of the signal at different times can be observed in Fig. 3.15. The signal width corresponds to the decrease from the peak value to a certain value. If there were no noise, or unwanted signals, or any other factors, the criterion would be simple: reducing the signal level or its power from the maximum value to zero. However, there should be some threshold in real conditions when the signal is still distinguishable against the noise. The decrease in signal power from the maximum to 1/3 of the maximum value was chosen as a criterion. That is, it should be noted that the actual width is slightly larger than the received one. It is possible to find the width for each moment. This width will match the width of the “ring” at the corresponding time (Fig. 3.16).

From Fig. 3.16 (a,b) it can be observed that although the change in ring width is small, it can be considered constant with some deviations. That is, from the time when it was possible to start observing the “ring” and until the end of the observation, when the “ring” disappeared, the width of the “ring” remained approximately unchanged (with reservations about the accuracy of measurement, random phenomena in the behavior of a colony of many microorganisms, noise, etc.).

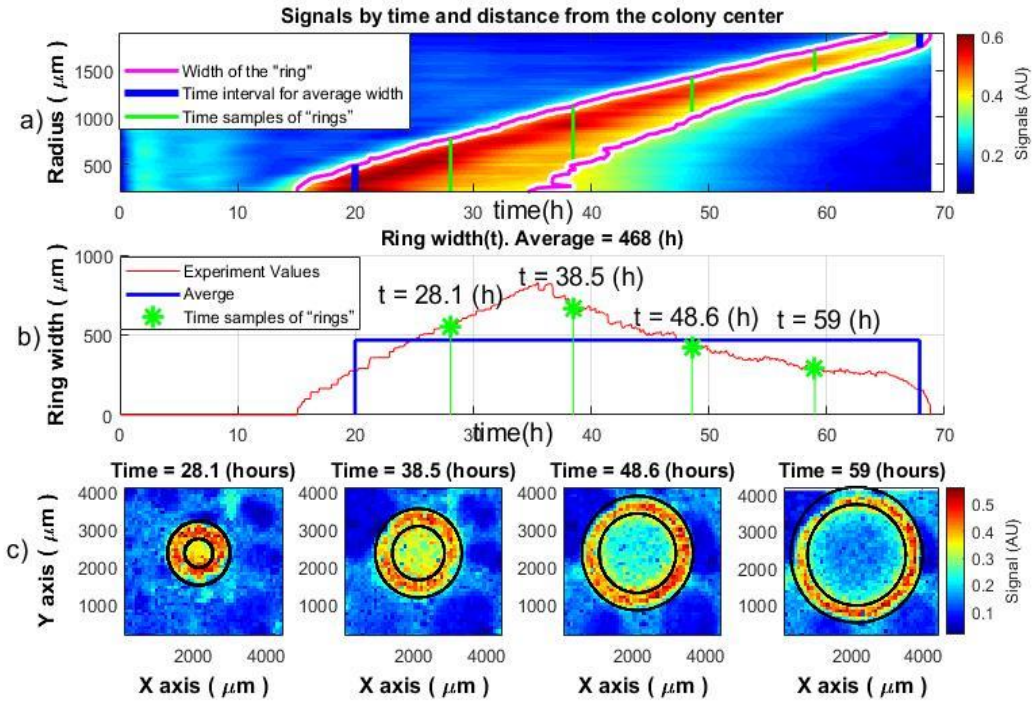

Figure 3.16. Determination of the width of the activity "ring" for the colony of *S. aureus*: a) signal values and determined width of the activity ring (purple line), b) the obtained width of the activity "ring", c) comparison of the obtained width of the activity "ring" (black lines) for one colony at different times. Similar spatiotemporal behavior of the signal was also observed within colonies of *E. coli* and *V. natriegens.*

The behavior described for one selected colony was observed for all types of bacteria considered in this study. The width of the "ring" is different for each type of bacteria. Fig. 3.17 shows the width of the "ring" for all types of bacterial colonies. The obtained results correspond to the mathematical model of microbial colony growth introduced by John Pirt ("Pirt model").

The Pirt study [113] provides a formula for calculating the width of the active zone or the "ring":

$$r = \frac{\omega\alpha}{2}t + r_0 \tag{3.13}$$

where ω is the width of the active cell proliferation zone of the colony, r is the colony radius at time t, and r_0 is the radius at t = 0; α is the specific growth rate also known as μ (h^{-1}), which can be found from the Gompertz equation (Eq. 3.8). Thus, having the experimental data (the radius of the colony growth, the corresponding time, and μ), it is possible to calculate the width of the active zone or the width of the "ring" using Eq. 3.13. The results obtained in this study and the Pirt model are compared in Fig. 3.17.

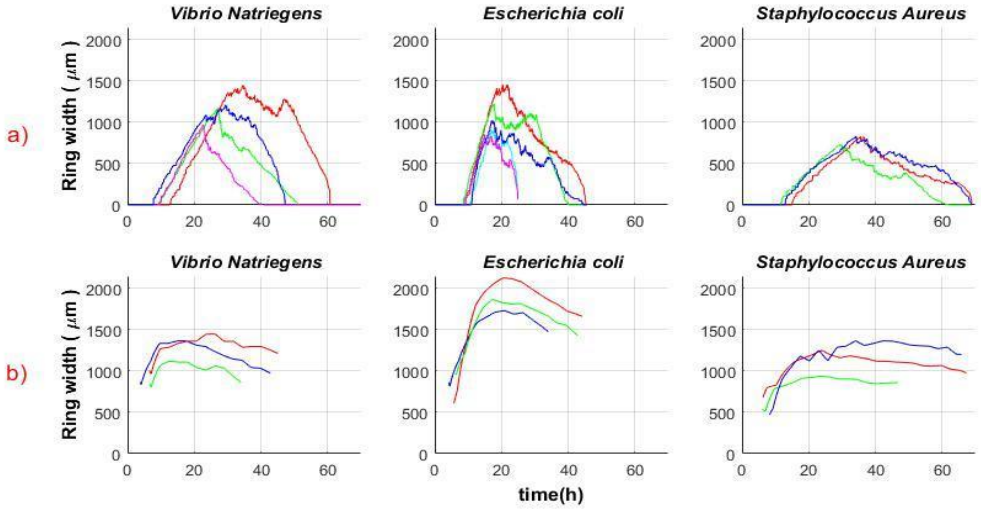

Figure 3.17. The width of activity "ring" as a function of time for different bacterial colonies; (a) width of activity "ring" determined by the speckle method; (b) calculated "ring" width using the Pirt model (Eq. 3.13). Parameters: alpha and r for the model are also obtained from speckle experiments. Each curve demonstrates the width of the activity "ring" over time of the one colony of a specific bacteria type.

The overall pattern of the ring width is unique and uniform for each bacterial species. However, the activity ring width dynamics of each colony of a microbial species might be shifted in time. For longer growing colonies, the proliferation and thus speckle activity of the colony retains its activity longer. It may be assumed that this is related to the distribution of the colonies on the plate. Since the bacterial colonies on the agar plates were distributed randomly, their growth was affected by the neighboring microbial colonies. The growth of microbial colonies is strongly affected by neighboring colonies in proximity, so the more near-neighboring colonies a given colony has, the earlier its growth ceases due to the depletion of common nutritional resources of the media [114,115].

To confirm the pattern in Figure 3.18 shows an example of part of a Petri dish with about 25 colonies. Each of the colonies after subpixel correlation analysis shows the formation of the activity ring effect described above.

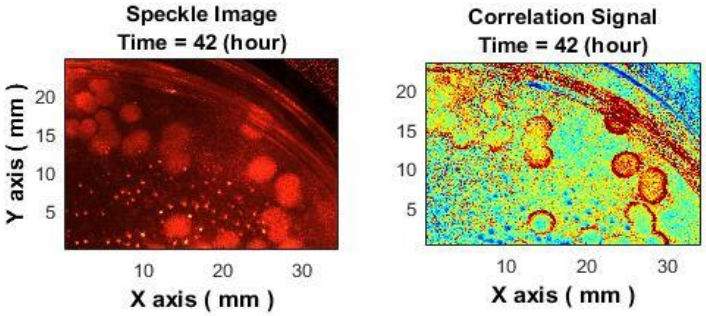

Figure 3.18. Demonstration of the ring effect on a part of a Petri dish with about 25 bacterial colonies

The Pirt model predicts that the actively growing edge of the microbial colony might be of similar width as measured by the speckle activity (compare Fig. 3.17, *V. natriegens* a and b), while it overestimates the width of the active edge of the microbial colony in the case of *E. coli* and *S. aureus.* It may be implied that the differences stem from the fact that growth rate α, h^{-1} in the Pirt equation is a constant, while in fact, it changes (decreases) during colony growth [111]. Another aspect to consider is that in both cases, experimental data were used for the calculations. However, as mentioned above, noise has influenced measurement accuracy.

3.9 Speckle pattern analysis against analysis under white light illumination

Colony imaging under white light illumination is a traditional microbial colony growth monitoring method. Thus, any new method should be benchmarked against it.

The images obtained by the laser speckle techniques are related to the fact that the rough surface produces many random reflections (are sensitive to changes on the surface itself) in the measurement field. Sensitive correlation subpixel analysis focuses on detecting these small changes. Accordingly, a growing colony leads to many changes that this analysis can detect.

If the measurement is performed under white light, situations with many random speckle patterns are not observed. Accordingly, correlation subpixel analysis, which is designed to detect small changes, will be less useful in this case. A colony growing under white light can be detected by changing the amplitude or statistical parameters. However, this will not allow the effects that can be observed with correlation subpixel analysis.

To compare these two technologies, measurements of colony growth were performed 1) under white light and 2) using laser speckle methods. Both experiments were carried out under the same conditions. The bacterium chosen for observation was *Escherichia coli*.

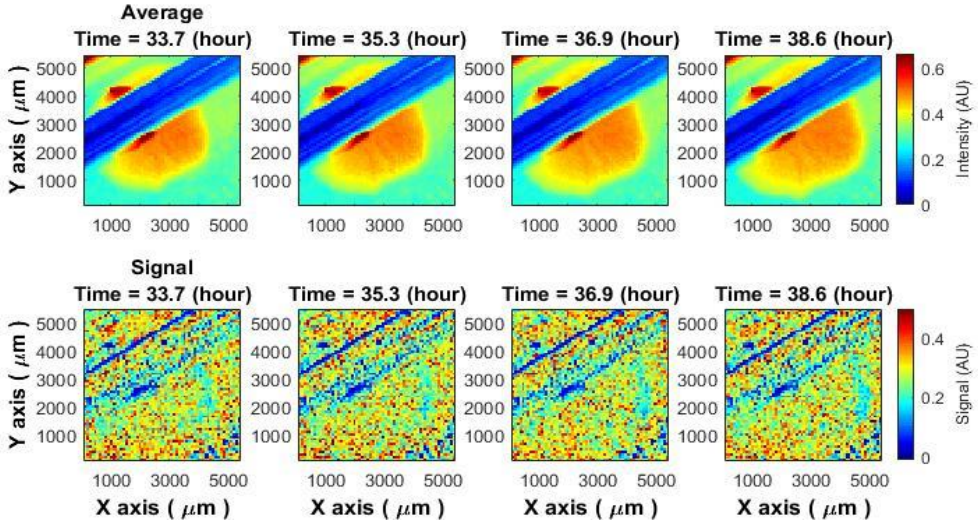

Figure 3.19. *Escherichia coli* colony growth under white light (top) and sub-pixel correlation analysis under white light (bottom). The blue structure of the picture series above is a wall of the cultivation chamber. The growth of the normal colony is visible in the lower part of the picture.

In the first experiment, colonies grew under white light illumination and subpixel analysis was performed. In this example demonstrated colony growth on agarised LB media. The results are shown in Fig.3.19.

To characterise the properties of the signal from white light or laser illumination, a place within the colony was chosen that was not directly in the center or on the edge of the colony but somewhere in the between. Two different signals - from the sub-pixel correlation algorithm: 1) under white light and 2) with the laser speckle technique were obtained and compared (Fig. 3.20 bottom). It can be noted that the sub-pixel analysis of laser speckle images allows to observe the behavior of the signal and the changes that occur with it, which can give additional info on colony characteristics. On the other hand - sub-pixel analysis of colonies under white light illumination - doesn't yield any signal pattern (Fig.3.20).

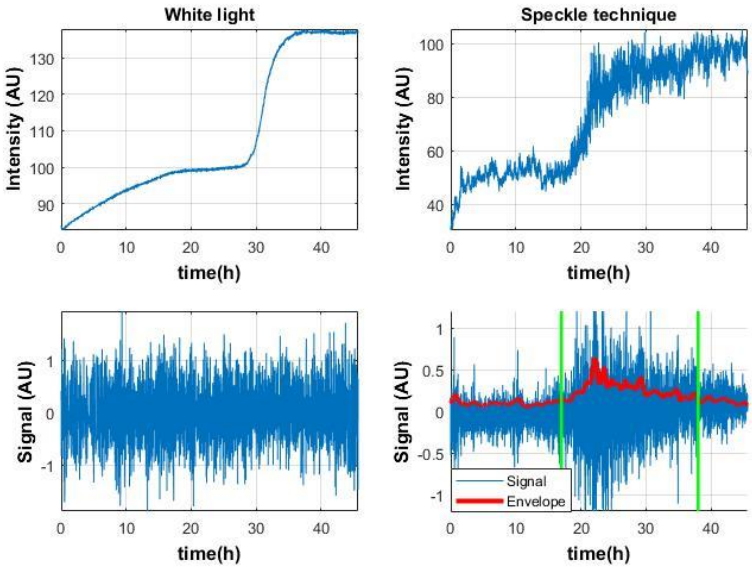

Figure 3.20. Intensity at the selected colony location under white light illumination (top - left). Signal obtained by the sub-pixel correlation algorithm at the same selected colony location under white light illumination (bottom - left). Intensity at the selected colony location by speckle technique (top–right). The signal obtained by the sub-pixel correlation algorithm at the same selected colony location by speckle technique (bottom - right).

The second experiment was to determine colony growth and activity using sub-pixel correlation analysis for images obtained by laser speckle techniques (Fig.3.21). Unlike white light analysis, the sub-pixel correlation analysis for laser speckle images detects the colony growth and additionally allows the observation of the effects inside the colony. These effects have been considered in subsection 3.8.

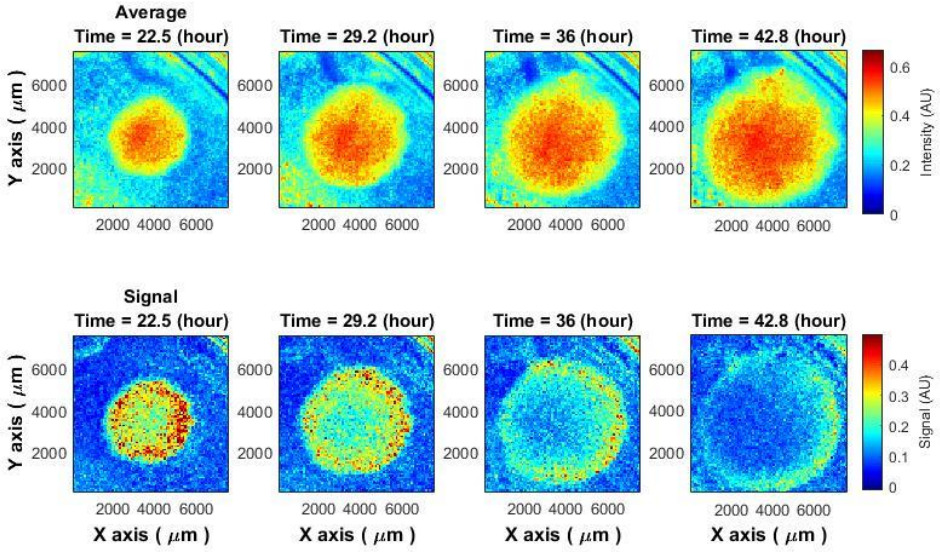

Figure 3.21. *Escherichia coli* colony growth over time (top) and the colony activity observed by sub-pixels correlation analysis (bottom) with laser speckle techniques.

It is clear from the signal obtained by the speckle technique that the signal rises, reaches a maximum, and then decreases (Fig. 3.20, bottom - right). The onset of colony growth when it becomes detectable by any technique (visual inspection or speckle analysis) is the "critical detection time", while the time from the beginning of the colony growth till the end of its growth - the duration of the activity. By using speckle analyses, the duration of the activity would be - the increase and decline of the signal, while the critical detection time - a time when the colony speckle signal becomes clearly distinguishable from the background noise.

While white light imaging clearly demonstrates colony growth, the sub-pixel correlation analysis method did not work under white light illumination. No colony growth, nor bacterial colonies were determined by sub-pixel correlation analysis under white light.

3.10 Chapter conclusions

The microbial colony growth was not affected by laser illumination, and the behavior of the growth curves obtained were highly similar to the behavior of the ones from the cultivation under white light.

The proposed method, based on the analysis of laser speckle patterns with correlation subpixel analysis, provides an earlier response of growing bacteria compared with classical CFU growth detection under white light illumination. Accordingly, it is possible to shorten colony detection time two or more times. Thus, speckle imaging offers an unprecedented analytic opportunity for CFU growth detection significantly earlier than visual inspection under white light.

The results (growing curves) demonstrate wide distribution, which can be attributed to unstable ambient temperature, which fluctuated across the experiments and, therefore, altered growth speed.
The speckle imaging method with sensitive correlation subpixel analysis revealed that distinct activity zone within the colony exist that migrate from the center to the edges during the growth of the colony. A similar pattern of activity zone ("ring") migration in the colonies was observed of three different microbial species. The migration speed of the “ring” varied across different microbial species reflecting the distinct growth rates characteristic of each microorganism. This promising, powerful technology has helped to visualise activity zones within the microbial colony. Previously, the presence of these zones was predicted mathematically.

4. LASER SPECKLE IMAGING FOR EARLY DETECTION OF ANTIBACTERIAL SUSCEPTIBILITY IN DISC DIFFUSION TESTS

Based on the posed aims and tasks, the fourth chapter of the Doctoral Thesis describes the application of the proposed analysis method for early detection of antibacterial susceptibility in disc diffusion tests as a research object. The chapter covers experimental confirmation of the capabilities of earlier detection of bacterial reactions to antibiotics and analyses the mathematical model of the inhibition (or sterile) zone size changing.

4.1 Introduction to the chapter

Rapid identification of antibacterial resistance plays a crucial role in treating acute infectious conditions such as sepsis and others. Empiric antimicrobial treatment must be replaced by pathogen-directed therapy as soon as possible to reduce patient mortality risk. Early identification of the pathogen and determination of its susceptibility to antibiotics can provide targeted pharmacological intervention at the early stages of the disease, increasing patient survival chances. This issue has become particularly relevant in treating elderly and immunocompromised patients. The EUCAST-standardized phenotypic resistance tests, such as disk diffusion and E-test, require 16-24 hours to obtain results [116]. Direct evidence of the sensitivity or resistance of the observed bacteria to the observed antibiotic is the manual measurement of the inhibition zone (if it has formed) using a ruler after a time interval determined according to the EUCAST standard.

At the same time, despite the widespread use in the detection of microorganisms by PCR method, the tests provide only genotypic information about antibacterial resistance, having limitations in the interpretation of antibiotic susceptibility results in gram-negative pathogens [117]. Therefore, new methods are needed that will allow for detecting changes in microorganisms faster than existing methods, significantly improving epidemiological work. Developing new, cost-effective methods for evaluating microbial activity to reduce detection time fully complies with the World Health Organization's (WHO) published Global Action Plan [118]. This is of great practical interest to technology developers and scientists.

The proposed technique of laser speckle imaging with correlation subpixel analysis allows for identifying dynamics and changes in the zone of inhibition (or sterile zone), which are impossible to observe with classical methods. Furthermore, it obtains the resulting zone of inhibition diameter earlier than the disk diffusion method, which is recommended by the European Committee on Antimicrobial Susceptibility Testing (EUCAST). These results could improve mathematical models of changes in the diameter of the zone of inhibition around the disc containing the antimicrobial agent, thereby speeding up and facilitating epidemiological analysis.

4.2 Comparison of the results obtained with the laser speckle technique without and with the algorithm

This subsection compares the behavior of the zone of inhibition for raw speckle images and for speckle images processed using subpixel correlation analysis. Two cases of bacterial susceptibility were considered: 1) bacteria that are susceptible to the antibiotic (Fig. 4.1) and 2) bacteria that are resistant to the antibiotic (Fig. 4.2).

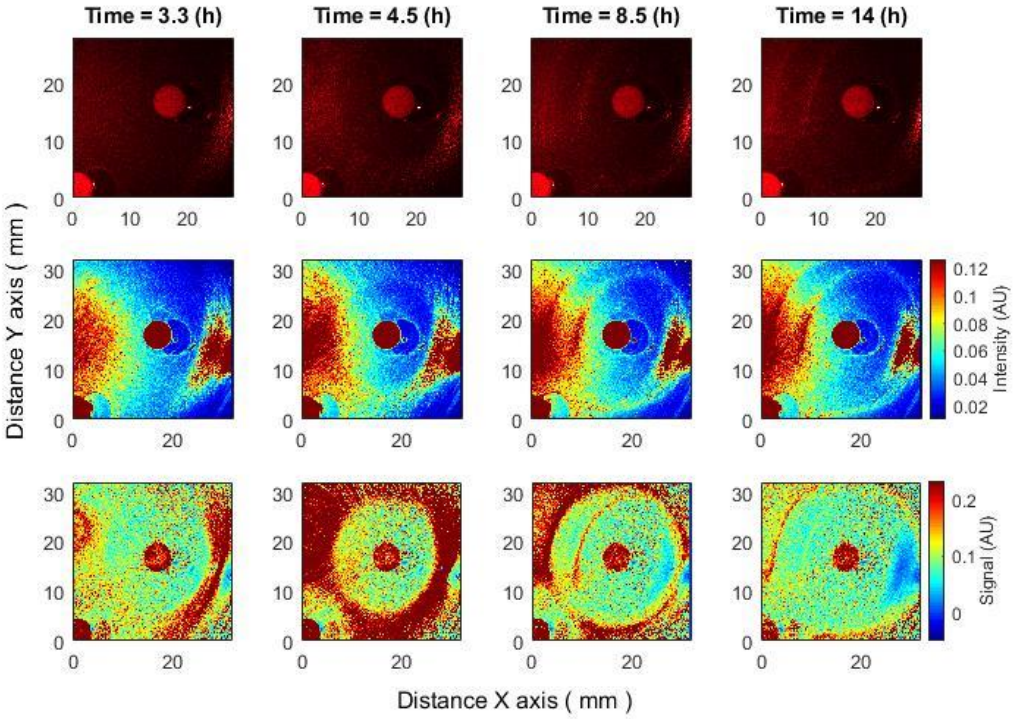

Figure 4.1. Changes of zone of inhibition as a function of time. Bacteria: *E. coli*, antibiotic CIP 5 μg. Recorded raw laser speckle images in time (top row), records processed by smoothing filter, and contrast enhancements (middle row) and resulting images after the subpixel correlation analysis (bottom row).

The correlation subpixel technique allows for the detection of submicron bacterial events (e.g., the formation of a zone of inhibition) earlier than without the algorithm (Fig. 4.1). It can be observed that by performing the subpixel correlation algorithm in the given experiment, the zone of inhibition can be detected after 3.3 hours, but without executing the algorithm, the zone of inhibition can be detected no earlier than after 4.5 or more hours.

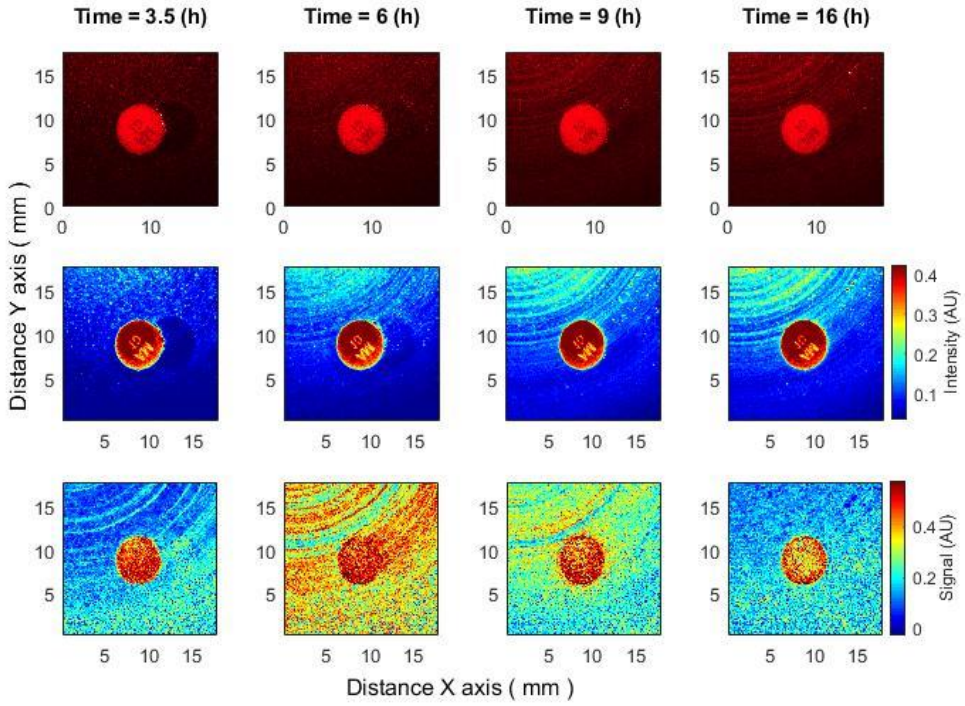

Figure 4.2. The behavior of bacteria that are resistant to antibiotics. Bacteria: *K. aerogenes*, antibiotic AM 10 μg. Recorded raw laser speckle images in time (top row), records processed by smoothing filter, and contrast enhancements (middle row) and resulting images after the subpixel correlation analysis (bottom row).

When the bacteria completely resist the antibiotic, raw speckle images and speckle images after subpixel correlation analysis will show that the zone of inhibition is not observed. However, since subpixel correlation analysis is designed to detect activity, there will be noticeable differences in bacterial behavior. Raw speckle images do not yet demonstrate the presence of bacteria (3.5 hours). Speckle images after subpixel correlation already detect it. That is, the activity of bacteria already exists. In the images showing data analysis using subpixel correlation analysis (i.e. Fig. 4.1-4.4, bottom row and Fig. 4.5-4.7, both top and bottom row), the blue color indicates low spatiotemporal activity, while red color indicates high bacterial activity. It is also worth noting that the antibiotic is in red color, that is, some processes take place on it, but these are chemical processes not related to the behavior of bacteria. The second interesting result is that raw speckle images still show the presence of spatiotemporal activity at late times (16 hours), while speckle images after subpixel correlation do not detect them. That is, bacteria are present but do not demonstrate activity (do not grow).

Another intriguing outcome can be observed when the bacteria are completely resistant to the antibiotic based on raw speckle images and the zone of inhibition is not observed at all, while the subpixel correlation analysis demonstrates the formation of a zone of inhibition (Fig. 4.3). This indicates that in some situations the zone of inhibition may form even if it is not detected by the "naked eye" at all and the described method is able to detect such situations.

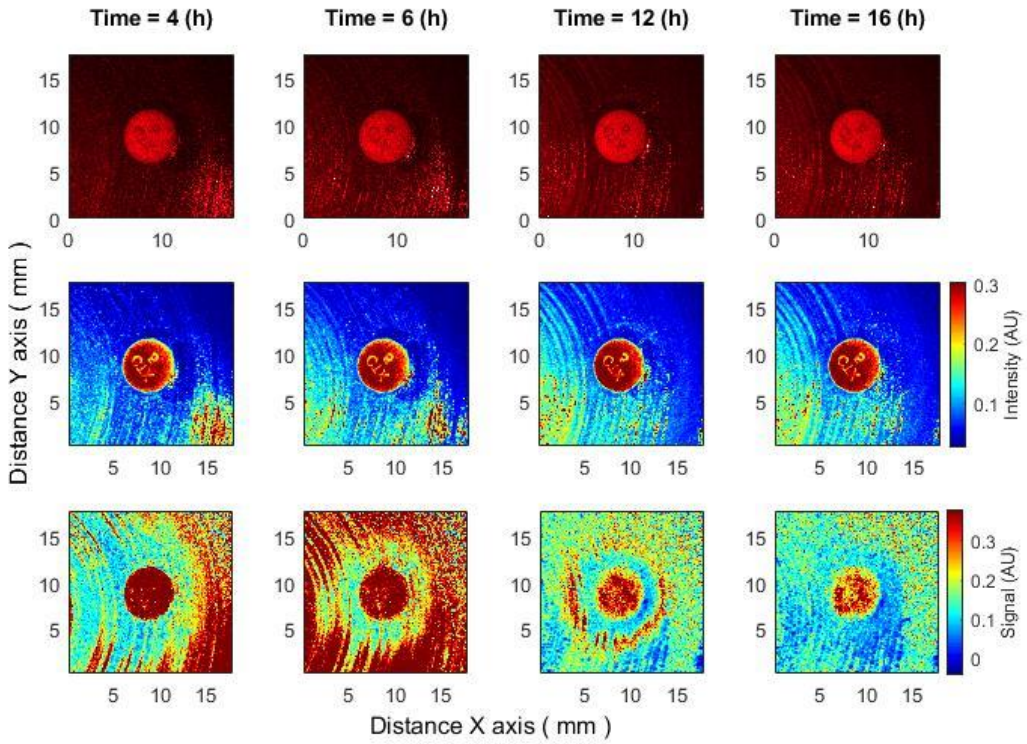

Figure 4.3. The behavior of bacteria on raw speckle images does not demonstrate the zone of inhibition, while the subpixel correlation analysis demonstrates the formation of a zone of inhibition. Bacteria: *K. aerogenes*, antibiotic CTX 5 μg. Recorded raw laser speckle images in time (top row), records processed by smoothing filter, and contrast enhancements (middle row) and resulting images after the subpixel correlation analysis (bottom row).

4.3 Early detection of the formation of a zone of inhibition

In cases where a zone of inhibition is formed, it becomes noticeable after 3-4 hours from the beginning of the experiment. It appears "suddenly", immediately possessing a certain radius. The question arises: what processes cause this sudden zone to appear? New experiments were conducted to understand these processes better. In previous experiments, bacteria were inoculated on agar medium in a Petri dish, and antibiotic discs were immediately placed on the prepared surface. In the new experiments, the antibiotic discs were placed on the surface 4-4.5 hours after the bacteria inoculation.

Bacterial activity using the correlation subpixel method can be detected 3-4 hours after inoculation (chapter 3). Until then, the signal level is very low. The zone of inhibition is noticeable only in contrast to the activity of bacteria; accordingly, it also cannot be visible until this moment. Since after 3.5-4 hours, the bacteria have grown to a sufficient concentration to obtain a signal from bacterial activity with the established method, it is expected that application of antibiotic discs 4-4.5 hours after bacterial inoculation would immediately allow the detection of the formation of the zone of inhibition.

This effect can be observed in a signal proportional to activity, i.e., after subpixel correlation analysis. When observing raw speckle images, then this effect may not be noticeable since it is not the activity of bacteria that is observed there but their presence. Bacteria are already present for several hours, and when the antibiotic disk is placed, they begin to "lose" activity. Hence, raw speckle images still do not demonstrate the formation of a zone of inhibition, while it is observed using subpixel correlation analysis of laser speckle images (Fig. 4.4).

Thus, using subpixel correlation analysis of laser speckle images, it is possible to measure the formation of a zone of inhibition already 1-1.5 hours after the time when the antibiotic was placed on already grown bacterial cultures. What is important is that the zone of inhibition did not appear "suddenly" but was formed with a small radius, continuously increasing, which can be explained by the spread of the antibiotic in the agar.

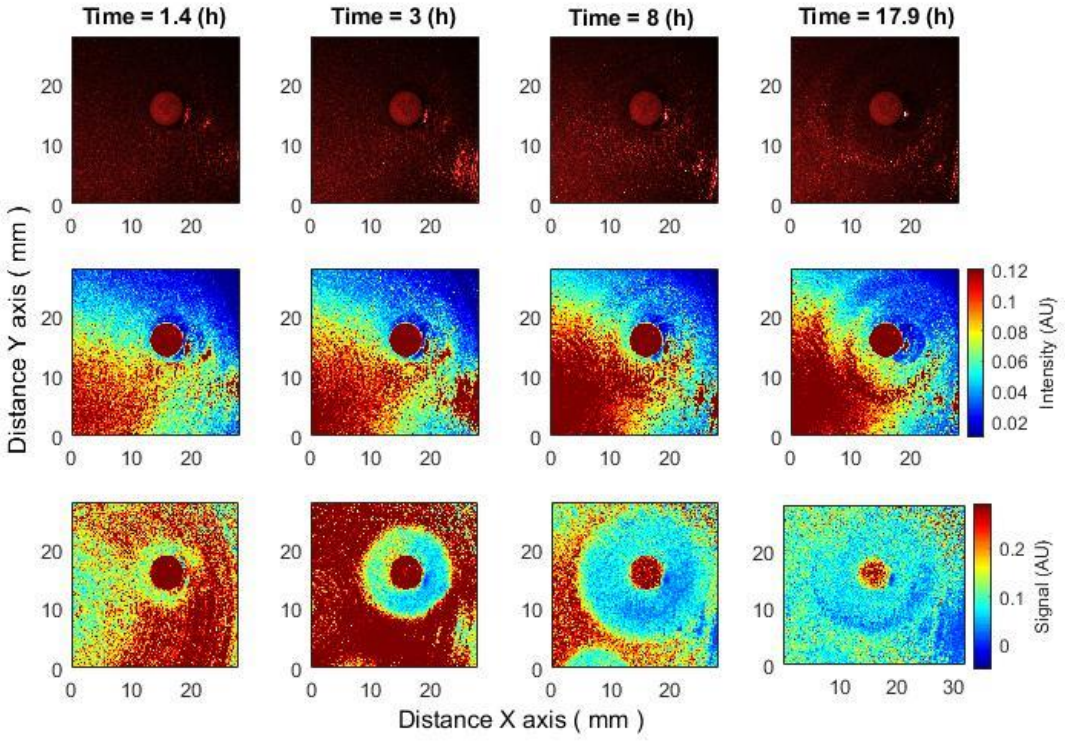

Figure 4.4. Antibiotics are placed 4-4.5 hours after bacteria inoculation. The zone of inhibition changes as a function of time. Bacteria: *E. coli*, antibiotic CIP 5 μg. Recorded raw laser speckle images in time (top row), records processed by smoothing filter, and contrast enhancements (middle row) and resulting images after the subpixel correlation analysis (bottom row).

4.4 Spatiotemporal analysis of the changes of the inhibition zone

It was obtained that after a few hours from the start of the experiment, an inhibition zone began to form around the antibiotic. The zone of inhibition becomes clearly visible within a

couple of hours after the beginning of formation. The result was obtained significantly earlier than by the disk diffusion method for the same bacterial species. The formation of a zone of inhibition is characterised by a decrease in activity. This means identifying a drop, defined as occurrences of low values following peaks in the signal envelope. It should be considered that detecting low signal values in noisy environments is more difficult than detecting high values. To avoid the influence of noise, it is worth averaging the signal envelopes over each radius as it moves away from the center (from the antibiotic). Consider one averaged signal envelope for each radius.

$$\overline{Env[r,n]} = \left[\frac{1}{M_{R1}}\sum_{m_{R1=1}}^{M_{R1}} Env_{m_{R1}}[n], \dots, \frac{1}{M_{Rk}}\sum_{m_{Rk=1}}^{M_{Rk}} Env_{m_{Rk}}[n]\right] \quad (4.1)$$

where M_{Rk} is the number of envelope signals at a given distance/radius from the center.

Consider the time when the signal envelope starts to drop as a function of time for several received radii. Note that the beginning of the signal envelope drop might indicate the appearance of a zone of inhibition in this place. Whereas in the situation where antibiotics are placed without bacteria such behavior was not found (Fig. 4.8).

Putting the averaged signal envelopes for all radii together, a spatio-temporal image can be obtained. This image enables the analysis of the behavior of the zone of inhibition. By emphasising the drop at each radius, a specific curve can be derived, representing the changes in the size of the zone of inhibition over time (Fig. 4.5). This behavior has been observed in several different experiments for different species of bacteria using different antibiotics.

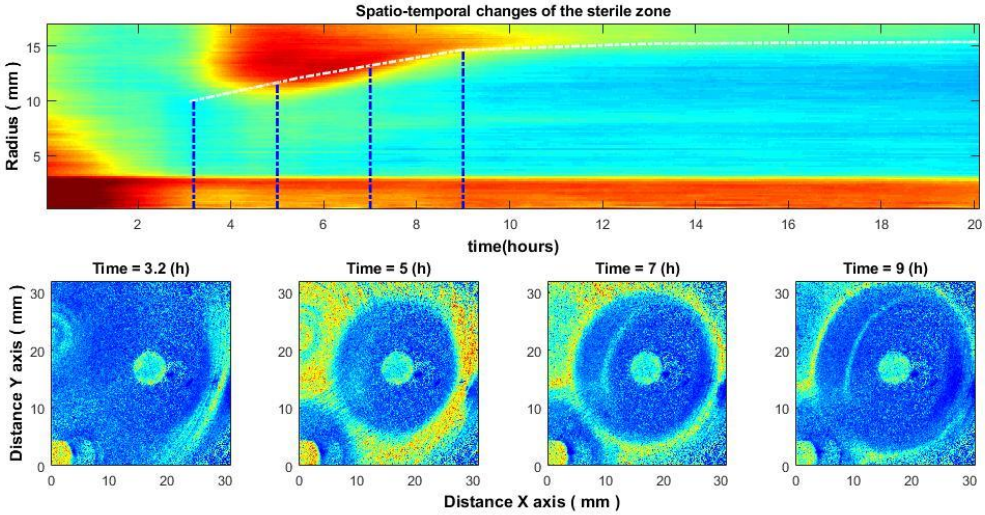

Figure 4.5. Spatio-temporal changes of the zone of inhibition (top), and zone of inhibition formation in the growth of bacteria around the antibiotic disc (bottom). Bacteria: *E. coli*, antibiotic CIP 5 μg. Antibiotics were placed on the Petri dish immediately after bacteria inoculation.

Fig. 4.5 illustrates the case of bacteria susceptible to antibiotics. Antibiotics were placed on the Petri dish immediately after the bacteria inoculation. It can be observed that there is no space-time reaction before 3.5-4 hours. This is due to the reason described above - the activity of bacteria is not noticeable; accordingly, the zone of inhibition is not visible. Consider similar

images when the antibiotic was placed on the Petri dish 4-4.5 hours after the bacteria inoculation (Fig. 4.6). Then there is no such "gap," and the spatio-temporal image is continuous.

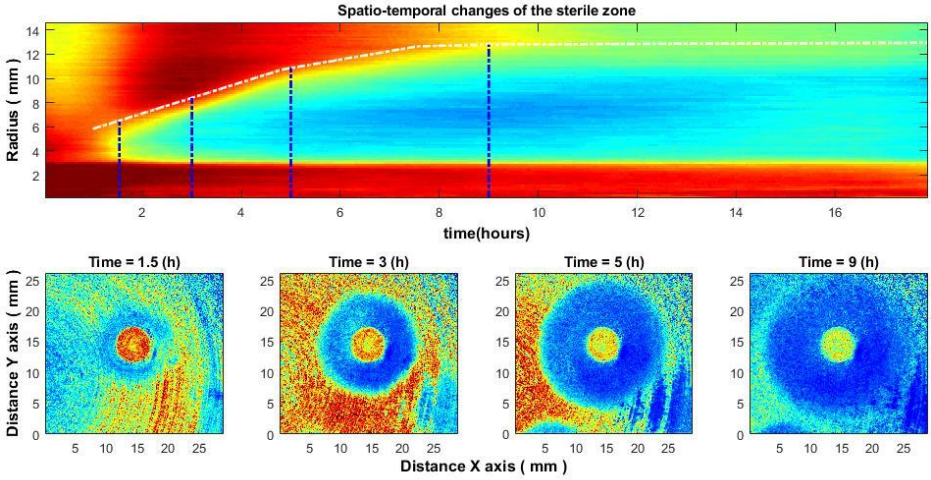

Figure 4.6. Spatio-temporal changes of the zone of inhibition (top) and zone of inhibition formation in the growth of bacteria around the antibiotic disc (bottom). Bacteria: *E. coli*, antibiotic CIP 5 μg. Antibiotics were placed on the Petri dish 4-4.5 hours after the bacteria inoculation.

For reference, experiments were performed with antibiotic diffusion discs placed on agar without inoculated bacteria. In such cases, the zone of inhibition was not observed (Fig. 4.7). This indicates that diffusion of the antibiotic without the presence of bacteria cannot be observed with the established method.

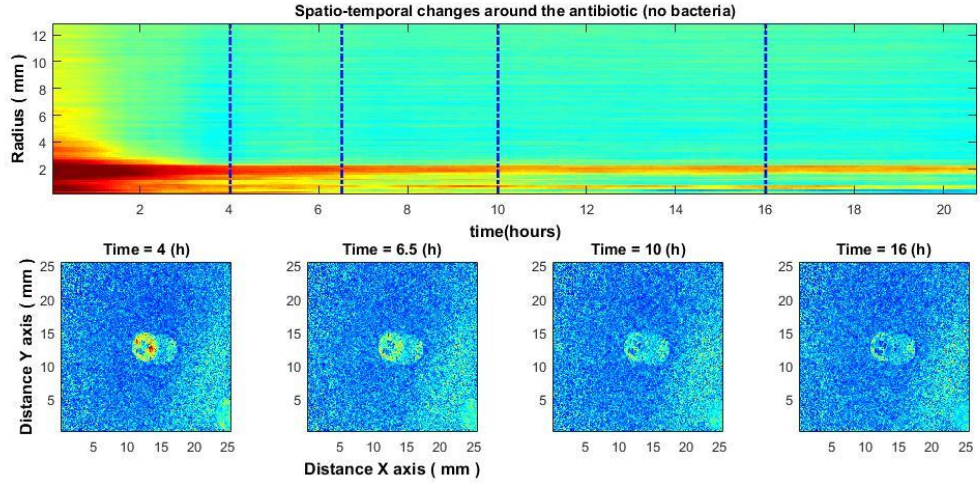

Figure 4.7. Experiment without bacteria. Spatio-temporal image of the area around the antibiotic AK 30 μg (top) and the spatial zone around the antibiotic at different times (bottom).

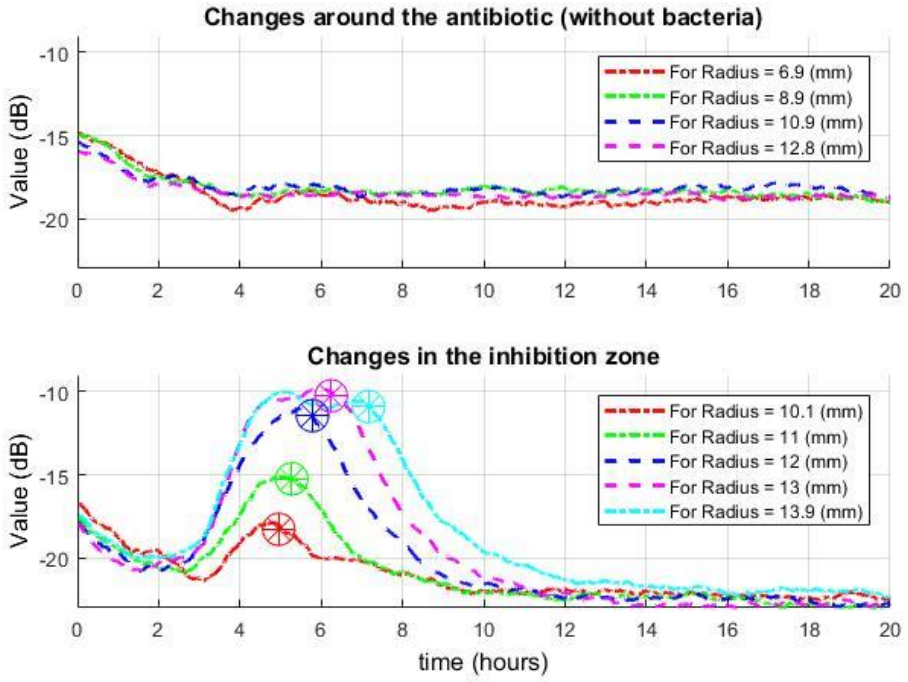

Figure 4.8. Change of signals envelope over time for several different radii around the antibiotic: without bacteria (top row) and with bacteria (bottom row). On the bottom graph, it is observed that as it moves away from the center, the drop (which means the appearance of a zone of inhibition in this place) occurs later (stars in a circle).

Having also analysed the signal in the time-frequency domain (spectrogram) (Eq. 3.4-3.5), it can be noted that as it moves away from the antibiotic, the energy level decreases (which means the appearance of a zone of inhibition in this place) occurs later, and also the signal becomes more high frequency, (spectrograms in Fig.4.9). This behavior is correlated with the averaged signal envelopes for the corresponding radii (Fig. 4.9 "Change in the zone of inhibition ").

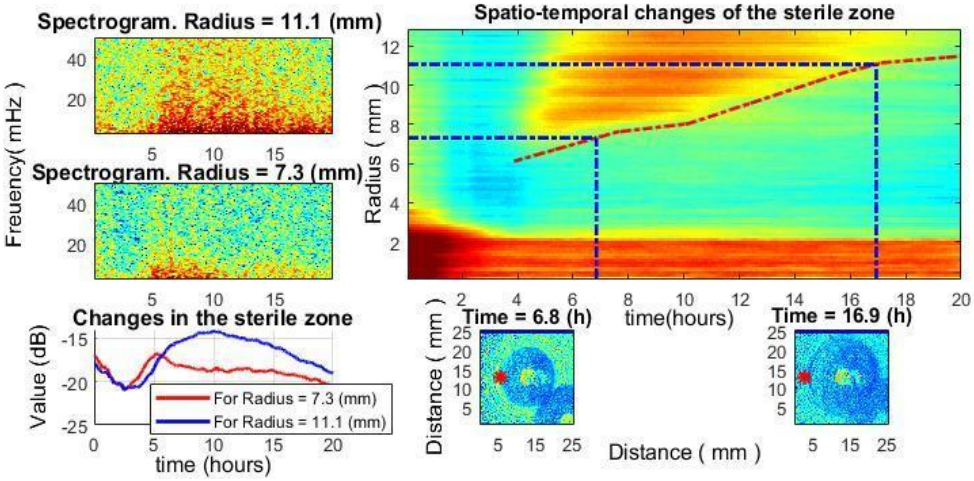

Figure 4.9. The growth of S. aureus around the Cefoxitin 30 μg disc. 1) Spatio-temporal changes of the zone of inhibition (top-right). Spatiotemporal inhibition zone growth curve (red). The blue lines in the direction to down indicate the times at which the disk images were taken. The blue lines in the direction to the left indicate the radii at which the spectrograms were taken. 2) Inhibition zone formation (2 time points) (bottom-right and bottom-center). The red stars indicate where the spectrograms were taken from. 3) Spectrogram for signal in near and in far radius from antibiotic (2 radius points). 4) Change of signal envelope over time for 2 different radii around the antibiotic (bottom-left).

4.5 The radius of the inhibition zone for different bacteria species

To study the change in the radius of the inhibition zone, several different bacteria species were used, which reacted to different antibiotic types. Spatiotemporal curves were obtained.

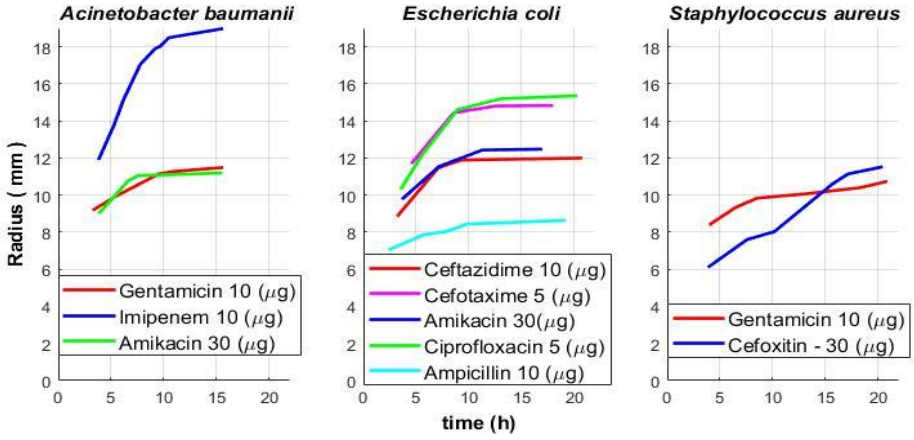

Figure 4.10. Spatio-temporal curves for different bacteria species as a response to different types of antibiotics.

From Figure 4.10, it can be seen that different types of antibiotics cause different reactions in the same bacteria species. That is, the radius of the inhibition zone and/or the growth rate of the inhibition zone for the same bacteria species are different for different antibiotics, as expected.

4.6 Mathematical model of the inhibition zone size changing

The agar diffusion analysis - a method for assessing the ability of antibiotics to inhibit bacterial growth. The minimum inhibitory concentration (MIC) in solid media is usually determined using the agar diffusion technique [119]. Antibiotic diffusion into the agarose medium leads to the inhibition of bacterial growth and the formation of inhibition zones. The diameter of inhibition zones increases with increasing antibiotic concentration.

It is possible to obtain a model of inhibition zone radius growth as a function of time [120]. The radius of the inhibition zone is proportional to the root square of the difference between the natural logarithm of the antibiotic concentration c and the natural logarithm of the MIC, multiplied by the diffusion coefficient and the time of antibiotic diffusion (Eq. 4.2).

$$r = \sqrt[2]{4D(\ln(c) - \ln(\mathrm{MIC})) \cdot \mathrm{t}} \tag{4.2}$$

where c is antibiotic concentration, and D is the diffusion coefficient received from Fick's second law of diffusion [121] (Eq. 4.3).

$$\frac{\partial c(x,t)}{\partial t} = D \frac{\partial^2 c(x,t)}{\partial x^2} \tag{4.3}$$

Fick called this coefficient: "a constant dependent upon the nature of the substances." Parameter c(x,t) describes the dependence of antibiotic concentration on time and on distance from the source. This approach has been applied to studies of two-dimensional diffusion of dyes and antibiotics, most notably penicillin [122], where it was assumed that D is independent of concentration. A newer study, such as [120] for agar diffusion assay of antibiotics to inhibit bacterial growth, is also based on these formulas and on the assumption that D is independent of concentration. Then, the authors consider the loss of antibiotics during diffusion and provide higher accuracy of the MIC, which was determined by the proposed new dissipative diffusion models for several antibiotics.

Thus, this model involves three unknown variables: MIC, D, and c. Their total influence in the formula can be replaced by one constant (in which it is also worth adding the number 4). Thus, a simple relationship is obtained between the radius of the zone of inhibition and time (Eq. 4.4).

$$r = \sqrt[2]{\mathrm{const} \cdot \mathrm{t}} \tag{4.4}$$

Having obtained the experimental curves, it is possible to choose the parameter of this constant, at which it will be as close as possible to the model. Then compare how much, in this case, the shape of the experimental curves corresponds to the shape of the curves from the model.

To compare the change in the theoretical and experimental growth curves of the zone of inhibition, several different bacterial species were used that reacted to different types of antibiotics. Consider the same bacterium: *E. coli*, and the same antibiotic: Ciprofloxacin, but for two different cases: 1) the antibiotic is placed immediately after the bacteria (almost simultaneously) (Fig. 4.5); 2) the antibiotic is placed 4.3 hours after the bacteria (Fig. 4.6). The results are presented in Fig. 4.11.

For each sensitive bacterium, these curves will be different. It is necessary to find the set of parameters for each bacterium against each antibiotic. In the case of resistant bacteria, these curves might be unpredictable and then approximations will not work here.

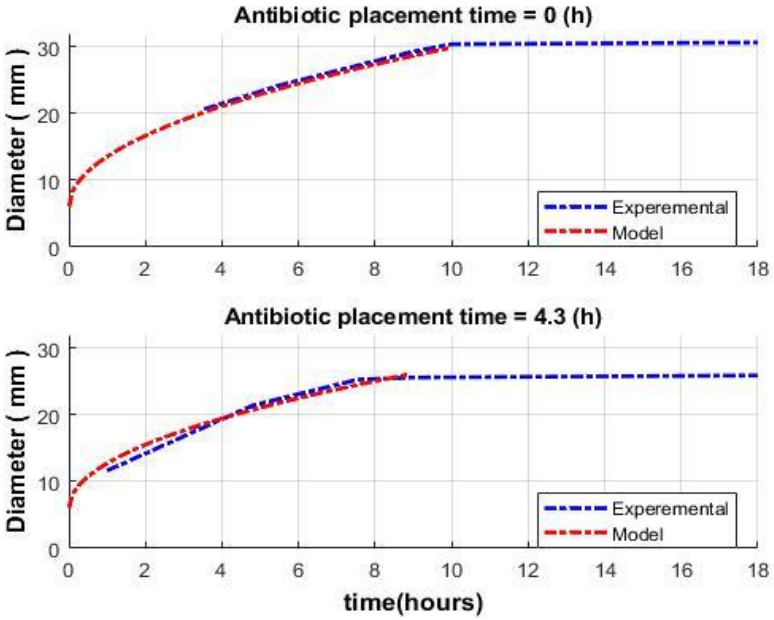

Figure 4.11. Spatio-temporal curves for experimental data and model for E. coli around the Ciprofloxacin disc (5 μg).

4.7 Chapter conclusions

In this chapter the clinically significant dynamics and changes of the zone of inhibition were evaluated by the processing of laser speckle images with the correlation subpixel analysis. The zone of inhibition is the "absence of signal;" accordingly, it can be detected on the "signal presence" background, that is, only when the bacteria are already visible (after 3-4 hours) when the surface density of bacteria increases to the level necessary for observation. However, if the antibiotic is placed on the Petri dish 4-4.5 hours after the bacteria inoculation, the bacteria are in sufficient concentration to be visible with the subpixel correlation method. In this case, the formation of the zone of inhibition becomes clearly visible almost immediately. While observing unprocessed (raw) speckle images in this case, the zone of inhibition is not immediately visible, but after a delay of several hours (approximately 5 hours delay). A case was observed where bacteria determined to be fully resistant to antibiotics using the conventional method could show a formation of a zone of inhibition when analysed using subpixel correlation analysis on laser speckle images (Fig. 4.3). This demonstrates that the established method allows the detection of small changes in activity that cannot be observed in the raw data. Hence, when developing a novel assay that deviates significantly from the current reference standard, it is crucial to consider various factors influencing antibiotic responses.

Many broad-spectrum antibiotics are given at intervals of 6 to 8 hours, allowing clinicians to reassess the choice of antibiotics based on the patient's condition. Future advancements in identification and antibiotic susceptibility testing (ID/AST) methods should focus on providing results within this time frame of less than 6 hours, enabling timely adjustments in antibiotic therapy to optimise patient care [123].

The accuracy of the proposed mathematical model of inhibition zone growth curves demonstrated in this chapter is verified in comparison with experimentally obtained curves. The approximation, fitted to the observed case, describes well the experimental curves obtained. For each sensitive bacterium, to determine the radius of the inhibition zone early, these curves will be different, and it is necessary to find the set of parameters for each bacterium against each antibiotic. Thus, the effort put into the determination of these parameters will contribute to the development of an algorithm that allows predicting the change in diameter of the inhibition zone around the antibiotic disk much earlier than using the standard disk diffusion method. However in the case of resistant bacteria, these curves might be unpredictable and then approximations will not work here. Accordingly, it is worth paying attention to other forecasting methods, for example, based on artificial intelligence.

5. APPLICATION OF AN ARTIFICIAL NEURAL NETWORK TO ANALYSE SPECKLE DATA TO CLASSIFY GROWING AND NON-GROWING COLONIES AND ZONES

Based on the posed aims and tasks, the fifth chapter of the Doctoral Thesis describes using artificial intelligence (artificial neural network) to analyse speckle data before and after the correlation subpixel analysis (proposed and described in previous chapters). This is done in order to classify between growing (active) colonies and not growing, or between zones of active growth and not growing (inhibition zones) around the antibiotic's discs. The chapter covers experimental confirmation of the capabilities of classification of growing / non-growing bacterial colonies, and also between inhibition and active bacteria growth zones around the antibiotic's discs using a neural network.

5.1 Introduction to the chapter

In biological tests centered on microbial growth analysis, the ability to detect when it ceases to grow can be important.

Laser speckle imaging can detect and monitor microbial presence, but without additional image processing, it lacks the capability to visualise zones of activity (growth). It also can't determine when the bacteria becomes inactive. Although the microorganisms are observed, their activity status, growing or non-growing, remains unknown. To distinguish areas with and without bacteria, a change in the statistical properties of the environment suffices. To classify an observed bacteria as either growing or non–growing, one needs to employ the described in the previous chapters subpixel correlation algorithm.

In the current chapter, two types of data are used: 1) laser speckle imaging without the utilisation of a subpixel correlation method, serving to identify the presence of a bacteria, and 2) laser speckle imaging integrated with a sensitive subpixel correlation algorithm, which ascertains the status of bacterial activity: growing or not. Utilising these datasets, both the location and the growth status of the microorganisms can be determined. The present chapter substantiates the capability of laser speckle imaging to categorise colonies (or zones with microorganisms) as growing or non–growing, a nonvisible parameter observed under white light illumination. Additionally, the subpixel correlation algorithm identifies the moment at which the microorganisms cease to grow. This analytical capability is instrumental for investigating the influence of chemical agents, such as drugs and antibiotics, on the dynamics of bacterial growth.

In a number of studies, the classification of zones of inhibition and zones of active growth of bacteria is performed upon reaching the zones of inhibition of the full area, for example, 24 h after the bacteria incubation. For the purpose of automating the classification of colonies (or zones with microorganisms) as either 'growing' or 'non–growing,' various algorithmic tools may be employed. These may include Linear Classifiers, Logistic Regression, Quadratic Classifiers, and Bayes Classifiers, among others [124]. For example, the study [125] for classifying bacterial regions based on laser speckle techniques using correlation values offers principal component analysis (PCA) and k-means clustering were exploited. Despite the fact that their

study demonstrates a good result, since the current study does not consider individual correlation values at a specific time from incubation but entire signals that very differ at different times from incubation, it was decided to use neural networks. A recent review study claims that the predominant selection for image classification and identification of bacterial species over the last decade are Convolutional Neural Networks (CNNs) [126]. CNNs are preferred for their superior computational efficiency with respect to calculations of model weights and bias values by which the model is optimised. For image classification aims, CNN is one of the popular types of neural networks [127]. For these reasons, neural networks were decided to be used. However, since in the current study, the analysis is performed not with images but with signals, a simpler version of neural networks was chosen, allowing the main emphasis to be placed on preprocessing and postprocessing. Having demonstrated the classification capabilities, a more detailed investigation of suitable machine learning tools will be carried out in the future.

Two types of algorithms are used in the current chapter:

The first algorithm is spatial averaging over a window of NxN pixels, and then the signal envelope with a certain window is used. Both of these procedures can reduce temporal and spatial noise. That is, this algorithm is almost raw data with spatial and temporal smoothing.

The second algorithm is described in detail in Chapter 3. This is converting a sequence of NxN pixels sections of images into signals. After which smoothing is also performed.

5.2 Tools for classification of growing / non-growing bacterial colonies

5.2.1 Colony analysis with laser speckle technique almost without additional processing (with spatial and temporal smoothing)

Correlation subpixel analysis, as outlined in Chapter 3, allows to reveal that colony growth is primarily driven by microbial proliferation at the colony's periphery. Images procured via laser speckle technique, when unaccompanied by correlation subpixel analysis, are insufficient for observing the ramifications of internal changes within the colonies.

To demonstrate the results of laser speckle imaging almost without additional processing (the first algorithm), one may consider a measurement of a bacterial colony recorded over a span exceeding 100 hours. In the initial 45 – 50 hours, the colony exhibits active growth. Subsequent to this phase, growth arrest occurs, presumably owing to nutrient depletion as a consequence of the expansion of the colony and the proximity of adjacent colonies. Examination of the colony's cross-sectional diameter as a function of time reveals certain growth dynamics (refer to Figure 5.1, top and middle rows). Initially, bacterial cells are observed at the colony's center, following which they manifest at increasing distances from the center. Upon attaining a specific diameter, the colony ceases to grow. While the images confirm the bacterial presence throughout the occupied diameter, they fail to elucidate the specific physiological state of the bacteria, i.e., whether they are in a state of growth or stasis.

Further insights can be gained by analysing the curves representing intensity levels at varying distances from the colony's center (Figure 5.1, bottom row).

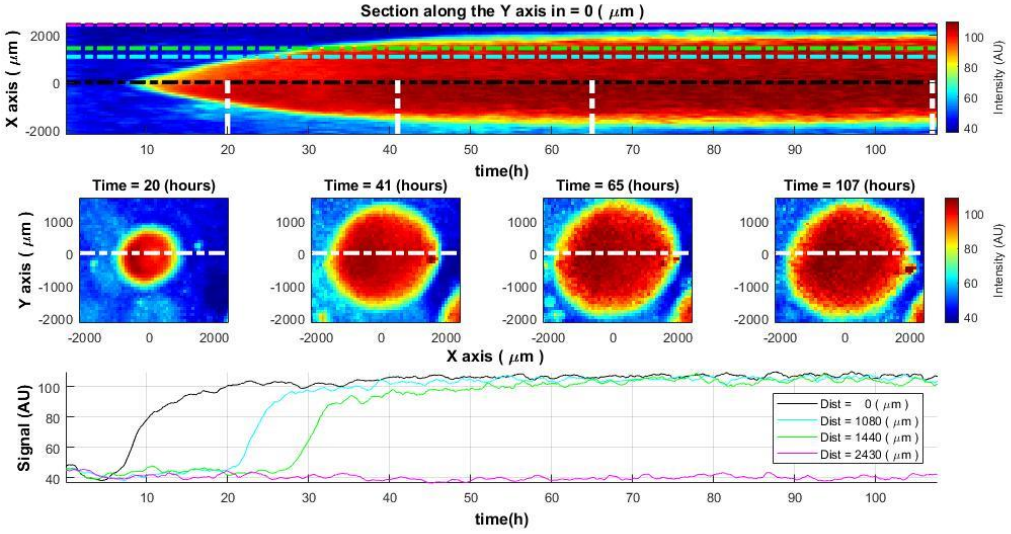

Figure 5.1. Spatiotemporal distribution of the laser speckle reflectance intensity across *V. natriegens* colony. The change of colony cross-sectional intensity over time (top) and colony size at specific time moments (middle row). The white lines in the top image define the time of the cross-section demonstration in the middle row images. Lines of different colors in the top and bottom images indicate the measurement of intensity level at the colony's center and at different distances from the colony center (bottom).

These curves depict an increment in intensity at distinct temporal intervals, contingent on the distance from the center. Once a specific intensity level is reached, it remains relatively constant. This information, however, does not furnish sufficient evidence to deduce the ongoing biological activities within the colony

5.2.2 Laser speckle technique with subpixel correlation analysis reveals growth changes within the colony

Alterations in the growth dynamics within a bacterial colony - whether spatial movement, increasing activity, or halt of the proliferation - can be effectively discerned by integrating laser speckle imaging techniques with correlation subpixel analysis (the second algorithm). Consequently, if a bacterial colony cease to grow at a certain juncture, this cessation is readily detectable. Such a halt in growth could be attributable to factors such as nutrient depletion in the media [114, 115] or the impact of external variables, like the presence of inhibiting compounds, including antibiotics.

Upon conducting subpixel correlation analysis, one can observe specific growth patterns within the colony across its diameter as a function of time (Figure 5.2, top and middle rows). Initially, bacterial activity is localised at the colony's center, expanding radially over time. Observations indicate that once a specific diameter is attained, growth arrests. Concurrently, the associated signal indicative of bacterial growth begins to attenuate and ultimately vanishes. Understanding that the signal is indicative of bacterial growth, it becomes clear that the growth of the colony has ceased.

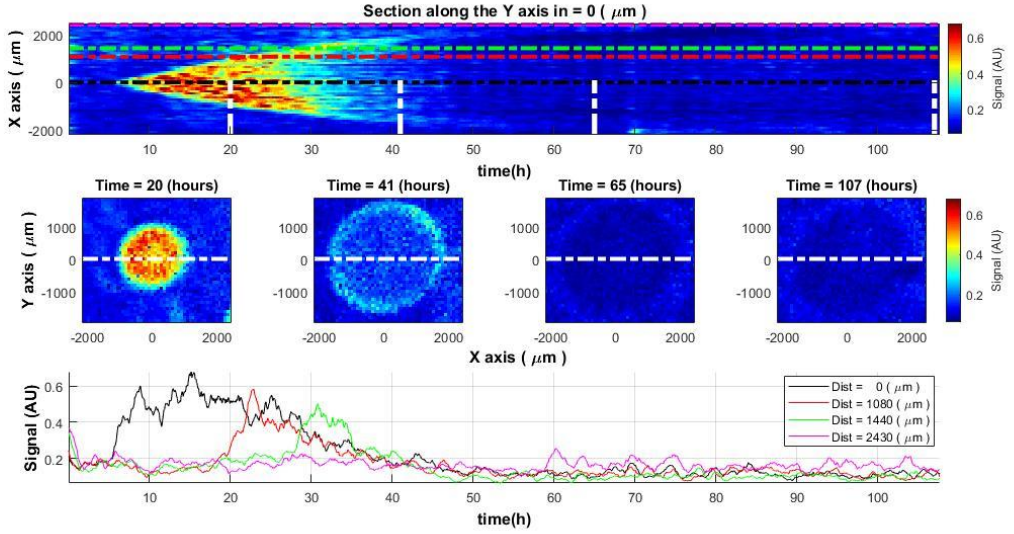

Figure 5.2. Spatiotemporal distribution of the activity signal across *V. natriegens* colony. The change of colony cross-sectional activity signal over time (top) and colony activity signal at specific time moments (middle row). The white lines in the top image define the time of the cross-section demonstration in central images. Lines of different colors in the top and bottom images indicate the measurement signals at the colony's center and at different distances from the colony center (bottom).

Examining signal curves along the temporal axis at various distances from the colony's center (Figure 5.2, bottom), one notes that bacterial growth (manifested as high signal values) migrates outward from the center. At first the strongest signal is observed at the center and diminishes as the distance from the center increases. Furthermore, the signal diminishes over time and vanishes approximately 45 – 50 hours into the initiation of the experiment, corresponding to the cessation of bacterial growth within the colony.

To verify the consistency of the aforementioned effect, analyses were conducted on 15 – 20 bacterial colonies.

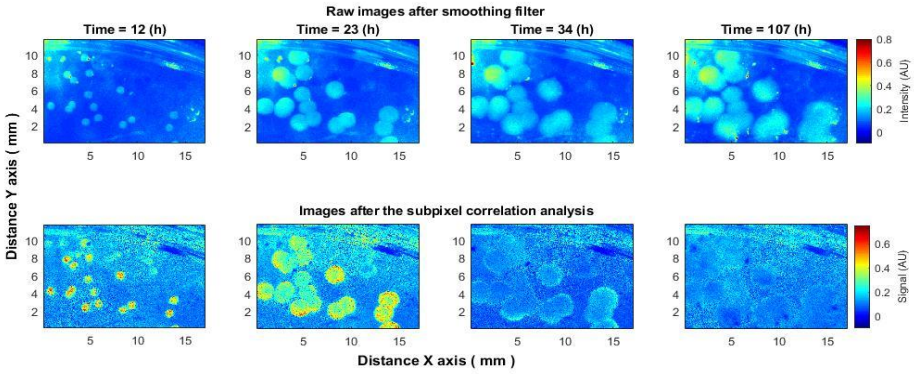

Figure 5.3. Laser speckle reflectance intensity images (top) and corresponding activity signal images (bottom) captured from 15-20 *V. natriegens* colonies at various time points during the incubation period.

Analogous behavior was discerned across all colonies. Elevated activity was observed in the initial hours of the experiment (Figure 5.3), followed by the 'ring' (chapter 3), after which activity ceased.

The observed behavior was consistent across different experiments and bacterial species, such as *E. coli* and *S. aureus*. Additional experiments were conducted where bacteria were dispersed across an entire Petri dish, covering species like *Klebsiella pneumoniae*, *Enterobacter cloacae*, and *Staphylococcus. aureus*. Using either raw or minimally processed speckle images (after spatial smoothing), the appearance and spread of bacteria could be observed. However, correlation subpixel analysis offered further insights: 1) It detected the presence of bacteria earlier than could be seen in raw speckle images (Figure 5.4, (4 hours)); 2) It captured a peak in activity that was not visible in raw images (Figure 5.4, (7 hours)); 3) It observed a decrease in activity that also was not visible in the raw images (Figure 5.4, (14 hours)). This behavior was consistent across all tested bacterial species, suggesting that the observed effects are neither random nor isolated but constitute a recurring phenomenon applicable across different bacteria.

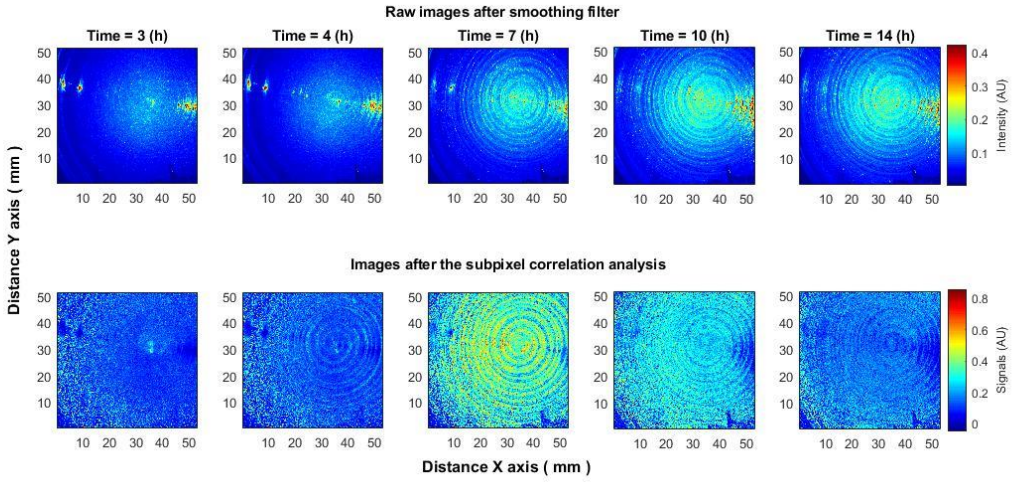

Figure 5.4. Bacteria *Klebsiella pneumoniae* put on the entire Petri dish. The subpixel correlation analysis of laser speckle images (bottom row) detects the appearance of bacteria earlier than raw speckle images (top row). Also increase (7 hours) and decrease (14 hours) of activity using subpixels correlation analysis can be observed, which is not visible on raw speckle images.

5.2.3 Overall evaluation of the growth-related activity within the colony

Observing that the colony is growing in the circle shape, in order to see the overall trend (and not only a cross-section along one of the axes, as shown in Figure 5.2) and reduce the influence of noise, the following analysis has been done:

1) The median of the signal envelope performed over each radius around the entire colony. It can be observed that the signal has become smoother (Figure 5.5 top-right vs top-left, respectively).

2) The beginning of the decrease in activity throughout the colony occurs after the signals reach the peak values. Therefore, peak values were found for all signal envelopes in space (throughout the colony) as a function of time (Eq. 5.1):

$$Env_{(peak\ activity)}[x,y] = \max_{n}(Env[x,y,n]) \tag{5.1}$$

where n is the time index.

the times when signal envelopes reach these peaks (Eq. 5.2):

$$Time\ Ind_{(peak\ activity)}[x,y] = \underset{n}{argmax}(Env[x,y,n]) \tag{5.2}$$

and their location relative to the center of the colony (the radii) (Eq. 5.3):

$$Rad[x,y] = \sqrt{(x - x_{centr})^2 + (y - y_{centr})^2} \tag{5.3}$$

For each time (Eq. 5.2) and radius (Eq. 5.3), the median of the obtained values is performed (Eq. 5.4)).

$$\widehat{Env}[Time\ Ind, Rad] = median(Env_{max}[x,y]\ ); \quad for\ n = Time\ Ind, r = Rad \tag{5.4}$$

This operation is performed because there is a spread in these values, as colony growth depends on various factors (availability of oxygen and nutrients, Brownian motion, push and/or pull from neighboring cells in the colony, asynchrony of cell growth, proliferation in the colony, etc.). This results in two curves: 1) "overall" signal as a function of time and 2) "overall" signal as a function of distance from the colony center.

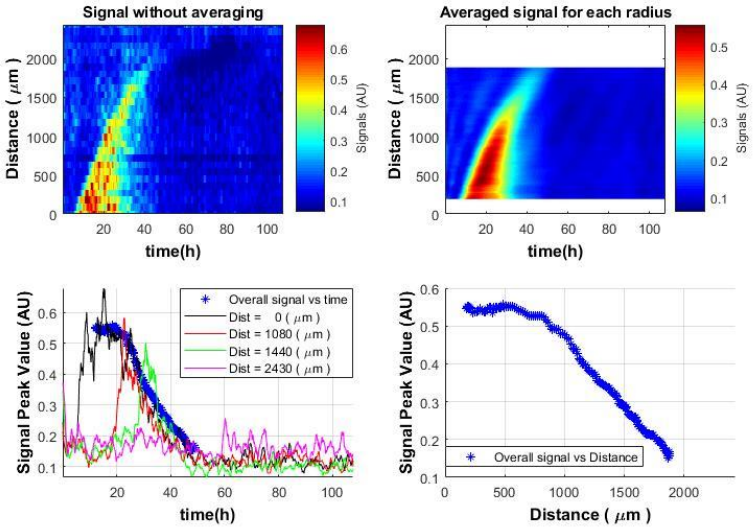

Figure 5.5. Spatiotemporal distribution of the "overall" signal envelope for colony radius (top-right); spatiotemporal distribution without averaging (top-left); signal dynamics over time at various distances from the colony center compared to the median signal envelope (blue bold stars curve, bottom-left); behavior of the median signal envelope vs distance (bottom-right).

When analysing the overall obtained spatiotemporal curve and the obtained signals separately in one graph, a coincidence can be observed (Figure 5.5 bottom-left). It is possible to detect changes in the signal level over time, which are similar to the pattern of bacterial growth within the colony. Thus, it is possible to evaluate the growth of the colony and identify whether the colony is active or not.

The observed decline in microbial activity as one moves away from the colony's center (Figure 5.5 bottom – right) is an intriguing finding. It aligns well with the notion that microbial colony growth is self–limiting over time, likely due to the depletion of essential nutrients in the media. This is consistent with earlier observations regarding microbial colony growth dynamics (chapter 3), and it also aligns with existing mathematical models describing such growth behavior [113, 111]. Therefore, this additional insight into spatial variability in microbial activity within the colony further substantiates the utility of using laser speckle imaging in conjunction with subpixel correlation for a more nuanced understanding of microbial growth patterns.

5.2.4 Automatic classification between growing and non-growing bacterial colonies using artificial neural network

The current subsection demonstrates the ability to classify between active and inactive bacterial colonies according to the features described in the previous subsections.

The training set is diversified, featuring 10 different colonies spanning three bacterial species and experiments conducted on different days. The duration of growth in these training experiments varies from 25 to 68 hours, providing a good range of data for machine learning. The decision to use *V. natriegens* colonies with a longer observation period of 107 hours for the test set is also noteworthy.

Dividing the x – y field into small NxN (10x10) pixel sections and applying two different algorithms—one for pixel spatial averaging and the other for subpixel correlation—adds layers of complexity and data richness to analysis. Further segmenting these signals into time windows of 3 hours allows a finer temporal resolution for classification tasks.

The aggregate data size is large enough, encompassing thousands of signals for each colony in the training set. Given that the 10 colonies are included in the training set, the overall sample size becomes statistically significant. This allows the creation of a robust and reliable machine-learning model capable of classifying active and inactive bacterial colonies based on the feature set described.

The decision to employ a Multilayer Perceptron (MLP), given the signal–based nature of the data, seems pragmatic, especially considering the ease of implementation and computational requirements compared to other more complex models like CNNs or RNNs.

Time–sliced classifier performance, illustrated in Figure 5.6. The ability to discern the evolving "ring" formation, its peak activity, and its eventual disappearance could offer substantial insights into bacterial colony growth dynamics. The time-resolved classification

should be especially useful for understanding the stages at which colonies are most active and the transition points between activity and inactivity.

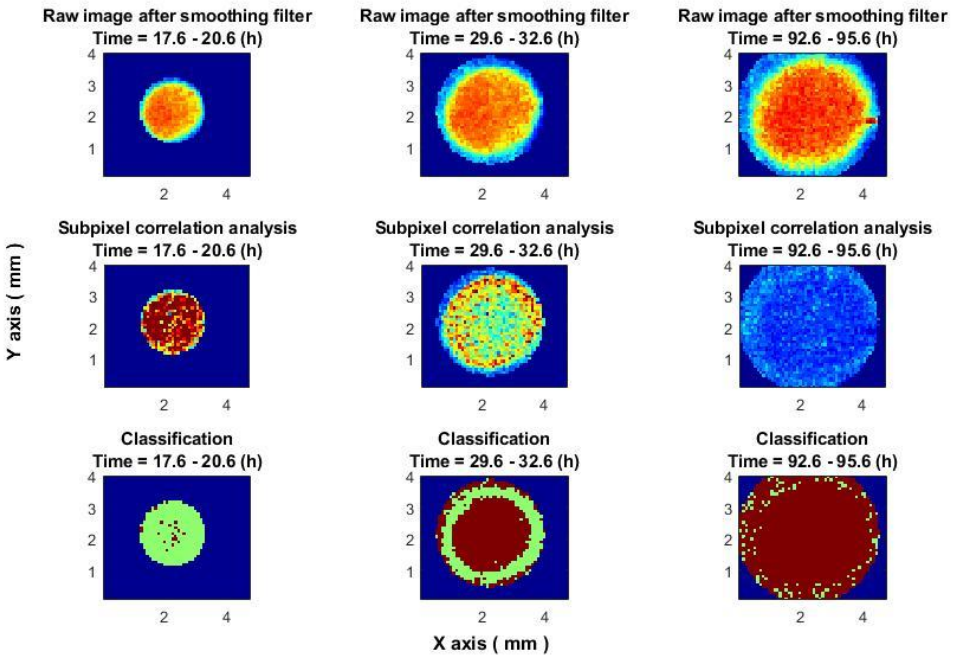

Figure 5.6. Classifier performance at different times. The images on the top row are raw images of the colony after a smoothing filter. Central images - subpixel correlation analysis. Images on the bottom - classification result. In all images, the blue color is the out-of-colony region. In the bottom images (classification result), the result of non-growing zones is in brown, and the results of growing zones are in green.

This methodology could have broader applications in both research and practical fields, such as monitoring bacterial resistance to antibiotics or assessing the efficacy of novel antimicrobial compounds.

5.3 Classifying between inhibition and active bacteria growth zones around the antibiotic's discs using a neural network

5.3.1 The signal behavior tendency at different radii from the antibiotic disc

As already described in Chapter 4 after placing bacteria in a nutrient medium, it begins to grow, multiply, and demonstrate "activity." After placing the antibiotic on this medium with bacteria, the antibiotic begins to create around itself an inhibition zone, which has an almost circular shape and grows over time. Bacteria grow over the entire Petri dish, but when the substance released by the antibiotic reaches them, growth stops in this place (along this radius from the antibiotic disk).

Consider the behavior of the first type of data under these conditions. The first type of data is a laser speckle image after spatially averaging pixels over each $N \times N$ pixel section and

temporal smoothing. That is, this is almost raw data after spatial and temporal smoothing (noise reduction). To avoid the local transient spikes, a signal envelope within a certain window [106] (like also in the case of correlation subpixel signal) was used (Eq. 3.3).

The formation of an inhibition zone is characterised by a stop of growth. That is, data from the inhibition zone before the antibiotic influence shows the same behavior as data outside the zone. However, in the time when the antibiotic influence reaches the measured area, the behavior of the data changes. The data value stops increasing. Thus, the closer the distance to the antibiotic, 1) the cessation of growth in data values will occur earlier, and 2) the achieved value will be lower than values at a far distance. That is, the shape of the signals at the same distance from the antibiotic (at the same radius) should be similar. Taken into account that these values are below the values outside the inhibition zone and accordingly more sensitive to the influence of noise, it is worth making a median of data over each radius as it moves away from the center (from the antibiotic) [106, 107,128], (Eq. 5.5). Fig. 5.7. demonstrates the behavior of this type of data inside and outside the inhibition zone.

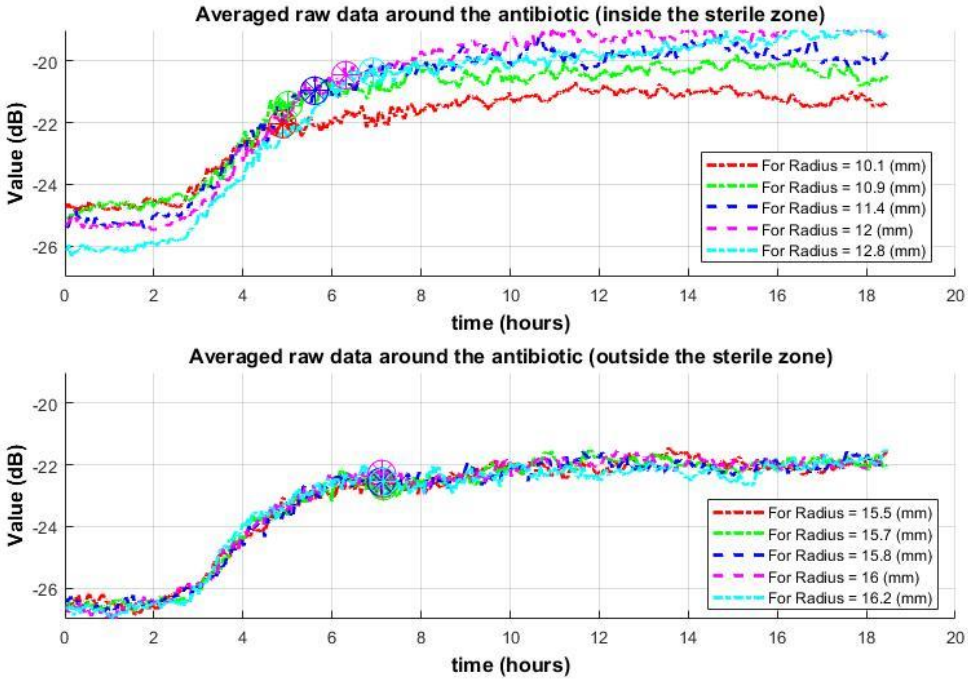

Figure 5.7 Behavior of median by radius data of first type over time for several different radii around the antibiotic. On the top, in inhibition zone. On the bottom out of inhibition zone (with active bacteria). On the top graph it is observed that as it moves away from the center, the cessation of data value growth (which means the appearance of an inhibition zone in this place) occurs later. Outside the inhibition zone (bottom graph), the cessation of value growth much later and simultaneously for different radii. The cessation of data values growth is indicated by circles.

Consider the second type of data: signal envelop after correlation subpixel algorithm. In this case, the inhibition zone in space is characterised by a fall of signal values (appearance of low values of signal - a decrease of activity after peak values of signals).

For a pronounced demonstration of the signal's behavior, like in the previous, it is to make a median of signal envelopes over each radius as it moves away from the center (from the antibiotic disc). Accordingly, even low signals (characterising the inhibition zone against the high values of the active growth zone) become noticeable (Chapter 4). That is, using a median signal envelope for each radius, less noisy curves will be considered (Eq. 5.5).

$$\overline{Env[r,n]} = \left[median_{\{over\ m_{r1}\}}\left(Env[m_{r1},n]\right),\ldots,median_{\{over\ m_{rk}\}}\left(Env[m_{rk},n]\right)\right] \quad (5.5)$$

where m_{rk} is the number of envelope signals at a given distance/radius (k) from the center. Consider the signal envelopes inside the inhibition zone for several radii. As it moves away from the antibiotic, the time of drop (appearance of low values) will be later. This happens because the signal envelope drop time indicates the appearance of an inhibition zone in this place.

If consider the signals envelopes for radii outside the inhibition zone, that is, in the bacterial active growth zone, then signals will be very similar to each other. The drop will occur later and almost simultaneously, supposedly due to the depletion of nutrients (Fig.5.8). Whereas in the situation where antibiotics are placed without bacteria no such behavior was found (Chapter 4).

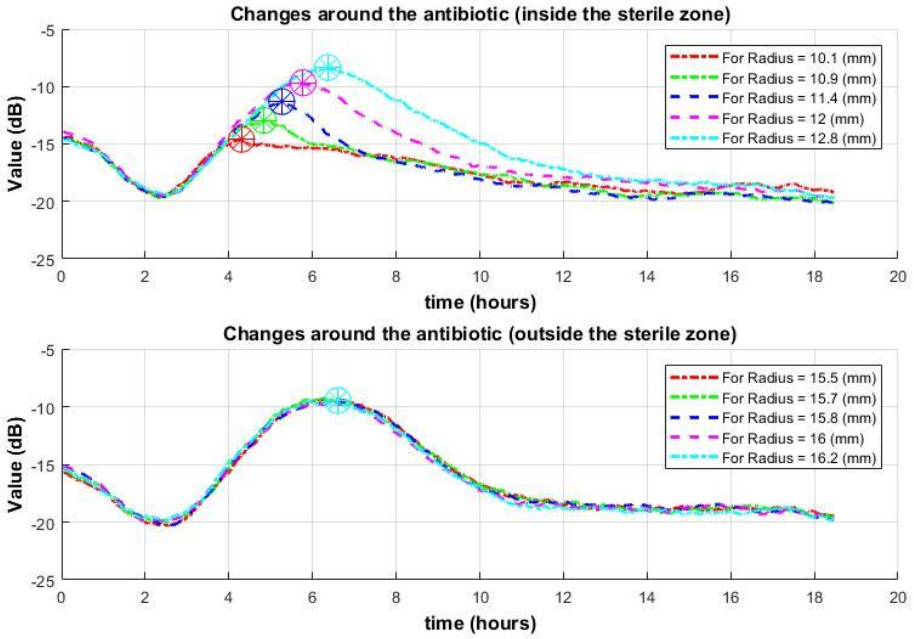

Figure 5.8. Change of median by radius data of the second type over time for several different radii around the antibiotic. On the top, in the inhibition zone. On the bottom out of the inhibition zone (with active bacteria). On the top graph, it is observed that as it moves away from the center, the drop (which means the appearance of an inhibition zone in this place) occurs later. Outside the inhibition zone (bottom graph), the signal falls much later and simultaneously for different radii. In this case, the drop is not due to antibiotics but for other reasons (for example, nutrient depletion).

Thus, it can be resumed that both types of data demonstrate an unconditional difference between the signals inside the inhibition zone and outside it. However, the signal after the correlation subpixel method looks cleaner, crisper, and better allows to distinguish zones.

It can also be noted that for the demonstrated experiment, the difference between signals after the correlation subpixel method is clearly noticeable in the interval of 4-10 hours. For averaged raw data, the differences are also noticeable after about 4-4.5 hours. That is, up to 4 hours there is almost no difference between the signals. After 9-10 hours, it is observed only for one of the two types of data – the first type. However, this type of data is more noisy; that is, it is more difficult to make a decision. Similar behavior is typical for other experiments.

Accordingly, it makes sense to check the classification on the interval where the signals are best distinguished from each other. This will be done using two approaches. 1) “Long-term” - the signal part where the difference is clearly visible (for example, 5 hours long), is processed in one indivisible piece. 2) “Short-term” - take the same 5-hour section, but break it into small time intervals (for example, 1 hour). The first approach should give a better result; however, this will happen only after the end of this interval (5 hours). The second approach may give worse results, but it will be every short-time interval (1 hour, that is, almost in real time).

5.3.2 Neural network for classification

The main goal of using a neural network in this subsection is to classify between 2 classes: 1) Zones of active bacterial growth and 2) Inhibition zones formed around antibiotic discs. And follow the change in the inhibition zone size. Let's describe considerations for designing a neural network in accordance with classification goals:

5.3.2.1 Neural network type

The perceptron (the first model for supervised learning [129]) is the simplest form of neural network used to classify patterns that are linearly separable [130].

The linear nature of the perceptron is not contingent on the assumption of Gaussianity and does not depend on the stochastic properties of the environment [131].

The perceptron consists of a linear combiner with a weight vector and bias. The perceptron convergence algorithm is adaptive and simple to implement.

Perceptron's consisting only of input neurons and output neurons called Single-Layer Perceptron's (SLP). This configuration includes only one layer of computationally active neurons (output layer) that modify data by summing and then applying the activation function.

The SLP's are restricted to linearly separable problems. To overcome this limitation, a more complex neural network structure called Multi-Layer Perceptron (MLP) is used (Fig.5.9).

The basic features of MLP:

1) The model of each neuron in the network includes a nonlinear (and differentiable) activation function. The most popular is the sigmoidal function [132]. 2) The network contains one or more hidden layers. 3) The network has a high degree of connectivity which is determined by synaptic weights of the network. 4) For updating weights, the backpropagation method of calculating the gradient is used [133].

For classification applications, the convolution neural network (CNN) is popular in use; it demonstrated good results with images; however, since the analysis involves the processing of signals (not images), a regular multilayer perceptron (MLP) is utilised.

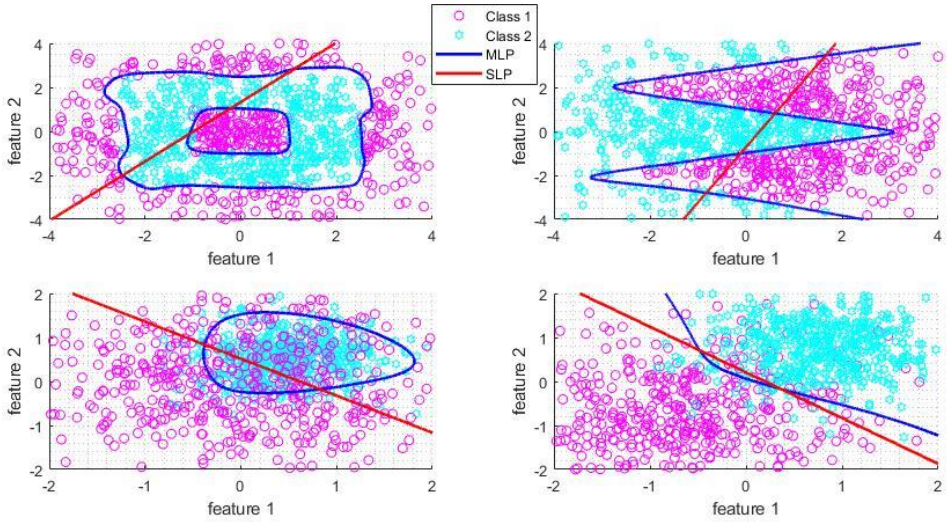

Figure 5.9. Simulation highlighting differences in classification results between SLP and MLP for different situations. Without classes overlapping (top images). With classes overlapping (bottom images).

5.3.2.2 The number of hidden layers

The MLP are universal approximators and can approximate any function that is needed [134]. The feedforward network with a single layer is sufficient to represent any function [135], but the layer may be infeasibly large and may fail to learn and generalise correctly. A study [136] claims that MLP with two hidden layers is sufficient to generate classification regions of any desired shape. However, the study does not specify how many neurons are in each layer. In some cases, a single hidden layer network may be less efficient than a network with more layers [137]. Each additional neuron in the second hidden layer enables the network to obtain results with a relatively small number of neurons in the first hidden layer, as explained by [138]. The study [139] applied a "transformative optimisation" method to compare single-hidden-layer and two-hidden-layer networks on ten separate datasets. In nine out of ten cases, a two-hidden-layer network was superior to a single-hidden-layer network, but the degree of improvement depended on the individual case. More than two hidden layers can be useful in certain special applications [140-141].

5.3.2.3 The number of neurons in the hidden layers.

A small number of neurons in the hidden layers will result in underfitting, (difficulty adequately detect). Too many neurons in the hidden layers will result in overfitting (the information in the training set is not enough to train all the neurons in the hidden layers).

The number of neurons must be such that the network can capture the complexity of the input-output connections. The general rules of thumb for determining the number of neurons to use in the hidden layers are [142]:

1) The number of hidden neurons should be between the size of the input layer and the size of the output layer. 2) The number of hidden neurons should be 2/3 of the input layer size plus the size of the output layer. 3) The number of hidden neurons should be less than twice the input layer size.

This puts some initial framework on the number of neurons in the hidden layers. It is obviously that the more complex the assumed input–output relationship, the more neurons there are in the hidden layers.

However, there are other approaches. For example, a study [143] for cases where a suitable neural network can be searched automatically offers formulas for determining the maximum number of hidden layers and the maximum number of neurons in a neural network design (upper bound). The efficient neural network can focus below certain upper bounds, and above them, it becomes pointless. This approach could provide starting points and guidance for choosing both the number of layers and the number of neurons in the layer for network building.

5.3.2.4 Database and neural network parameters.

In practice, a wide variety of networks and their purposes make it challenging to find a universal solution for choosing an appropriate topology. Accordingly, a process or algorithm for searching for parameters such as the number of hidden layers, the number of neurons in layers, learning rate, epochs, etc, is determined. For efficiency, criteria are introduced to determine within what limits these parameters should be changed.

Based on literature recommendations, a network with 1, 2, and 3 hidden layers was tested. The effect of changing the number of neurons in the layers was also tested. Figure 5.10 A illustrates the result: Mean squared error (MSE) as a function of epochs. The result shows that for a network with 2 and 3 hidden layers, the MSE is lower than with one hidden layer. A comparison of a network with 2 and 3 hidden layers shows that there is almost no difference.

With an increase in the number of neurons from a small number, the result improves, but after a certain number of neurons, the result hardly improves anymore (Figure 5.10 B).

The learning rate was also checked. Figure 5.10 C illustrates the result: Increasing the learning rate reduces MSE; however, after certain values of the learning rate, instability will begin, which is expressed as an increase in the MSE values (instead of a decrease), or the form of “jumps” of MSE values.

Figure 5.10 D shows the improvement in the result when moving from using a signal of the first type, raw data after spatial and temporal smoothing, to a signal of the second type, a signal after the correlation subpixel method, and to using these two signals simultaneously.

Figure 5.10 E analyses the influence of the time window. During time windows after 3-4 hours from the beginning of the experiment, bacterial activity is high for several hours; against this background, the effect of the antibiotic is also clearly observed. Then, as the activity decreases (depletion of nutrients, etc.), the growth of the antibiotic’s influence also decreases.

The number of epochs was chosen so that the MSE values would almost stop decreasing (Figure 5.10 F).

Based on the considerations described above, the network parameters are as follows: The network is Multilayer Perceptron [131]: 1) two hidden layers. The first hidden layer is 30 neurons. The second hidden layer is 20 neurons, and the output layer is 2 neurons, according to the number of classes - bacteria or an inhibition zone. 2) Learning Rate = 0.03. 3) Momentum = 0.5, 4) Epochs = 200.

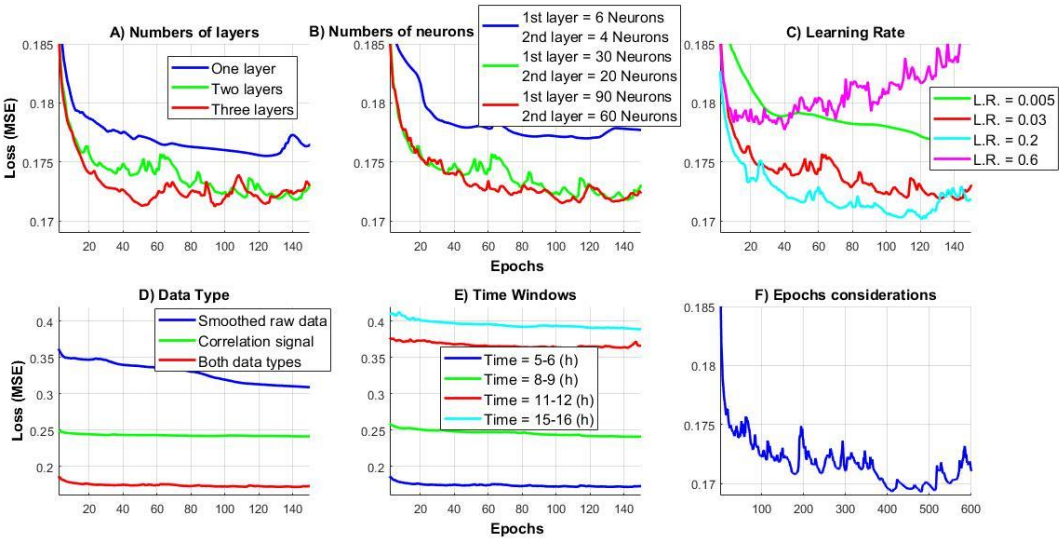

Figure 5.10. Parameter analysis: number of layers (5.10.A), number of neurons (5.10.B), learning rate (5.10.C), data type (5.10.D), time window (5.10.E), number of epochs (5.10.F).

To train the neural network, 8 experiments with E. coli bacteria were used. Testing of the neural network was performed in 1 experiment with E. coli bacteria. Each such experiment involved an almost entire Petri dish in which 2 antibiotics were placed, around which zones of inhibition were formed.

In each experiment, there were approximately 80-100 thousand signals of one type and the same number of signals of the second type of length T (15-18 (h)). The signals were divided into time windows of 1 hour in order to obtain a classification result during this short period of time, which increases the number of signals by 15-18 times.

5.3.3 Results

5.3.3.1 Classification results

As already noted in Chapter 4, the inhibition zone becomes visible approximately 3-4 hours after the start of the experiment, and it becomes visible immediately with some already noticeable radius. Chapter 4 explained the reason for this and demonstrated how the inhibition zone could be observed almost from its time of appearance. However, the current Chapter operates according to the standard [144]. Accordingly, it is expected that the classifier will not be able to detect the inhibition zone until 3-4 hours from the beginning of the experiment and let's check this statement.

As a reference, consider the "long-term" classification. As described in Subsection 5.3.1, the signal part, where the difference is clearly visible, is processed in one indivisible piece. After checking different sections of the signal with a length of 3-6 and 12 hours, a section with a length of 5 hours was selected at a time of 4-9 hours from the start of the experiment. In this time interval, the classifier provided the best results. Fig. 5.11 shows the result for the correlation subpixel algorithm only, and Fig. 5.12 shows the improvement in the result when using both types of data.

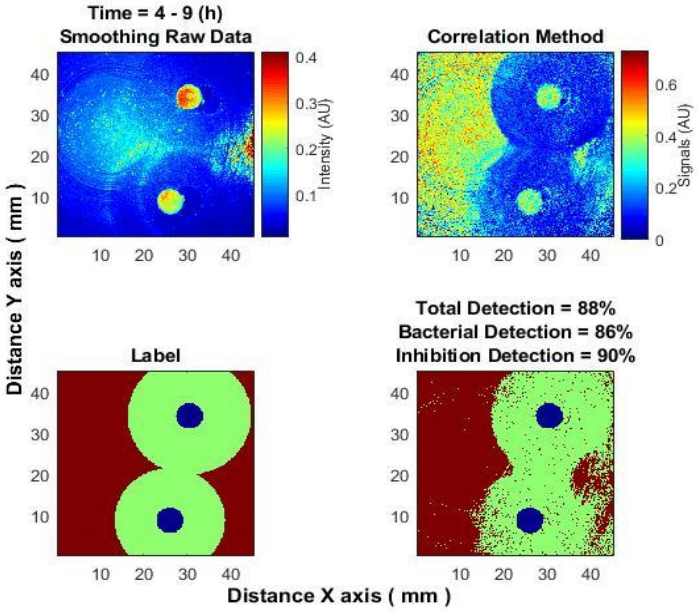

Figure 5.11. “Long-term” classification. Top left - smoothed raw date; top right - correlation subpixel method; bottom left - labels; bottom right - classification result.

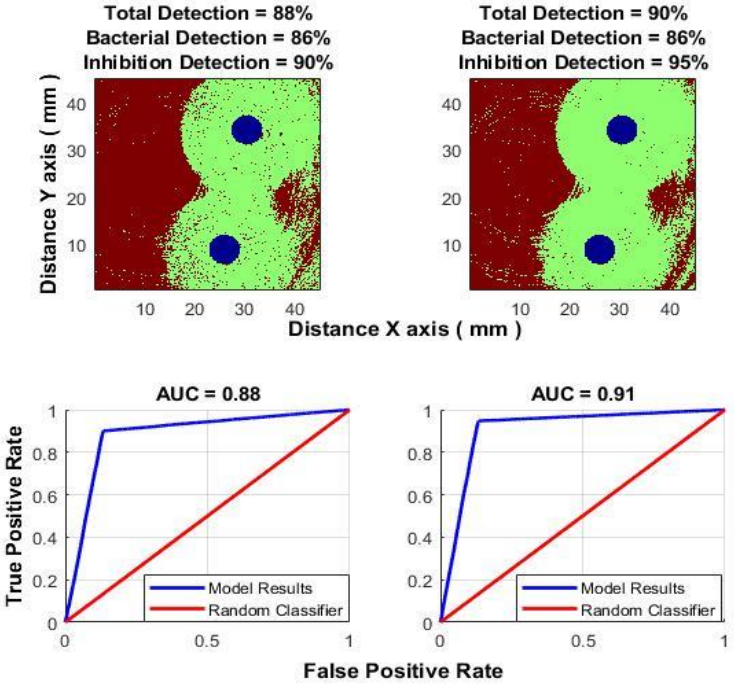

Figure 5.12. “Long-term” classification. Top left - classification result for correlation subpixel method; top right classification result for both methods together: correlation subpixel method and smoothed raw date; bottom ROC curves accordingly.

5.3.3.2 Improving classification results.

This subsection described two methods to improve classification results by using knowledge about the antibiotic position and the growth process of the inhibition zone, using signal processing.

5.3.3.2.1 Improving classification results by class changing function as distance from antibiotic

Taking into account: 1) That inhibition zones occur around the antibiotic, and antibiotic location and size are known 2) That the inhibition zone grows in a shape close to a circle. So, the classification result can be improved.

For this aim, the median of the class values obtained over each radius as it moves away from the antibiotic to the edges for each time window of 1 hour is performed. The class characterising the inhibition zone can be designated as class 1, and the class characterising the area with bacteria can be as class 2. At a radius close to the antibiotic, the median of class result will be close to 1 (since this is an inhibition zone). At a radius far from the antibiotic, the median of class result will be close to 2 (since this is an area with active bacteria). The distance of switching from class 1 to class 2 will correspond to the radius of the inhibition zone for each considered time window (Eq.5.6).

$$\langle Class(r) \rangle = [median\,(Class[m_{r1}]), \ldots, median(Class[m_{rk}])] \tag{5.6}$$

where m_{rk} is the number of class points per radius "k" from the center.

Fig. 5.13 (middle and bottom row) shows the class change as a function of radius around 2 antibiotic discs, and improving classification results for one selected time window.

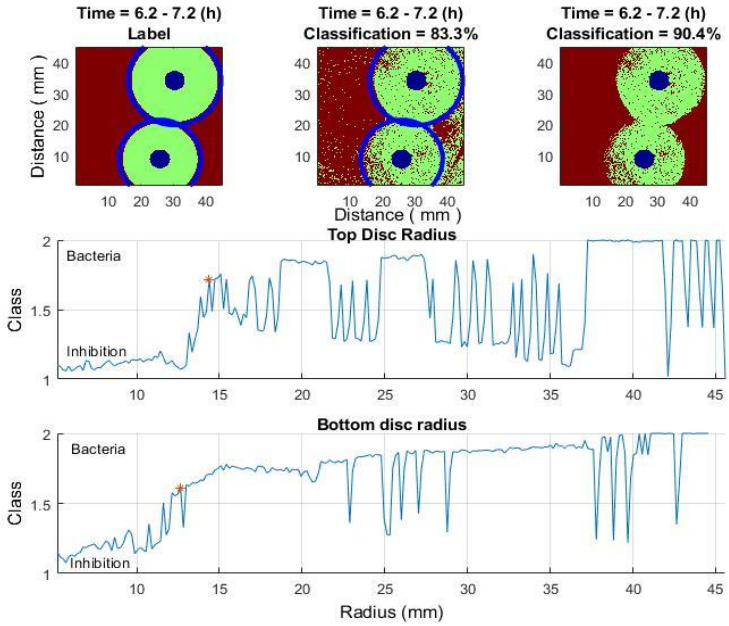

Figure 5.13. Improving classification results. Time window 6.2-7.2 h. Top row: 1) left image-labelling, 2) central image-classification result. 3) right image-classification result after class estimation algorithm Middle row class change as a function of radius (top antibiotic disc). Bottom row class change as a function of radius (bottom antibiotic disc).

Figure 5.14 shows improving classification results by using a class-changing function for three different time windows: in the beginning, middle and the end.

Where for the time window: 4.1-5.1 (h), total correct detection before improving = 70 %: correct bacteria detection = 68 %, and correct inhibition zone detection = 74 %. Total correct detection after improving = 87 %.

For the time window: 8.2-9.2 (h), total correct detection before improving = 88 %, correct bacteria detection = 86 %, and correct inhibition zone detection = 90 %. Total correct detection after improving = 92.5 %.

For the time window: 16.4-17.4 (h), total correct detection before improving = 70 %, correct bacteria detection = 69 %, and correct inhibition zone detection = 70 %. Total correct detection after improving = 83 %.

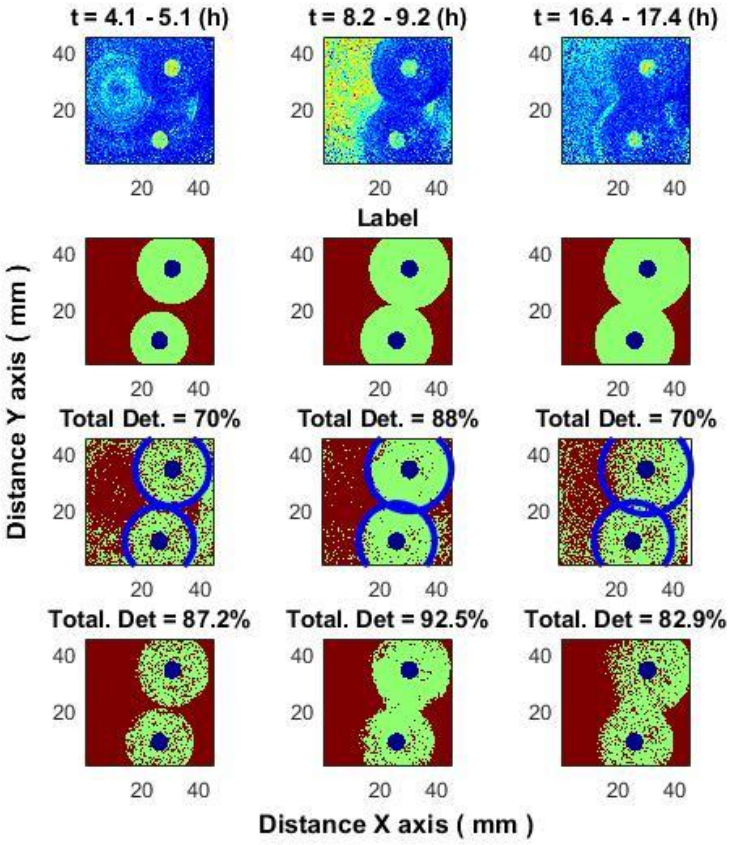

Figure 5.14. Improving classification results for three different time windows: in the beginning, middle and the end.

5.3.3.2.2 Improving classification results using the median signal per radius

Another approach to improve the classification result, like the previous case, uses the same two factors: 1) That inhibition zones occur around the antibiotic, and antibiotic location and size are known, and 2) That the inhibition zone grows in a shape close to a circle. Using this

knowledge, it is possible to make median the signals over the radius around the antibiotic. Thus, instead of a large number of signals, for each radius, there will be only one median signal from the correlation subpixel method and one from the average by NxN pixels window. The median signal preserves the trend of the signals, but the noise is suppressed [106, 107, 128], which will improve the performance of the classifier. Also, replacing many signals with a small amount of median signals will reduce the operating time of the classifier.

The implementation of this approach makes it possible to achieve higher classification performance (Fig. 5.15).

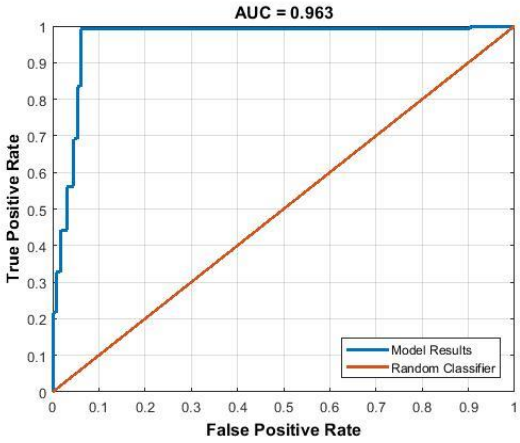

Figure 5.15. ROC curve of classification using the median signal.

However, if a classification error occurs, an incorrect result will be obtained not at one point in space but along an entire specific radius (in the "ring" shape) (Fig. 5.16). If a "ring" is located deep in another class, then it can be easily detected and removed using additional algorithmic tools.

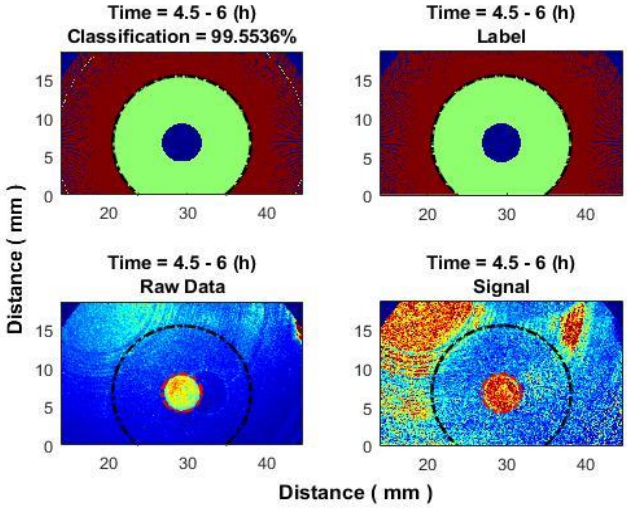

Figure 5.16. Improving classification results by one median signal over each radius Time window: 4.5-6 (h). top left - classification result; top right – labels; bottom left – average over NxN pixes window; bottom right - correlation subpixel algorithm.

If it is located at the transition place from one to another class, then it is more difficult to detect the error (Fig. 5.17).

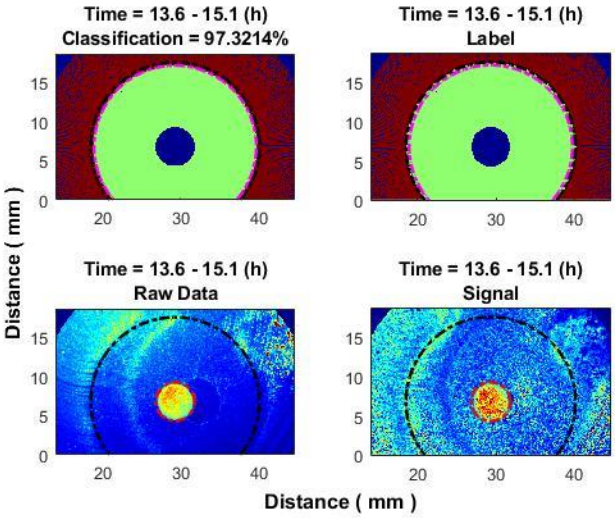

Figure 5.17. Improving classification results by one median signal over each radius Time window: 13.6-15.1 (h). top left - classification result; top right – labels; bottom left – average over NxN pixes window; bottom right - correlation subpixel algorithm.

5.4 Chapter conclusions

The laser speckle imaging with correlation subpixel algorithm allows the detection of subtle changes in the object under observation, effectively distinguishing colonies where bacteria are still proliferating colonies (or zones) from dormant or dead colonies (or zones), which is not achievable with laser speckle without correlation subpixels algorithm or white – light imaging alone.

This technique gives a mechanism for distinguishing between growing and non–growing bacterial colonies. Such capabilities pave the way for deeper studies into the complex interactions occurring within microbial communities.

In the inhibition zone, the decrease in the signals' value occurred in a dynamic manner (as one moves away from the antibiotic, this occurs later), representing the radius of the inhibition zone. Outside the inhibition zone, the signal decreased much later and simultaneously for different radii. The signals in both zones definitely differed from each other. The correct classification reached 88 percent (in the time window 8.2-9.2 h). However, at the beginning of the formation of the inhibition zone, or vice versa, after long hours from the onset of formation, the percentage of correct classification decreases to 70 percent. Using the proposed methods: 1) Finding the radius at which the inhibition zone ends, the correct classification reaches 92,5 percent (in the time window 8.2-9.2 h). And 83-87 percent, at the beginning of the formation of the inhibition zone or after long hours from the beginning of formation. 2) Median signal per each radius, the correct classification reaches over 96 percent (up to 99 percent) in all time windows.

Thus, by understanding the specificity of signals using an algorithmic appropriate base, high classification can be achieved.

The method could become instrumental in various research domains, from studying bacterial growth dynamics to evaluating the efficacy of antimicrobial substances.

6. COMPARISON OF THE PROPOSED METHOD WITH OTHER METHODS BASED ON THE USE OF LASER SPECKLE TECHNIQUES

Based on the posed aims and tasks, the sixth chapter of the Doctoral Thesis performs a comparison of proposed in the literature algorithms for microorganism's behavior monitoring with described in previous chapters of this study correlation subpixels algorithm as a research object.

6.1 Introduction to the chapter.

In this chapter, using experimental data of the microorganisms' growth (fungi and bacteria), these methods are compared with the proposed subpixel correlation algorithm (Chapter 3), which has proven to be a worthy tool for detecting microbial growth activity and detecting hidden effects in microorganism's behavior. The comparison results and the advantages of the algorithm are demonstrated. By combining laser speckle technology with conventional methods of cultivation, identification and antimicrobial sensitivity, it would be possible to obtain results faster and thus improve the quality of treatment and survival of patients.

6.2 Algorithms of the microorganism's behavior analysis proposed in the literature.

6.2.1 Spatial contrast analysis.

Studying the growth of any microorganism in culture is crucial for understanding its growth process and improving its yield. To prove that the laser speckle imaging technique is a reliable and robust method for monitoring microbial concentration, the literature suggests analysing such parameters as the spatial contrast [145] (Chapter 1 (Eq. 1.20)) and the speckle grain size [35]. This is because as the concentration of scatterers in the sample increases, the dynamics of Brownian motion also increase. Consequently, the spatial contrast decreases. The spatial contrast of the speckle image can provide information about the nature of the medium, for example, its viscosity [146] or the number of diffusers [147]. The image's contrast can also detect the dynamics in the medium due to variation of the speckle grains. When microorganisms move on the observed surface, the speckle pattern will be blurred, and the standard deviation of the intensity will be small compared to the unchanged mean intensity. Accordingly, speckle contrast is reduced. Thus, lower contrast values correspond to more intense dynamic changes in the observed medium.

Study [55] believes that the decline in contrast can be linked to the variation of the ratio of the speckle grain size and the pixel size of the camera. They assume that the contrast could be indirectly connected to increased cell concentration during fermentation.

6.2.2 Speckle size analysis.

The speckle grain size is a parameter affected by the number or the size (dimension) of the scatterers in the medium [46]. The demonstrated results in [57] show that both speckle grain

size and spatial contrast decrease with microorganisms' growth. The study [55] even proposes to use speckle grain size to compare bacterial growth efficiency among different strains. The average speckle size may be estimated by the full width at half maximum (FWHM) of the autocovariance function (Chapter 1 (Eq. 1.19)).

Thus, speckle size can be calculated from the speckle image, and it is useful for measuring the roughness of a surface. The study [57] uses this assay to analyse bacterial growth in liquid culture media. It was found that speckle grain size decreases with bacterial growth. However, since the current study works on the surface, on the solid (agar) media, the result may be different, and this needs to be checked.

6.2.3 Decorrelation time analysis.

Another useful approach to using the laser speckle technique to determine a microorganism's activity is to measure the time or rate of decorrelation [88] (Chapter 1 (Eq. 1.32)). The decreases in the temporal correlation value are proportional to the microorganism's concentration and activity.

6.2.4 Temporal contrast analysis.

Along with the spatial contrast method, several studies for the characterisation of the activity of a dynamic speckle pattern suggest using the temporal contrast method [16] or other methods based on the difference between time frames. For example: Average Difference or Fujii Method [48], Generalized Difference Method [148], etc. These methods can indeed provide certain benefits compared to spatial contrast analysis and also highlight those hidden effects that were discovered in this work using the correlation subpixels algorithm. Let's analyze this using the temporal contrast method as an example.

Using temporal contrast instead of spatial contrast allows operation with higher spatial resolution, however, at the expense of temporal resolution.

The study [53] showed that if temporal samples are statistically independent (the time between samples is greater than the correlation time), then temporal contrast analysis provides high results when estimated from 15 or more speckle frames, while for spatial contrast, a window of 7x7 = 49 spatial points is used. The study [16] assumes that the temporal contrast analysis will likely perform better than the spatial one with fewer samples, provided that temporal samples are more statistically independent than the spatial samples. This is based on the fact that static scattering does not produce an additive offset in the temporal speckle contrast but instead scales the speckle contrast by a factor related to the relative contribution of statically and dynamically scattered photons. It is also worth noting that temporal speckle contrast is generally less computationally expensive than spatial speckle contrast [149].

Temporal speckle contrast appears inherently less sensitive to the contribution of static scattering than spatial speckle contrast [150].

6.2.5 Interim summary

The current subsection describes four algorithms proposed for observing the behavior of microorganisms. The first three of them, during microorganisms' growth on the observed specimen, react by decreasing parameters. That is, spatial contrast decreases with microorganisms' growth, the temporal correlation value decreases with microorganisms' growth, and speckle grain size (in liquid culture media) decreases with bacterial growth. In the

next subsection, the behavior of microorganisms for solid (agar) media will be tested, and the results of the algorithms described above will be compared with the algorithm for spatial correlation subpixel analysis.

6.3 Comparison of algorithms.

6.3.1 Spatial contrast analysis.

The calculation of spatial contrast was tested in experiments with bacteria and with fungi on the solid (agar) media. For a more visual comparison with the correlation subpixel algorithm, a bacterial colony of *Vibrio natriegens* was selected. The ability to obtain the “ring of activity” effect, which characterises the growth of a colony, was tested in Chapter 3. Fig. 6.1 demonstrates the result of the comparison by the algorithm. The contrast demonstrates the presence of a colony but does not reveal the "ring effect" that is noticeable using the correlation subpixel algorithm.

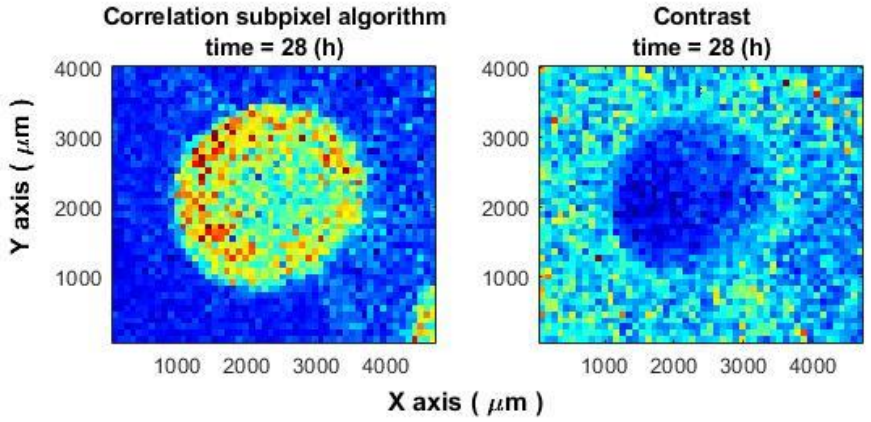

Figure 6.1. Comparison of correlation subpixel algorithm with spatial contrast analysis. The contrast analysis does not reveal the "ring effect"

6.3.2 Decorrelation time analysis.

To analyse the decorrelation method, experiments with bacteria and fungi were used. Fig. 6.2 shows the change in the normalised cross-correlation value over time between the 1st frame and subsequent frames in 2 cases: with and without microorganisms. This method allows to distinguish microorganisms from their absence. However, after a short time in both cases the correlation will drop below the detection level. Additionally, like in contrast method, this method detects the presence of microorganisms but does not reveal hidden effects within colonies**.**

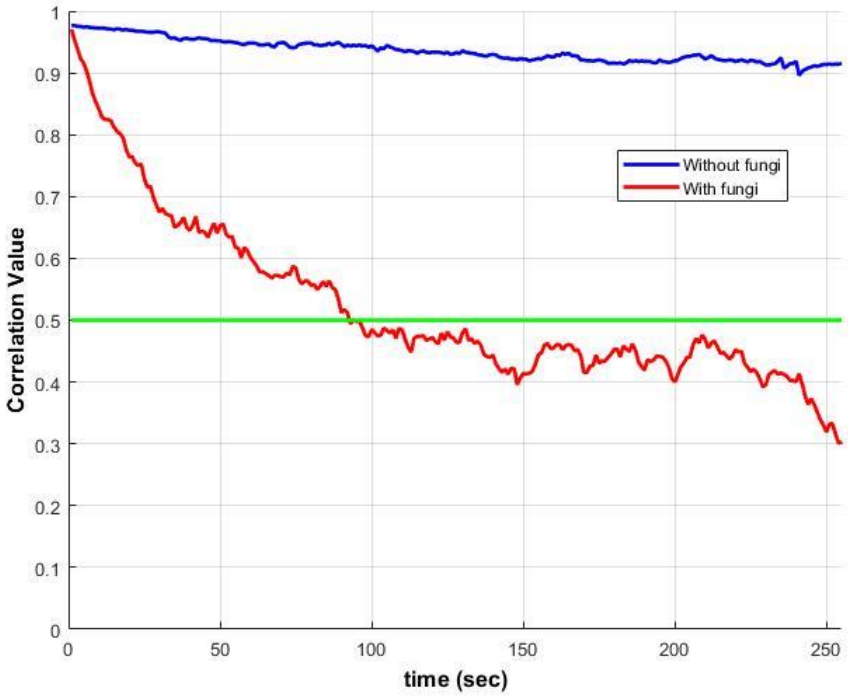

Figure 6.2. Change in the value of the normalized cross-correlation over time between the 1st frame and subsequent frames in 2 cases: 1) without microorganisms (blue) and 2) with microorganisms (red).

6.3.3 Speckle size analysis.

Speckle size measurements in experiments with bacteria and with fungi on the solid (agar) media before and after the appearance of microorganisms in the observation area were carried out several times and with different cultures. This is demonstrated using the example of *Candida albicans* fungi. The experimental field was divided into MxM pixels, and the speckle size was measured for each such window (Fig.6.3). Next, the average speckle size and standard deviation over the entire field were calculated (Fig.6.4). The algorithm demonstrated the following result: The speckle size remains almost unchanged (measured changes can be attributed to statistical errors).

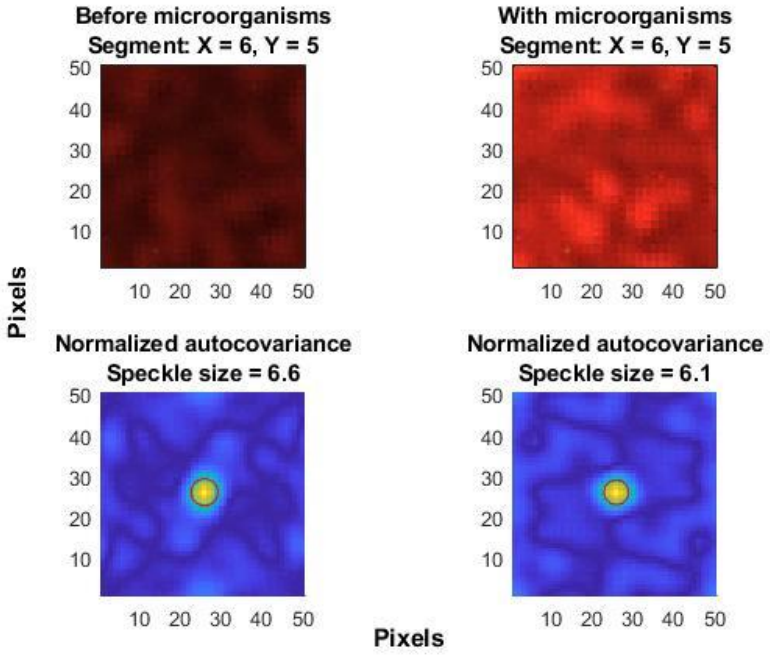

Figure 6.3 Analysis of microorganism's behavior by speckle size calculation. For one spatial window.

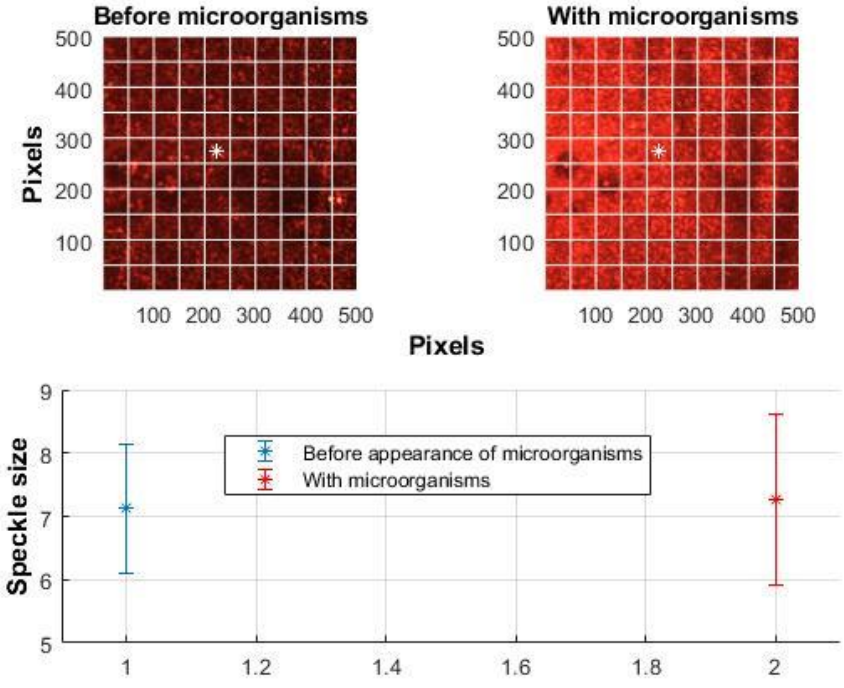

Figure 6.4 Analysis of microorganism's behavior by speckle size calculation. For many spatial windows (entire field).

6.3.4 Temporal contrast analysis.

As mentioned in subsection 6.2.4, it is expected that methods based on the difference between time samples, such as the temporal contrast method [16] and others, along with the subpixel correlation algorithm, can also detect hidden effects on the growth, behavior, and inhibition of microorganisms. Figure 6.5 shows a comparison of a part of a *V. Natriegens* bacterial colony processed by two methods: subpixel correlation algorithm and temporal contrast method. In both cases, the ring effect is visible. As described in subsection 6.2.4, the spatial resolution of the temporal contrast method is better than the subpixel correlation algorithm.

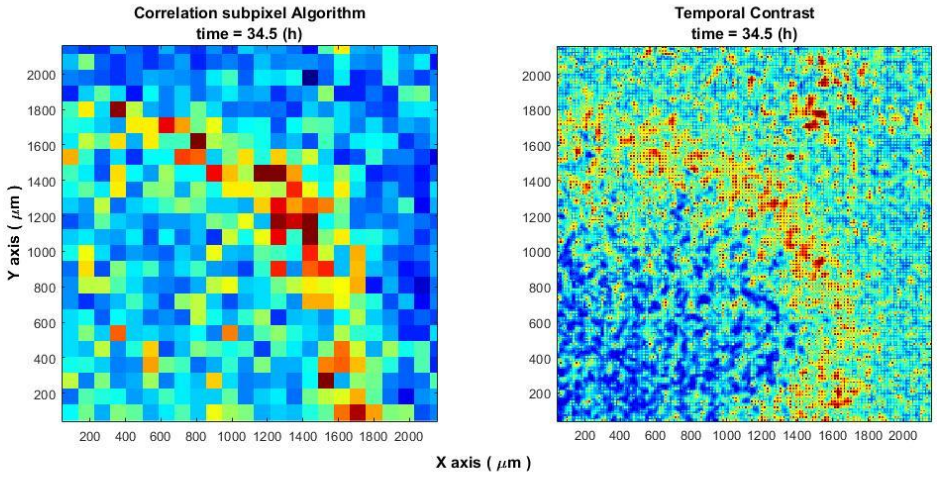

Figure 6.5 Edge of a bacterial colony. On the left is the correlation subpixel analysis. On the right is the temporal contrast analysis. Both methods detect the "ring effect" described in Chapter 4.

However, a time analysis will also be carried out. To demonstrate the behavior of a signal, it is worth using not recordings of microorganisms but a deterministic signal with clearly known changes in the time and frequency domains. For this purpose linear sweep was chosen. Such a signal was described as used in subsection 2.3.

Signal parameters: linear sweep, frequency increase between 5-185 mHz during 2500 sec, Fs = 400 mHz, (the time between consecutive frames 2.5 sec, which is an acceptable sampling frequency for the processing of fungi). Since a time window is used to calculate temporal contrast or similar algorithms, 2 simulations were carried out to describe this process:

1) Averaging frames (or time samples) in this signal. The averaging was performed in the signal itself, every N sample. Despite the fact that in subsection 6.2.4 it is written that N is longer than 15, for greater graphical clarity, a smaller number is used: N = 4. Figure 6.6 demonstrates that, in this case, temporal frequencies higher than Fs/N will “curl up” into the area of lower. That is, the effect of temporary aliasing is observed. So this simulation

demonstrates the problem. However, to make sure that the problem is real, need to perform a simulation with speckle images.

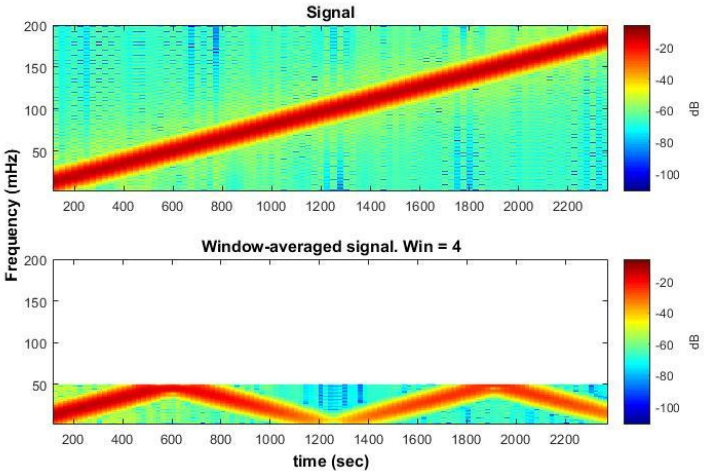

Figure 6.6 Spectrogram of linear sweep signal. Top image - the sampling frequency satisfies the Nyquist criterion. The bottom is the same signal but averaged over the time window N = 4. In this case, the effect of temporal aliasing is observed.

2) A speckle image is created (described in subsection 1.2). The image is shifted according to the same linear sweep function. The signal is checked pixel by pixel. In one case, the signal is taken as it is; in the other, with averaging over the same window N = 4. Figure 6.7 demonstrates the results. As with the simple simulation, the speckle images simulation also demonstrates the effect of time aliasing.

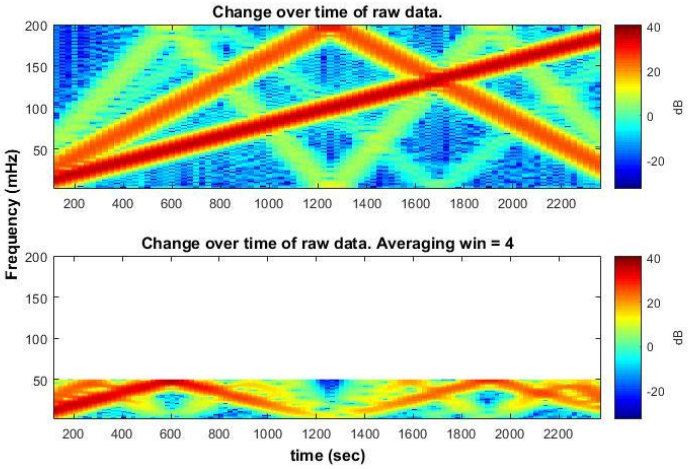

Figure 6.7 Simulation of a sequence of speckle images shifted according to linear sweep. Top image - the spectrogram demonstrates that the sampling frequency satisfies the Nyquist criterion for the signal. However, in contrast to the "clean" signal, due to the nonlinearity of the system or algorithm limitations, higher harmonics can appear, which also cause the aliasing effect. The bottom is the same simulation but averaged over N = 4 frames. In this case, the effect of temporal aliasing is observed. The appearance of high harmonics further emphasises the aliasing effect

6.4 Chapter conclusions

In this chapter, the widely described in the literature algorithms for analysing speckle data of microorganism behavior were considered and compared with the proposed method - correlation subpixel analysis.

The spatial contrast analysis detects a growing bacterial colony but cannot detect migration of activity within the colony, which is detected using subpixel correlation analysis.

The decorrelation method allows the detection of the presence of microorganisms but does not reveal hidden effects within colonies (the "ring effect").

Speckle size measurements in experiments with bacteria and fungi on the solid (agar) media did not reveal significant changes in this parameter. Accordingly, for these conditions, it is worth resorting to other methods.

Methods based on the difference between time frames, such as the temporal contrast method, are able to detect hidden effects. This can be done with high spatial resolution, but the undesirable effect is decreased temporal resolution. Lowering the temporal resolution will require a higher frame rate. Failure to take this aspect into account will lead to the effect of temporary aliasing. The challenge of temporal aliasing in such methods is a topic for future research.

It is also worth noting that, unlike the methods described in this Chapter, the proposed correlation subpixels algorithm, in addition to spatial analysis, converts a speckle image sequence into a time signals array. An important advantage of this approach is that signal processing algorithms can be applied to the array of obtained signals. As demonstrated in previous chapters, the toolkit includes filtering operations in the time, frequency, or time-frequency domains. Using spatial signal processing algorithms, the advantage of signal and image processing is demonstrated by analysing the behavior and changes in the time-spatial domain.

The results obtained in the current chapter demonstrate the advantages of the proposed method - correlation subpixel analysis.

RESULTS AND CONCLUSIONS

The goal of the Thesis was to develop a novel approach for non-contact detection and assessment of submicron activity or growth of submicron objects over a large area, as well as the ability to classify and evaluate specific submicron objects or events. One of the challenges was the approach to signal processing, for which a correlation subpixel algorithm was implemented to convert a sequence of video images into signal arrays. Another challenge stemmed from the fact that changes in the growth and inhibition of microorganisms manifest as very low-frequency signals (mHz). Technologies designed for processing such low-frequency signals typically require complex equipment and are suited for observing "global-scale" processes. Therefore, it was essential to develop compact, small-scale equipment capable of operating within this frequency range and processing these signals. The developed approach holds potential for application in other areas that require the processing of very low-frequency signals, which could stimulate further research in this field. The proposed method demonstrated sensitivity to hidden effects that were either undetectable by other approaches or would have required significantly higher frame rates for detection. Additionally, it was shown to perform effectively in noisy environments. The use of artificial neural networks to analyze signals obtained from the sequence of images (processed using the proposed algorithm), along with additional post-processing based on an understanding of the signal properties, resulted in significant improvements in the classification of active (growing) and inactive zones - an outcome not achievable with raw speckle data alone.

The goal of the Thesis was effectively achieved, and in the process, the following steps were completed, giving the following results:

- An analytical study of similar research and studies revealed the most popular and accurate approaches and methods in this field:
  - analysis of speckle contrast;
  - analysis of speckle size;
  - analysis of decorrelation time or rate of speckle images.
- There is a relationship between all the studied approaches with correlation analysis. Thus, it becomes clear that correlation analysis is an important, powerful, and promising tool for analysing speckle patterns (including the medical/biological field).
- Correlation analysis methods of speckle images described in the literature for detecting mechanical vibrations and reconstructing audio signals were studied. The conclusions drawn were used. However, due to the distinctive features of signals characteristic of microorganism behavior, the algorithm was modified. Methods for fast and, at the same time, accurate implementation of the algorithm were considered, and the most suitable one was proposed.
- An approach that allows monitoring of the dynamics of submicron events, highlighting hidden effects, was developed for medical and microbiological needs in the analysis of the behavior of microorganisms.

All developed methods and algorithms were experimentally analysed to test the hypotheses defined for this study:

- The first hypothesis was validated through experiments designed to observe colony growth using two distinct illumination methods: 1) white light illumination, and 2) the laser speckle technique, followed by subsequent analysis. Analysis of laser speckle patterns using a subpixel correlation algorithm enabled earlier detection of bacterial growth compared to the conventional colony-forming unit (CFU) method under white light illumination. The bacterial colony formation on the agar media was detected using the laser speckle technique with subpixel correlation analysis approximately 3 hours after bacterial inoculation. In contrast, the CFU growth under white light could be detected later, after an additional delay of approximately 3–4 hours, corresponding to 7–9 bacterial doublings. During this time, the concentration of *V. natriegens* bacteria is expected to increase by at least 2 orders (hundreds of times). However, as colony growth follows Gompertz kinetics, characterised by a decreasing growth rate over time; accordingly, this difference may take an even longer time delay. The use of speckle imaging thus provides an unprecedented and highly sensitive analytical approach for CFU growth detection significantly earlier than visual inspection under white light.
- The second hypothesis was validated through experiments observing colony growth using the laser speckle technique under two approaches: 1) without additional analysis, and 2) with correlation subpixel algorithm analysis. The proposed correlation subpixel analysis revealed the presence of a distinct activity zone within the colony, which migrates from the center to the edges during growth. The experimental data on the actual size of activity zones within growing microbial colonies remain limited. The proposed technique offers a promising and powerful method for visualizing these activity zones, which were previously either predicted through mathematical models or observed using invasive methods. The migration speed of the "ring of activity" varies across microbial species, reflecting the distinct growth rates characteristic of each species. Experimentally determined approximate migration speeds are as follows: E. coli at 125 μm/h, V. natriegens at 65 μm/h, and S. aureus at 35 μm/h. The "ring of activity" was observed to appear approximately 10–12 hours after inoculation for E. coli, 13–15 hours for V. natriegens, and 15–18 hours for S. aureus, and it persisted throughout the colony growth process. The experimental width of the "activity ring" also varied among species, with recorded ranges of 800–1400 μm for E. coli, 900–1400 μm for V. natriegens, and 600–800 μm for S. aureus. Variability in the measured parameters, including activity ring width, maximum migration distance from the center, and microbial colony growth curves, was observed. This variability may result from changes in the properties of the agar medium, biological variability within the samples, and/or measurement inaccuracies. To enhance the precision of these measurements for medical or microbiological research, it is necessary to perform statistical analyses on larger datasets, encompassing multiple colonies from various microbial species.
- The third hypothesis was validated through the execution and analysis of experiments observing colony growth in a highly noisy environment using two approaches: 1) the laser speckle technique without additional analysis, and 2) the laser speckle technique with correlation subpixel algorithm analysis. The proposed correlation subpixel algorithm successfully detected the presence of a colony, whereas the laser speckle

technique, without additional analysis, failed to do so. In a high-noise environment, where noise levels were 3–4 times higher than the normal background noise and exceeded the useful signal level by more than a factor of 2, colony formation was detected using the proposed technique 7 hours after bacterial inoculation, corresponding to a time delay of approximately 3–4 hours. In contrast, colonies were not detectable under white light illumination or using the laser speckle technique without the application of the proposed correlation subpixel algorithm.

- The fourth hypothesis was validated through the analysis of experimental data involving both bacterial colonies and zones of inhibition around antibiotic disks using two approaches: 1) the laser speckle technique without additional analysis, and 2) the laser speckle technique with correlation subpixel algorithm analysis. Although the laser speckle technique without additional analysis enables the visualisation and detection of colonies and zones of inhibition, the laser speckle technique with correlation subpixel algorithm exhibits enhanced sensitivity to subtle changes, allowing for reliable differentiation between various data types. This capability was further confirmed through the implementation of a classifier. The proposed method, correlation subpixel analysis of laser speckle images, enables the detection of inhibition zone formation around an antibiotic disk on average 1–1.5 hours earlier than unprocessed (raw) speckle images. Specifically, the inhibition zone can be observed 3–3.5 hours after inoculation using the proposed method, compared to 4.5 hours with raw speckle imaging. It is also worth paying attention to the following cases: 1) When an antibiotic disk was placed on a bacterial culture inoculated according to the EUCAST standard after a delay of 4–4.5 hours post-inoculation (allowing the bacteria to reach a high concentration), the formation of the zone of inhibition became clearly visible almost immediately using the proposed technique. In contrast, when observing unprocessed (raw) speckle images, the zone of inhibition became apparent only after a delay of several hours (approximately 5 hours). 2) Additionally, the proposed technique identified cases where bacteria determined to be fully resistant to antibiotics using conventional methods demonstrated the formation of a zone of inhibition. This suggests the technique's potential sensitivity to subtle antimicrobial effects not detected by standard approaches. The practical implementation of this technology could significantly accelerate laboratory workflows, enabling faster transmission of results and their interpretation to clinical settings.

All theoretical questions posed in this study were experimentally validated through the proposed and developed approaches and methods. As a result, a non-invasive, non-contact method was introduced within the scope of this Thesis, enabling earlier detection of bacterial growth compared to conventional colony-forming unit (CFU) detection under white light illumination. This method allows for the visualisation of previously undetectable, hidden activity zones within microbial colonies and facilitates the identification of dynamic changes in the zone of inhibition around antibiotic disks, which would otherwise remain undetected. Consequently, classifiers developed based on this method accurately distinguished between active and inactive zones. Future research may focus on developing simulation models and forecasts of microorganism colony growth and inhibition zone dynamics.

BIBLIOGRAPHY

[1] Newton, I., Opticks (Reprinted by Dover Press, New York 1952) Book I, Part I, Prop. VIII, Prob. II. (1730).
[2] Exner, K., Sitzungsbericht, Kaiserl. Akademie der Wissenschaft (Wien), 76, 522, (1877).
[3] Exner, K., Wiedemanns. Ann. Physik 9, 239, (1880).
[4] Von Laue, M. (1914). Sitzungsber. Akad. Wiss.(Berlin), 44, 1144, (1914).
[5] de Haas, W. J. On the diffraction phenomenon caused by a great number of irregularly distributed apertures or opaque particles. In Koninklijke Nederlandse Akademie van Wetenschappen (Amsterdam), Proceedings, Vol. 20, No. 11, pp. 1278-1288, (1918).
[6] von Laue, M., Mitt. Physik. Ges. (Ziirich) 18,90 (1916)
[7] von Laue, M., Verhandl. Deutsch. Phys. Ges. 19, 19 (1917)
[8] Rigden, J. D., Gordon, E. I., "Granularity of scattered optical maser light." Proceedings of the Institute of Radio Engineers, 50(11), 2367, (1962).
[9] Oliver, B. M. "Sparkling spots and random diffraction.", Proceedings of the IEEE, 51(1), 220-221, (1963).
[10] Singh, P., Shree, R. "Analysis and effects of speckle noise in SAR images.", In 2016 2nd International Conference on Advances in Computing, Communication, & Automation (ICACCA)(Fall) (pp. 1-5). IEEE, (2016, September).
[11] Michailovich, O. V., Tannenbaum, A., "Despeckling of medical ultrasound images.", IEEE transactions on ultrasonics, ferroelectrics, and frequency control, 53(1), 64-78., (2006).
[12] Racine, R., Walker, G. A., Nadeau, D., Doyon, R., Marois, C., "Speckle noise and the detection of faint companions.", Publications of the Astronomical Society of the Pacific, 111(759), 587, (1999).
[13] Fujii, H., and T. Asakura. "Effect of surface roughness on the statistical distribution of image speckle intensity." Optics communications 11.1, pp.:35-38., (1974)
[14] Hamed, A. M., and M. Saudy. "Computation of surface roughness using optical correlation." Pramana 68, pp.: 831-842., (2007)
[15] Heikkinen, J., Schajer, G. S., "Remote surface motion measurements using defocused speckle imaging.", Optics and Lasers in Engineering, 130, 106091, (2020).
[16] Boas, D. A., Dunn, A. K. “Laser speckle contrast imaging in biomedical optics,” J. Biomed. Opt., vol. 15, no. 1, p. 11109, (2010).
[17] Hahn, F., Hernández, G., Echeverría, E., Romanchick, E. “Escherichia coli detection using thermal images,” Canadian Biosystems Engineering, vol. 48 (4), 7–13, (2006).
[18] Volpe, P. L. O. “Flow microcalorimetric measurements of the antibacterial activity of the homologous series m-alkoxyphenols and p-hydroxybenzoates on Escherichia coli,” J. Braz. Chem. Soc., vol. 8, no.4 (1997).
[19] Skarstad, K., Steen, H. B., Boye, E. "Cell cycle parame-ters of slowly growing Escherichia coli B/r studied by flow cytometry," J. Bacteriol. 154 (2), 656–62, (1983).
[20] Tan, W., Oldenburg, A. L., Norman, J. J., Desai, T. A., Boppart, S. A. “Optical coherence tomography of cell dynamics in three dimensional tissue models,” Opt. Exp. 14, 7159–7171, (2006).
[21] Goodman, J. W.: "Speckle Phenomena in Optics. Theory and Application", Chapter 8, Roberts and Company, Englewood, Colorado, (2007).

[22] Battista, D. Di., Ancora, D., Zacharakis, G., Ruocco, G., Leonetti, M.: "Hyperuniformity in amorphous speckle patterns." Opt. Express 26, 15594–15608 (2018).
[23] Goodman, J. W.: "Introduction to Fourier Optics", 3rd ed., Roberts, (2005).
[24] Gascon F, Salazar F.: "A simple method to simulate diffraction and speckle patterns with a PC", Optik-International Journal for Light and Electron Optics, Vol 117, pp. 49–57, (2006)
[25] Duncan, D. D., Kirkpatrick, S. J.: "The copula: a tool for simulating speckle dynamics", Journal of Optical Society of America A 25(1), 231-237 (2008).
[26] Rabal, H., Arizaga, R., Cap, N., Grumel, E., Trivi, M.: "Numerical model for dynamic speckle: an approach using the movement of scatterers". Journal of Optics A: Pure and Applied Optics, (2003)
[27] Federico, A., Kaufmann, G. H., Galizzi, G. E., Rabal, H., Trivi, M., Arizaga, R.: "Simulation of dynamic speckle sequences and its application to the analysis of transient processes," Opt. Commun. 260, 493–499 (2006).
[28] Fricke-Begemann, T., Beyrau, F., Gulker, G., Hinsch, K. D., Jaschke, P., Wolff, K.: "Analysis of microstructure changes and dynamic processes at rough surfaces using speckle correlation," in Scattering and Surface Roughness II, Z. Gu and A. Maradudin, eds., Proc. SPIE 3426, pp. 113–123 (1998).
[29] Duncan, D. D., Kirkpatrick, S. J.: "Algorithms for simulation of speckle (laser and otherwise)," Biomedical Optics (Optical Society of America), V, 6855, p. 685505, (2008)
[30] Oulamara, A., Tribillon, G., Duvernoy, J.: "Biological activity measurement on botanical specimen surfaces using a temporal decorrelation effect of laser speckle," J. Mod. Opt. 36, pp. 165–179 (1989).
[31] Kenny, E., Coakley, D., Boyle, G.: "Biospeckle in the human sclera and impact on laser speckle correlation measurement of eye tremor," J. Biomed. Opt. 18, 097009 (2013).
[32] Lehmann, P., "Surface-roughness measurement based on the intensity correlation function of scattered light under speckle-pattern illumination," Appl. Opt. 38, 1144-1152 (1999)
[33] Ennos, A., "Speckle interferometry," in Laser Speckle and Related Phenomena, J.C. Dainty, ed. (Springer-Verlag, 1975)
[34] Kirkpatrick, S. J., Duncan, D. D., Wells-Gray, E. M.: "Detrimental efects of speckle-pixel size matching in laser speckle contrast imaging", Opt. letters 33, 2886–2888 (2008).
[35] Piederriere Y., Cariou J., Guern Y, Le Jeune B., Le Brun G., Lotrian J., Scattering through fluids: speckle size measurement and Monte Carlo simulations close to and into the multiple scattering, Optics Express 12, 176-188, (2004).
[36] Goodman, J. W, Statistical Optics (Wiley, 1985).
[37] Vaz, P. G., Humeau-Heurtier, A., Figueiras, E., Correia, C., and Cardoso, J., Laser speckle imaging to monitor microvascular blood flow: a review. IEEE reviews in biomedical engineering, 9, 106-120., (2016).
[38] Draijer, M., Hondebrink, E., Van Leeuwen, T., Steenbergen, W., Review of laser speckle contrast techniques for visualizing tissue perfusion. Lasers in medical science, 24, 639-651, (2009).
[39] Duncan, D. D., Kirkpatrick, S. J. "Can laser speckle flowmetry be made a quantitative tool?" J. Opt. Soc. Am. A. Opt. Image Sci. Vis., vol. 25, no. 8, pp. 2088–2094, (2008).
[40] Goodman, J. W. "Statistical properties of laser speckle patterns," in Laser Speckle Relat. Phenom., ser. Topics in Applied Physics. Springer Berlin Heidelberg, vol. 9, pp. 9–75, (1975)

[41] Briers, J. D., and Fercher, A. F., “Retinal blood-flow visualization by means of laser speckle photography.” Invest. Ophthalmol. Vis. Sci., vol. 22, no. 2, pp. 255–259, (1982)
[42] Briers, J. D., Webster, S. “Laser speckle contrast analysis (LASCA): A nonscanning, full-field technique for monitoring capillary blood flow,” J. Biomed. Opt., vol. 1, no. 2, pp. 174–179, (1996)
[43] Yu, G., Durduran, T., Zhou, C., Cheng, R., Yodh, A. G., “Near-infrared diffuse correlation spectroscopy for assessment of tissue blood flow.”, Handbook of biomedical optics, ch. 10, pp. 195-216, (2011).
[44] Nadort, A., Woolthuis, R. G., van Leeuwen, T. G., Faber, D. J., “Quantitative laser speckle flowmetry of the in vivo microcirculation using sidestream dark field microscopy.”, Biomedical optics express, vol. 4, no. 11, pp. 2347-2361, (2013).
[45] Siegert, A. J. F. On the fluctuations in signals returned by many independently moving scatterers. Report: Radiation laboratory, Massachusetts Insitute of Technology, (1943)
[46] Goldfischer, L. I. Autocorrelation function and power spectral density of laser-produced speckle patterns. JOSA. 55, 247–253 (1965)
[47] Fercher, A.F., Briers, J.D., “Flow visualization by means of single-exposure speckle photography.”, Opt. Commun. 37, 326–330, (1981), https://doi.org/10.1016/0030-4018(81)90428-4
[48] Fujii, H., Nohira, K., Yamamoto, Y., Ikawa, H., Ohura, T., "Evaluation of blood flow by laser speckle image sensing. Part 1.", Applied Optics, 26(24), 5321-5325, (1987)
[49] Senarathna, J., Rege, A., Li, N., Thakor, N. V. “Laser Speckle Contrast Imaging: Theory, Instrumentation and Applications,” Biomed. Eng. IEEE Rev., vol. 6, pp. 99–110, (2013)
[50] Parthasarathy, A. B., Tom, W. J., Gopal, A., Zhang, X., Dunn, A. K. “Robust flow measurement with multi-exposure speckle imaging.” Opt. Express, vol. 16, no. 3, pp. 1975–89, feb 2008.
[51] Bandyopadhyay, R., Gittings, A. S., Suh, S. S., Dixon, P. K., Durian, D. J., “Speckle-visibility spectroscopy: A tool to study time-varying dynamics.”, Review of scientific instruments, vol. 76, no. 9, (2005).
[52] Draijer, M., Hondebrink, E., Van Leeuwen, T., Steenbergen, W. “Review of laser speckle contrast techniques for visualizing tissue perfusion,” Lasers Med. Sci., vol. 24, no. 4, pp. 639–651, 2009.
[53] Cheng, H., Luo, Q., Zeng, S., Chen, S., Cen, J., Gong, H. “Modified laser speckle imaging method with improved spatial resolution,” J. Biomed. Opt., vol. 8, no. 3, p. 559, 2003.
[54] Dragojević, T., Bronzi, D., Varma, H. M., Valdes, C. P., Castellvi, C., Villa, F., Tosi, A., Justicia, C., Zappa, F., Durduran, T. “High-speed multi-exposure laser speckle contrast imaging with a single-photon counting camera,” Biomed. Opt. Express, vol. 6, no. 8, pp. 2865–2876, 2015.
[55] Loutfi, H., Pellen, F., Le Jeune, B., Lteif, R., Kallassy, M., Le Brun, G., Abboud, M., "Real-time monitoring of bacterial growth kinetics in suspensions using laser speckle imaging." Scientific reports, 10(1), 408, (2020).
[56] Gutt, C., Stadler, L. M., Duri, A., Autenrieth, T., Leupold, O., Chushkin, Y., Grübel, G., "Measuring temporal speckle correlations at ultrafast x-ray sources.", Optics express, 17(1), 55-61, (2009).

[57] Zdunek, A., Muravsky, L. I., Frankevych, L., Konstankiewicz, K., "New nondestructive method based on spatial-temporal speckle correlation technique for evaluation of apples quality during shelf-life.", International Agrophysics, 21(3), 305-310, (2007).
[58] Nader, C. A., Pellen, F., Loutfi, H., Mansour, R., Jeune, B. L., Brun, G. L., Abboud, M., "Early diagnosis of teeth erosion using polarized laser speckle imaging.", Journal of biomedical optics, 21(7), 071103-071103, (2016).
[59] Cheng, H., Duong, T. Q. "Simplified laser-speckle-imaging analysis method and its application to retinal blood flow imaging.", Optics letters, 32(15), 2188-2190, (2007).
[60] Bonner, R., Nossal, R., "Model for laser Doppler measurements of blood flow in tissue.", Applied optics, 20(12), 2097-2107, (1981).
[61] Ji, Y., Chao, Z., Zhang, Y., Wu, Z., Miao, P. "Effects of scattering particles' concentration in laser speckle contrast imaging." 2014 7th International Conference on Biomedical Engineering and Informatics. IEEE, (2014)
[62] Zakharov, P., Völker, A. C., Wyss, M. T., Haiss, F., Calcinaghi, N., Zunzunegui, C., Buck, A., Scheffold, F., Weber, B., "Dynamic laser speckle imaging of cerebral blood flow.", Optics express, 17(16), 13904-13917, (2009).
[63] Mahé, G., Humeau-Heurtier, A., Durand, S., Leftheriotis, G., Abraham, P., "Assessment of skin microvascular function and dysfunction with laser speckle contrast imaging.", Circulation: Cardiovascular Imaging, 5(1), 155-163, (2012).
[64] Vaz, P. G., Humeau-Heurtier, A., Figueiras, E., Correia, C., Cardoso, J., "Effect of static scatterers in laser speckle contrast imaging: an experimental study on correlation and contrast.", Physics in Medicine & Biology, 63(1), 015024, (2017).
[65] Lemieux, P. A., Durian, D. J., "Investigating non-Gaussian scattering processes by using nth-order intensity correlation functions.", JOSA A, 16(7), 1651-1664, (1999).
[66] Dunn, A. K., Bolay, H., Moskowitz, M. A., Boas, D. A., "Dynamic imaging of cerebral blood flow using laser speckle.", Journal of Cerebral Blood Flow & Metabolism, 21(3), 195-201, (2001).
[67] Duncan, D. D., Kirkpatrick, S. J., Gladish, J. C., "What is the proper statistical model for laser speckle flowmetry?", In Complex Dynamics and Fluctuations in Biomedical Photonics V (Vol. 6855, pp. 9-15). SPIE, (2008, February)
[68] Boas, D. A., Yodh, A. G., "Spatially varying dynamical properties of turbid media probed with diffusing temporal light correlation.", JOSA A, 14(1), 192-215, (1997).
[69] Ramirez-San-Juan, J. C., Regan, C., Coyotl-Ocelotl, B., Choi, B., "Spatial versus temporal laser speckle contrast analyses in the presence of static optical scatterers.", Journal of biomedical optics, 19(10), 106009-106009, (2014).
[70] Yuan, S., Devor, A., Boas, D. A., Dunn, A. K. “Determination of optimal exposure time for imaging of blood flow changes with laser speckle contrast imaging.” Appl. Opt., vol. 44, no. 10, pp. 1823–1830, (2005)
[71] Ohtsubo, J., Asakura, T. Velocity measurement of a diffuse object by using time-varying speckles. Optical and Quantum Electronics, 8, 523-529. Opt. Quant. Electron. 8 523–9, (1976)
[72] Ruth, B., "Velocity measurement by the laser speckle method using optical fibres.", Optics & Laser Technology, 19(2), 83-90, (1987).
[73] Ruth, B., "Non-contact blood flow determination using a laser speckle method." Optics & Laser Technology, 20(6), 309-316, (1988).

[74] Fujii, H., Asakura, T., Nohira, K., Shintomi, Y., Ohura, T., "Blood flow observed by time-varying laser speckle.", Optics letters, 10(3), 104-106, (1985).
[75] Aizu, Y., Ogino, K., Koyama, T., Takai, N., Asakura, T., "Evaluation of retinal blood flow using laser speckle phenomena", Nippon Laser Igakkaishi, 8(3):89-90, (1987)
[76] Li, H., Liu, Q., Lu, H., Li, Y., Zhang, H. F., Tong, S., "Directly measuring absolute flow speed by frequency-domain laser speckle imaging." Optics express, 22(17), 21079-21087, (2014).
[77] Zhou, K., Zhou, C., Sapre, A., Pavlock, J. H., Weaver, A., Muralidharan, R., Noble, J., Kovac, J., Liu, Z., Ebrahimi, A. "Dynamic Laser Speckle Imaging meets Machine Learning to enable Rapid Antibacterial Susceptibility Testing (DyRAST)," ACS Sens. 5(10), 3140-3149 (2020).
[78] Peters, W. H., Ranson, W. F. “Digital image techniques in experimental stress analysis,” Optical Engineering 21, 427-431 (1982).
[79] Sutton, M. A., Wolters, W. J., Peters, W. H., Ranson, W. F., McNeill, S. R. “Determination of displacement using an improved digital correlation method,” Image and Vision Computation 1, 133-139 (1983).
[80] Argyriou, V., Vlachos, T. "A Study of Sub-pixel Motion Estimation using Phase Correlation", In BMVC (pp. 387-396), (2006).
[81] Sjödahl, M., Benckert, L. R. "Electronic speckle photography: analysis of an algorithm giving the displacement with subpixel accuracy," Applied Optics 32 (13), 2278-2284 (1993).
[82] Chen, D. J., Chiang, F. P., Tan, Y. S., Don, H. S. “Digital speckle-displacement measurement using a complex spectrum method,” Appl. Opt. 32(11), 1939 –1849 (1993).
[83] Barcellona, C., Halpaap, D., Amil, P., Buscarino, A., Fortuna, L., Tiana-Alsina, J., Masoller, C. “Remote recovery of audio signals from videos of optical speckle patterns: A comparative study of signal recovery algorithms,” Opt. Express, 28, 8716–8723, (2020).
[84] Zalevsky, Z., Beiderman, Y., Margalit, I., Gingold, S., Teicher, M., Mico, V., Garcia, J. "Simultaneous remote extraction of multiple speech sources and heart beats from secondary speckles pattern", Opt. Express 17, 21566–21580, (2009).
[85] Li, L., Gubarev, F. A., Klenovskii, M. S., Bloshkina, A. I. "Vibration measurement by means of digital speckle correlation", In 2016 International Siberian Conference on Control and Communications (SIBCON) (pp. 1-5). IEEE, (2016).
[86] Hao, X., Zhu, D., Wang, X., Yang, L., Zeng, H. "A Speech Enhancement Algorithm for Speech Reconstruction Based on Laser Speckle Images". Sensors, 23(1), 330, (2023).
[87] Nadkarni, S. K., Bouma, B. E., Helg, T., Chan, R., Halpern, E., Chau, A., Minsky, M. S., Motz, J. T., Houser, S. L., Tearney, G. J. “Characterization of atherosclerotic plaques by laser speckle imaging,” Circulation 112(6), 885–892 (2005).
[88] Yoon, J., Lee, K., Park, Y., “A simple and rapid method for detecting living microorganisms in food using laser speckle decorrelation,” arXiv:1603.07343 (2016).
[89] Rose, L. J., O'Connell, H., “UV Light Inactivation of Bacterial Biothreat Agents.”, Appl Environ Microb 75, 2987-2990 (2009).
[90] Bolton, J. R., Linden, K. G., “Standardization of methods for fluence (UV dose) determination in bench-scale UV experiments.”, J Environ Eng-Asce 129, 209-215 (2003)
[91] Yoo, J. C., Han, T. H. "Fast normalized cross-correlation", Circuits, systems and signal processing, 28, 819–843, (2009).

[92] Di Stefano, L., Mattoccia, S., Tombari, F. "ZNCC-based template matching using bounded partial correlation", Pattern recognition letters, 26(14), 2129–2134, (2005).
[93] Kuglin, C. D., Hines, D. C. “The phase correlation image alignment method,” in Proc. IEEE 1975 Inf. Conf. Cybernet. Society, New York, No. 4, 163–165, (1975).
[94] Lewis, J. P. “Fast Template Matching”, Vision Interface, 120–123, (1995).
[95] Kim, S., Kim, J., Lim, W., Jeon, S., Kim, O., Koh, J. T., Kim, C., Choi, H., Kim, O. “In Vitro Bactericidal Effects of 625, 525, and 425 nm Wavelength (Red, Green, and Blue) Light-Emitting Diode Irradiation,” Photomed. Laser Surg. 31(11), 554–562, (2013).
[96] Chang, C.-W., Grinshpun, S. A., Willeke, K., Macher, J. M., Donnelly, J., Clark, S., Juozaitis, A., “Factors Affecting Microbiological Colony Count Accuracy for Bioaerosol Sampling and Analysis.”, American Industrial Hygiene Association Journal, 56(10), 979–986, (1995).
[97] Sieuwerts, S., de Bok, F. A. M., Mols, E., de Vos, W. M., & van Hylckama Vlieg, J. E. T., “A simple and fast method for determining colony forming units”, Letters in Applied Microbiology, 47(4), 275–278, (2008).
[98] Murialdo, S. E., Sendra, G. H., Passoni, L. I., Arizaga, R., Gonzalez, J. F., Rabal, H., Trivi, M. “Analysis of bacterial chemotactic response using dynamic laser speckle,” J. Biomed. Opt. 14(6), 064015, (2009).
[99] Murialdo, S. E., Passoni, L. I., Guzman, M. N., Sendra, G. H., Rabal, H., Trivi, M., Gonzalez, J. F. “Discrimination of motile bacteria from filamentous fungi using dynamic speckle,” J. Biomed. Opt. 17(5), 056011, (2012).
[100] Kim, H., Singh, A. K., Bhunia, A. K., Bae, E. “Laser-induced speckle scatter patterns in Bacillus colonies,” Front. Microbiol. 5, 537, (2014).
[101] Grassi, H. C., García, L. C., Lobo-Sulbarán, M. L., Velásquez, A., Andrades-Grassi, F. A., Cabrera, H., Andrades-Grassi, J. E., Andrades, E. D."Quantitative Laser Biospeckle Method for the Evaluation of the Activity of Trypanosoma cruzi Using VDRL Plates and Digital Analysis," PLoS Negl. Trop. Dis. 10(12), e0005169, (2016).
[102] Grassi, H. C., Velásquez, A., Belandria, O. M., Lobo-Sulbarán, M. L., Andrades-Grassi, J. E., Cabrera, H., Andrades, E. D. “Biospeckle laser digital image processing for quantitative and statistical evaluation of the activity of Ciprofloxacin on Escherichia coli K-12,” Laser Phys. 29(7), p.075603, (2019).
[103] Váchová, L., Cáp, M. & Palková, Z. Yeast colonies: a model for studies of aging, environmental adaptation, and longevity. Oxid. Med. Cell. Longev. 2012, 601836 (2012)
[104] Gåsvik, K. J. “Optical Metrology”, 3rd ed., Chapter 8, John Wiley & Sons, New York (2002).
[105] Lai, X., Torp, H. “Interpolation methods for time-delay estimation using cross-correlation method for blood velocity measurement. Ultrasonics, ferroelectrics, and frequency control,” IEEE Transactions 46(2), 277–290 (1999).
[106] Tukey, J. W. Nonlinear (nonsuperimposable) methods for smoothing data. Proc. Con. Rec. EASCON. 673 (1974).
[107] Lehmann, E. L. Teory of Point Estimation (Wiley, 1983).
[108] Jwo, D. J., Chang, W. Y., Wu, I. H., "Windowing techniques, the Welch method for improvement of power spectrum estimation.", Comput. Mater. Contin, 67, 3983-4003. (2021).
[109] Nyquist, H., “Certain Topics in Telegraph Transmission Theory. Transactions of the American Institute of Electrical Engineers”, 47(2), 617–644, (1928).

[110] Shannon, C. E., “Communication in the presence of noise”, Proceedings of the Institute of Radio Engineers. 37 (1): 10–21, (1949).
[111] Rivas, E.-M., Gil de Prado, E., Wrent, P., de Silóniz, M.-I., Barreiro, P., Correa, E. C., Conejero, F., Murciano, A., and Peinado, J. M.: "A simple mathematical model that describes the growth of the area and the number of total and viable cells in yeast colonies," Lett. Appl. Microbiol. 59, 594-603 (2014).
[112] Hoff, J., Daniel, B., Stukenberg, D., Thuronyi, B. W., Waldminghaus, T., and Fritz, G.: "Vibrio natriegens: an ultrafast-growing marine bacterium as emerging synthetic biology chassis," Environ Microbiol. (2020).
[113] Pirt, S. J. "A kinetic study of the mode of growth of surface colonies of bacteria and fungi.", J. Gen. Microbiol. 47(2), 181–197 (1967)
[114] Chacón, J. M., Möbius, W., Harcombe, W. R., “The spatial and metabolic basis of colony size variation.”, ISME J. 12(3), 669–680, (2018).
[115] Cooper, A. L., Dean, A. C., Hinshelwood, C, “Factors afecting the growth of bacterial colonies on agar plates.”, Proc. R. Soc. Lond. B. Biol. Sci. 171(1023), 175–199 (1968)
[116] Tenover, F.C., Antimicrobial Susceptibility Testing, 4th ed., pp. 166-175 (Academic Press, 2019).
[117] Bard, J.D., Lee, F., "Why can't we just use PCR? The role of genotypic versus phenotypic testing for antimicrobial resistance testing," Clin. Microbiol. Newsl. 40(11), 87-95 (2018).
[118] World Health Organization, "Global antimicrobial resistance surveillance system (GLASS) report: early implementation 2020," WHO, https://apps.who.int/iris/handle/10665/332081 (2020).
[119] Abraham, E.P., Chain, E., Fletcher, C.M., Florey, H.W., Gardner, A.D., Heatley, N.G., Jennings, M.A., "Further observations on penicillin". Lancet, 177–89, (1941).
[120] Bonev, B., Hooper, J., Parisot, J., "Principles of assessing bacterial susceptibility to antibiotics using the agar diffusion method.", J Antimicrob Chemother 61, 1295–1301 (2008).
[121] Fick, A., Poggendorff’s Annalen. (1855) 94, 59-86. and (in English) Phil.Mag. S.4, Vol.10, 30-39 (1855).
[122] Cooper, K.E., Woodman, D., "The diffusion of antiseptics through agar gels, with special reference to the agar cup assay method of estimating the activity of penicillin", J Pathol Bacteriol,58: 75–84 (1946).
[123] Tjandra, K.C., Ram-Mohan, N., Abe, R., Hashemi, M.M., Lee, J.-H., Chin, S.M., Roshardt, M.A., Liao, J.C., Wong, P.K., Yang, S., “Diagnosis of Bloodstream Infections: An Evolution of Technologies towards Accurate and Rapid Identification and Antibiotic Susceptibility Testing,” Antibiotics 11, 511 (2022).
[124] McCullagh, P. and Nelder, J.A. Generalized Linear Models, 2nd Edition, Chapman and Hall, London, (1989).
[125] Kim, D., Lee, J., Yoon, J. “Accurate estimation of the inhibition zone of antibiotics based on laser speckle imaging and multiple random speckle illumination.”, Computers in Biology and Medicine, 174, 108417, (2024)
[126] Wu, Y., Gadsden, S. A., "Machine learning algorithms in microbial classification: a comparative analysis.", Frontiers in Artificial Intelligence, 6, 1200994, (2023).
[127] Rawat, W., Wang, Z., "Deep convolutional neural networks for image classification: A comprehensive review.", Neural computation, 29(9), 2352-2449, (2017).

[128] Sun, X. X., Qu, W., "Comparison between mean filter and median filter algorithm in image denoising field", Applied Mechanics and Materials, 644, pp. 4112-4116 (2014)
[129] Rosenblatt, F., “The Perceptron: A probabilistic model for information storage and organization in the brain,” Psychological Review, vol. 65, pp. 386–408, (1958).
[130] McCulloch, W. S., and W. Pitts. "A logical calculus of the ideas immanent in nervous activity." The bulletin of mathematical biophysics5, pp. 115-133, (1943).
[131] Haykin, S. "Neural Networks and Learning Machines". Third Edition, Pearson Education, Inc., McMaster University, Hamilton, Chapter 1 and Chapter 4, (2009)
[132] Menon, A., Mehrotra, K., Mohan, C. K., & Ranka, S., Characterization of a class of sigmoid functions with applications to neural networks. Neural networks, 9(5), 819-835, (1996)
[133] Rumelhart D.E., Hinton G.E., Williams R.J., Learning Internal Representations by Error Propagation. In: Parallel Distributed Processing, vol. 1, pp. 318—362. Cambridge, MA, MIT Press, (1985).
[134] Ian, G., Yoshua, B., & Aaron, C., Deep learning: Adaptive computation and machine learning, Chapter 6, (2017)
[135] Hornik, K., Stinchcombe, M., and White, H., Multilayer feedforward networks are universal approximators. Neural Networks , 2, 359–366, (1989).
[136] Lippmann, R., An introduction to computing with neural nets. IEEE Assp magazine, 4(2), 4-22, (1987)
[137] Reed, R., MarksII, R. J., Neural smithing: supervised learning in feedforward artificial neural networks. Mit Press, (1999)
[138] Chester, D. L.: Why two hidden layers are better than one. In: Caudhill, M. (ed.) International Joint Conference on Neural Networks, vol. 1, pp. 265-268. Laurence Erlbaum, New Jersey, (1990)
[139] Thomas, A. J., Petridis, M., Walters, S. D., Gheytassi, S. M., Morgan, R. E., Two hidden layers are usually better than one. In Engineering Applications of Neural Networks: 18th International Conference, EANN 2017, Athens, Greece, August 25–27, 2017, Proceedings (pp. 279-290). Springer International Publishing, (2017)
[140] Fahlman, S., & Lebiere, C., The cascade-correlation learning architecture. Advances in neural information processing systems, 2, (1989)
[141] Le Cun, Y., Boser, B., Denker, J. S., Henderson, D., Howard, R. E., Hubbard, W., & Jackel, L. D., Backpropagation Applied to Handwritten Zip Code Recognition, Neural Computation, vol. 1, (1989)
[142] Jeff, H. T., Introduction to Neural Networks with Java. Chapter 5, (2005)
[143] Yotov, K., Hadzhikolev, E., Hadzhikoleva, S., Cheresharov, S., Finding the optimal topology of an approximating neural network. Mathematics, 11(1), 217, (2023)
[144] The European Committee on Antimicrobial Susceptibility Testing. (2023) Clinical breakpoints – breakpoints and guidance. Available at: https://www.eucast.org/clinical_breakpoints/
[145] Briers, J. D., Richards, G. J., He, X. W. Capillary blood flow monitoring using laser speckle contrast analysis (LASCA). J. Biomed. Opt. 4, 164–176 (1999).
[146] Abou Nader, C., Loutfi, H., Pellen, F., Le Jeune, B., Le Brun, G., Lteif, R., Abboud, M. Assessing white wine viscosity variation using polarized laser speckle: A promising alternative to wine sensory analysis. Sensors, 17(10), 2340, (2017)

[147] Abou Nader, C., Pellen, F., Roquefort, P., Aubry, T., Le Jeune, B., Le Brun, G., Abboud, M. Evaluation of low viscosity variations in fluids using temporal and spatial analysis of the speckle pattern. Opt. Lett. 41, 2521–2524 (2016)
[148] Arizaga, R. A., Cap, N. L., Rabal, H. J., Trivi, M., Display of local activity using dynamical speckle patterns. Optical Engineering, 41, 287-294, (2002)
[149] Le, T. M., Paul, J. S., Al-Nashash, H., Tan, A., Luft, A. R., Sheu, F. S., Ong, S. H., New insights into image processing of cortical blood flow monitors using laser speckle imaging. IEEE transactions on medical imaging, 26(6), 833-842, (2007)
[150] Cheng, H., Yan, Y., Duong, T. Q., Temporal statistical analysis of laser speckle images and its application to retinal blood-flow imaging. Optics express, 16(14), 10214-10219, (2008)

Ilya Balmages was born in 1978 in Kyiv, Ukraine. He obtained a Bachelor's degree in Electrical and Power Systems Engineering from Sami Shamoon College of Engineering (SCE), Beer-Sheva, Israel, in 2000, and a Master's degree in Electro-Optical Engineering from Ben-Gurion University of the Negev (BGU), Beer-Sheva, Israel, in 2006.

From 2007 to 2018, he worked at the EORD company in Haifa, Israel. Since 2019, he has been working at Riga Technical University (RTU), where he has held the positions of scientific assistant and researcher. He is currently a researcher at Riga Technical University (RTU). His scientific interests are related to non-invasive methods for detecting microorganism activity and the classification of microbial behaviour using image and signal processing, as well as machine learning techniques.